Theoretical and Experimental Constraints on Modified Gravity

A thesis presented for the degree of

Doctor of Philosophy

by

Seyyed Ali Mozaffari-Chinjani

Department of Physics

Imperial College London

2013

Submitted in part fulfilment of the requirements for the degree of Doctor of Philosophy in Physics of Imperial College London and the Diploma of Imperial College London.

Acknowledgements

No thesis is written alone, no academic work stands in isolation, we must always remember the family, friends and colleagues whom each in their own small way helped me through all the times, both troubling and worry-free.

I am indebted to my mum and dad for the all the encouragement, support and help they have provided me since my childhood. I would not be the scientist I am today without them. I would also thank my brothers for the endless supply of questions and answers we give one another and the realism that only siblings can bring to ones own pursuits.

In a similar vein, my supervisor João Magueijo has always a source of inspiration and knowledge, even perhaps when I least expected it and I thank him greatly for it. He always knew when to let me hang on to a problem until I had figured out how to deal with it and when to jump in with similar uncertainty.

I must also give thanks to Johannes Noller, Dan Thomas, Tom Zlosnik, Dominic Galliano, Alex Adam and Benjo Fraser, be it about work or anything else, I've always enjoyed our many fruitful discussions, be them long or short.

I would also pay tribute to the help and support of the STFC and the Theoretical Physics Group at Imperial, as well as to all the fellow Masters and PhD students that I encountered during my time here have, in some capacity, enriched my studies and thoughts. Additionally I would like to Rocca di Papa for their amazing hospitality.

Declaration

I herewith certify that, to the best of my knowledge, all of the material in this dissertation which is not my own work has been properly acknowledged. The research described has been done either in collaboration with João Magueijo or on my own and the presentation in Chapters 1-4 follows the papers [1, 2, 3, 4].

Seyyed Ali Mozaffari-Chinjani

2013

Abstract

In this thesis, we consider techniques to characterise a Solar System test for modified gravity theories with an inherent preferred acceleration scale (reducing to MOdified Newtonian Dynamics (MOND) in its non-relativistic limit). We further explore the use of measurements from the forthcoming LISA Pathfinder mission to test these theories. Employing gravitational wave techniques such as the expected signal-to-noise ratio as well as considering effects from a variety of instrumental noise models, saddle trajectories and systematics such as self gravity, we show such a test appears very viable. The possibility of constraints in the event of a null result is explored, as well as designing free functions to evade such a test. The symmetries present in such a scheme allowed us to we develop a simple algorithm for scaling tidal stresses in the event of parameters a_0 and κ assuming values different to those originally considered (short cutting a lot of computational work). In doing so, we are able to show broadly, that the scaling of parameters (within an order of magnitude) could potentially save or slaughter a dubious result. Similarly constraints from fifth force experiments and bounds on anomalous accelerations on solar system scales could feed into our theories, but these would appear as parameters in the (otherwise unconstrained) free function μ. We present a similar scaling algorithm to rescale results previously computed from a particular μ, as well as look at methods to constrain it from data. We also explore the behaviour of previously poorly constrained parameters, such as the MONDian scaling C and its behaviour between models. We also extend our formalism to investigate results from more general free functions, perhaps resulting from scalar tensor or other modified gravity theories.

Contents

List of Figures

List of Abbreviations

- **AQUAL** - AQUAdratic Lagrangian Theory
- **ASD** - Amplitude Spectral Density
- **BBN** - Big Bang Nucleosynthesis
- **CMB** - Cosmic Microwave Background
- **CDM** - Cold Dark Matter
- **DM** - Deep MONDian
- **EA** - Einstein Æther theory
- **EFE** - Einstein Field Equations
- **FT** - Fourier Transform
- **GEA** - Generalised Einstein Æther theory
- **GR** - General Relativity
- **GW** - Gravitational Wave
- **LISA** - Laser Interferometer Space Antenna
- **LTP** - LISA Technology Package
- **LPF** - LISA Pathfinder

- **MG** - Modified Gravity
- **MOND** - MOdified Newtonian Dynamics
- **NR** - Non-Relativistic
- **QN** - Quasi-Newtonian
- **SET** - Stress Energy Tensor
- **SNR** - Signal to Noise Ratio
- **SOR** - Successive Over-Relaxation
- **SP** - Saddle Point
- **TeVeS** - Tensor Vector Scalar theory
- **vev** - vacuum expectation value
- **wrt** - with respect to

Chapter 1

Introduction

The concordance model of modern cosmology rests soundly on two cornerstones, a universe filled mostly with cold dark matter and dark energy (described by a cosmological constant), ie ΛCDM, with underlying dynamics characterised by Einstein's theory of General Relativity (GR). Whilst this model explains the early universe with ever increasing accuracy [9], as long as there remains the lack of direct detection of a dark matter particle (baring unviable candidates such as neutrinos [10, 11]), it remains prudent to consider alternatives. One such pathway available is to modify the underlying dynamics themselves, subject to the condition that above certain scales we restore our familiar Newtonian limit. MOdified Newtonian Dynamics (MOND) provides just such a scheme. The MONDian paradigm seeks to explain away galactic dynamics through the use of a modified force law, introducing a preferred acceleration scale, on the scale of typical galactic accelerations (see [7] for a detailed review). On galactic scales, these modified effects become dominant, but at larger accelerations, gravity becomes idyllically described by Newtonian dynamics.

Although ideas of "modifying" gravity in some way have been nothing new, it was Milgrom in 1983 who first proposed a theory of modified inertia [12]. It was this idea that in 1986 was developed into the theory known as AQUAL [13] by Bekenstein and Milgrom, formulating a Lagrangian theory which would satisfy energy and momentum conservation. Investigating the equations of motion from that leads us to a modified Poisson relation (as we will detail later in Section 1.2) - a common way to present such

theories. In the past decade, the potential accomplishments of MONDian theories have been put on an equal pedestal to GR with the development of fully relativistic modified gravity (MG) theories. We find in the literature now a litany of examples of such[1], starting in 2004 with Bekenstein's ground breaking theory of TeVeS [14]. TeVeS attempted to overcome previous issues in this field by introducing a vector and scalar field into the mix, fixing acausal and light deflection issues, at least at the payoff of having to fix more variables. Similarly, the lorentz violating work of Einstein Æther theories [15, 16][2], these various ideas were expanded on and generalised by Zlosnik, Ferreira and Starkman in 2006 [17, 18, 19], as well as attempts by Skordis and others to generalise and investigate the cosmology of these theories [44, 20, 46]. Since 2009, Milgrom has produced Bimetric theories [21], motivating a quasi-linear MONDian theory from a relativistic perspective. There have also resulted various other ideas [22, 23, 24]. Whilst the MONDian paradigm provides a useful framework for making connection to observables, the free functions and parameters in these theories remain relatively unconstrained, leading to a problem of fine tuning. Much work has been done investigating these modified effects on the largest scales, for instance applying constraints from galactic data when seeking dark matter alternatives [25, 26, 27, 28, 29]. The much hailed Bullet Cluster (1E 0657-558) has been considered for what it can tell us about the necessity or needlessness of dark matter and MOND [30, 31, 32, 33, 34]. These gravitational lensing studies in the past decade have suggested that Cold Dark Matter (CDM) fits the data very well and modified gravitational force laws are statistically unlikely to explain away the results. There remains however a lack of consensus on interpreting the weak lensing survey and also there are clusters, such as Abell 520 [35], which are not easily explained by any current paradigm. Quite a different tack has come from applying Lorentz violating mechanisms (typically well constrained in the matter sector) to the gravity sector [36, 37]. Constraints from high energy experiments, such as those at the LHC, especially in the light of the most recent data, have provided some of the best detailed constraints to be seen in the Solar System. Perhaps a good way to investigate general modified non-relativistic theories is to examine deviations from the inverse square law, as considered in [38, 39, 40]. Little more however seems to be known about constraining modified

[1] The original work on AQUAL [13] did describe a relativistic extension for MOND, however it was soon realised it could not take into account observations of light deflection from galaxies nor could it properly restrict the tachyonic behaviour of its field.

[2] In fact the original Einstein Æther theory reduces just to Newtonian dynamics in its weak field, but its construction introduces an acceleration scale, a feature that was later used in generalisations to reduce to MOND.

gravity theories purely in the Solar System. A chance of extending the forthcoming LISA Pathfinder (LPF) mission [41, 42, 43], to include probing the low acceleration regime around gravitational saddle points (SP), appears to provide just such an opportunity, both for testing and also cleanly constraining these theories. In this work, we will extend the analysis for using LPF in such a test, however first we must understand the standard constructions of GR and those resulting from MG theories.

1.1 General Relativity

We start from differential geometry and the constructions of General Relativity (GR). We can begin with a spacetime described by a metric $g_{\mu\nu}$ which we can easily connect with, using the distance relation

$$ds^2 = g_{\mu\nu}dx^\mu dx^\nu \tag{1.1}$$

In "flat" (often denoted Minkowski) spacetime, the metric (denoted by $g_{\mu\nu} = \eta_{\mu\nu}$) takes the form

$$ds^2 = -dt^2 + dx^2 + dy^2 + dz^2 \tag{1.2}$$

or through the diffeomorphism invariance of relativity, we can express equivalently in different coordinate systems, for instance polar coordinates

$$ds^2 = -dt^2 + dr^2 + r^2(d\theta^2 + sin^2\theta\, d\phi^2) \tag{1.3}$$

By flat spacetime, we simply mean we have generalised the three dimensional Euclidean space into four dimensions. Recall in 3D Euclidean space, angles in a triangle add up to 180 degrees and the shortest distance between two points (known as a geodesic) is just a straight line. Throughout this work, we will follow the metric signature $-+++$. From the metric $g_{\mu\nu}$, we can define the torsion free (Christoffel) connection

$$\Gamma^\alpha{}_{\mu\nu} \equiv \frac{g^{\alpha\beta}}{2}\left(g_{\mu\beta,\nu} + g_{\nu\beta,\mu} - g_{\mu\nu,\beta}\right) \tag{1.4}$$

where $_{,\mu} \equiv \partial_\mu = \frac{\partial}{\partial x_\mu}$, such that we define the metric compatible (ie $\nabla_\rho g_{\mu\nu} = 0$) covariant derivative of some (n, m) rank tensor $T^{\alpha_1\alpha_2\ldots\alpha_n}{}_{\beta_1\beta_2\ldots\beta_m}$

$$\begin{aligned} \nabla_\mu T^{\alpha_1\alpha_2\ldots\alpha_n}{}_{\beta_1\beta_2\ldots\beta_m} &= \partial_\mu T^{\alpha_1\alpha_2\ldots\alpha_n}{}_{\beta_1\beta_2\ldots\beta_m} \\ &+ \Gamma^{\alpha_1}{}_{\mu\nu} T^{\nu\alpha_2\ldots\alpha_n}{}_{\beta_1\ldots\beta_m} + \ldots \\ &- \Gamma^{\nu}{}_{\mu\beta_1} T^{\alpha_1\alpha_2\ldots\alpha_n}{}_{\nu\beta_2\ldots\beta_m} - \ldots \end{aligned} \tag{1.5}$$

where we notice the change of sign between the co- (i.e. upstairs) and contra- (i.e. downstairs) variant indices. We can also define the Riemannian curvature tensor, from the identity

$$R^\alpha{}_{\beta\mu\nu} V^\beta \equiv (\nabla_\mu \nabla_\nu - \nabla_\nu \nabla_\mu) V^\alpha \tag{1.6}$$

$$R^\alpha{}_{\beta\mu\nu} \equiv \partial_\mu \Gamma^\alpha{}_{\beta\nu} - \partial_\nu \Gamma^\alpha{}_{\beta\mu} + \Gamma^\alpha{}_{\epsilon\mu} \Gamma^\epsilon{}_{\beta\nu} - \Gamma^\alpha{}_{\epsilon\nu} \Gamma^\epsilon{}_{\beta\mu} \tag{1.7}$$

and can also define Ricci curvature,

$$R^\alpha{}_{\mu\alpha\nu} = R_{\mu\nu} \tag{1.8}$$

and similarly the Ricci scalar

$$R_{\mu\nu} g^{\mu\nu} = R \tag{1.9}$$

Einstein put together these constructions, along with the energy-matter content to form his much heralded Einstein field equations (EFE)

$$G_{\mu\nu} = R_{\mu\nu} - \frac{1}{2} R\, g_{\mu\nu} = \frac{8\pi G}{c^4} T_{\mu\nu} \tag{1.10}$$

The addition of the Ricci scalar term here is needed, such that we satisfy the Bianchi identity $\nabla_\rho G^{\mu\nu} = 0$ (which here can be seen as a consequence of the conservation of stress energy $\nabla_\rho T^{\mu\nu} = 0$). We can also consider GR as being derived from a Lagrangian, such that the equations of motion will give us the field equations. We consider the Einstein-Hilbert action, with cosmological constant, minimally coupled to

matter

$$S = S_{EH} + S_m + S_{GHY} = \int \left[\frac{c^4}{16\pi G} (R - 2\Lambda) + \mathcal{L}_m \right] \sqrt{-g}\, d^4x + \frac{1}{8\pi G} \int_{\partial M} d^3x \sqrt{-g} K \tag{1.11}$$

where $g = det(g_{\mu\nu})$, R is the Ricci scalar curvature and K is the trace of the extrinsic curvature of the boundary. The last term, known as the Gibbons-Hawking-York boundary term, is added to ensure S has a well defined variation principle. If our underlying manifold M is closed (meaning it is compact and without boundary), then it is simply zero, but with some non-trivial boundary ∂M, it adds additional dynamics, in this work however we will stick to the former case. We find the field equations by varying S with respect to (wrt) $g^{\mu\nu}$

$$R_{\mu\nu} - \frac{1}{2} R\, g_{\mu\nu} + \Lambda\, g_{\mu\nu} = \frac{8\pi G}{c^4} T_{\mu\nu} \tag{1.12}$$

and we can take, without loss of generality, $c = 1$ (by definition of units).

1.1.1 Weak field limit and Newtonian dynamics

As a note in history, we knew of Newton's theory of gravity long before Einstein's, so we need to make a connection with the Newtonian theory we are more familiar with, using the so called "weak field" or non-relativistic (NR) limit of GR (by which, we mean small Ricci curvature regime). Considering metric perturbations around the flat Minkowski background,

$$g_{\mu\nu} = \eta_{\mu\nu} + \epsilon\, h_{\mu\nu} \tag{1.13}$$

we can consider only linear terms when expanding in ϵ, with $|\epsilon| \ll 1$. One issue here that of the gauge, so we will fix it using Poisson gauge, $h_{00} = -2\Phi$, $h_{ij} = -2\Psi\delta_{ij}$ (we will take $\partial_0 h_{\mu\nu} = 0$, such that these perturbations are not dynamical) . Here the connection and Ricci tensor take the form

$$\Gamma^{\alpha}{}_{\mu\nu} = \epsilon \frac{\eta^{\alpha\beta}}{2} (h_{\beta\mu,\nu} + h_{\beta\nu,\mu} - h_{\mu\nu,\beta}) + \mathcal{O}(\epsilon^2) \tag{1.14}$$

$$R_{\mu\nu} = \epsilon \frac{\eta^{\alpha\beta}}{2} (h_{\beta\nu,\alpha\mu} + h_{\alpha\mu,\beta\nu} - h_{\mu\nu,\alpha\beta} - h_{\alpha\beta,}) + \mathcal{O}(\epsilon^2) \tag{1.15}$$

Meaning for our purposes

$$R_{00} = \epsilon\,\delta^{ij}\,\partial_i\partial_j\Phi \tag{1.16}$$

$$R_{ij} = \epsilon\,\left(\delta_{ij}\delta^{kl}\partial_l\partial_k\Psi + \partial_i\partial_j[\Psi-\Phi]\right) \tag{1.17}$$

$$R = 2\epsilon\,\delta^{ij}\,\left(2\partial_i\partial_j\Psi - \partial_i\partial_j\Phi\right) \tag{1.18}$$

Similarly, the stress-energy tensor (SET) will take the form

$$T^{\mu\nu} = T^{\mu\nu}_{(0)} + \epsilon\,T^{\mu\nu}_{(1)} + \dots \tag{1.19}$$

We use a perfect fluid form for the SET, with the proviso that for $\epsilon = 0$, i.e. flat spacetime, there is no curvature[3]. At leading order, it takes the form

$$T^{\mu\nu}_{(1)} = \rho U^\mu U^\nu + P(g^{\mu\nu} + U^\mu U^\nu) \tag{1.20}$$

where U_μ is velocity 4-vector, taking the form $U_\mu = (1,0,0,0)$ in the rest frame, ρ is the rest frame mass density and P is the isotropic pressure. Whilst in general we would require ten functions to fully specify a fluid in this relativistic form, a perfect fluid requires only two, making it much easier to find solutions. Under the assumption of dust (i.e. pressureless matter sources), we find two conditions on the potentials from (respectively) the G_{ij} and G_{00} equations,

$$\Phi = \Psi \tag{1.21}$$

$$\nabla^2\Phi = 4\pi G\rho \tag{1.22}$$

The equality of these two scalar potentials, in the absence of anisotropic fluid stresses (i.e. T_{ij} for $i \neq j$) is a feature true of GR, although not necessarily for all modified gravity theories. In such cases however,

[3]Cosmological solutions to the EE suggest that even in the absence of "three curvature" k, there can still be a perfect fluid form for the SET - the spacetime however is still conformally flat, ie $g_{\mu\nu} = a(\tau)\eta_{\mu\nu}$ where τ is some conformal time coordinate and so $\Gamma, R, \dots$ etc remain non-zero even for $k = 0$.

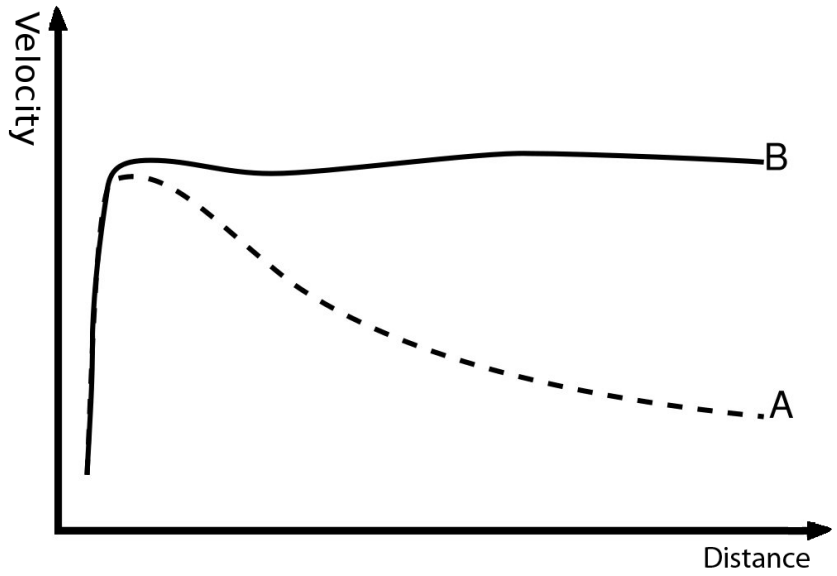

Figure 1.1: The resulting velocity distance relations between a theoretical galaxy, labelled A and an observed galaxy, labelled B. Instead of the predicted fall off going as $1/\sqrt{r}$, we find they flatten out. Such observations suggest either a breakdown of Newtonian mechanics or a different mass distribution at the edges of the galaxy.

it can be of great help in simplifying our equations [23].

1.2 Modified Gravity

1.2.1 Milgrom's MOND

One of the big discrepancies between GR and observations (from considering just visible matter sources) comes in the form of galactic rotation curves. From $\mathbf{F} = m\mathbf{a}$, we see that balancing the Newtonian force with the centripetal acceleration as we move out from the centre of the galaxy gives

$$\frac{GMm}{r^2} = m\frac{v^2}{r} \Rightarrow v \sim \frac{1}{\sqrt{r}} \tag{1.23}$$

Observation however shows $v \to$ constant, as we see in Figure 1.1. One solution clearly could be to have some theory with $F \sim \sqrt{F_N}$, such that $v \sim \sqrt{GM/m}$. Milgrom's [12] original formulation of a modified

gravity theory amounted to a modified inertia law,

$$\mathbf{F} = m\mathbf{a} \longrightarrow \mathbf{F} = m\tilde{\mu}\left(\frac{|a|}{a_0}\right)\mathbf{a} \tag{1.24}$$

where the $\tilde{\mu}$ function (often called the interpolating function) takes the form

$$\tilde{\mu}(x) \to 1 \qquad x \gg 1$$

$$\tilde{\mu}(x) \to x \qquad x \ll 1$$

and the Milgrom characteristic acceleration is $a_0 \simeq 10^{-10}\,\mathrm{ms}^{-2}$. The idea being that on "larger" acceleration scales, gravity behaves as expected (i.e. Newtonian). On "smaller" scales, such as the galactic regime, typical accelerations are $\leq a_0$ and the dynamics are modified to explain observation in this way. In doing so the $v \to$ constant behaviour we were seeking is realised.

Similarly it is possible to write down such a theory in a Lagrangian formulation, the so-called AQUAL theory [13]

$$\mathcal{L} = -\frac{a_0^2}{4\pi G} f\left(\frac{|\nabla\Phi|^2}{a_0^2}\right) - \rho\Phi \tag{1.25}$$

where $\tilde{\mu}(\sqrt{y}) = df(y)/dy$ and the subsequent equations of motion encode this theory as a modified Poisson equation

$$\nabla \cdot (\tilde{\mu}\nabla\Phi) = 4\pi G\rho \tag{1.26}$$

Interest in these MG theories peaked when it appeared to be possible to pick a particular $\tilde{\mu}$ (often motivated by certain features) that would provide a good fit to galactic data. Popular examples of $\tilde{\mu}$'s included

$$\tilde{\mu}(x) = \frac{x}{1+x} \quad , \quad \tilde{\mu}(x) = \frac{x}{\sqrt{1+x^2}}$$

where as before $x = |\nabla\Phi|/a_0$. However, as astrophysical data and instrumentation become more sophisticated and precise, other probes of these theories became necessary. Given that these results were

obtained from a strictly non-relativistic theory, a fully relativistic theory with MOND-like behaviour in its weak field limit became a necessity. It was not until the advent of theories such as TeVeS [14], GEA [19, 17, 18] and others [21, 22], that a side-by-side comparison with GR + ΛCDM was possible [7]. Here we will summarise a few of these and derive the weak field limits thereof, showing how they reduce to MOND.

1.2.2 Bekenstein's Tensor Vector Scalar theory - TeVeS

Bekenstein's seminal work in this area consists of his Tensor Vector Scalar theory (TeVeS), which seeks to source modified gravity effects in the weak field from a fifth force field ϕ and vector field A_μ, whilst not jeopardising the agreement to observation found in GR from effects such as gravitational lensing. In addition the theory is constructed to be Bimetric, with the gravity ($g_{\mu\nu}$) and matter ($\tilde{g}_{\mu\nu}$) metrics related:

$$\tilde{g}_{\mu\nu} = e^{-2\phi}\left(g_{\mu\nu} - A_\mu A_\nu\right) + e^{2\phi} A_\mu A_\nu \tag{1.27}$$

such a disformal relation is needed to avoid problems such as superluminal propagation (see Section IIC of [14]). Here we present the action in a slightly different form to that originally considered in the literature (for reasons of clarity):

$$\begin{aligned} S &= \frac{1}{2}\int\left[\frac{1}{8\pi G}(R-2\Lambda) - \frac{\mu}{\kappa G}h^{\mu\nu}\partial_\mu\phi\partial_\nu\phi - \frac{\mu^2}{2\kappa\ell^2 G}F(\mu) - \frac{K}{16\pi G}\mathcal{F}^{ab}\mathcal{F}_{ab} + \frac{\lambda}{8\pi G}(A^\mu A_\nu + 1)\right]\sqrt{-g}\,d^4x \\ &+ \int\mathcal{L}_m\left(\tilde{g}_{\mu\nu}, f^\alpha, f^\alpha_{|\mu}\ldots\right)\sqrt{-\tilde{g}}\,d^4x \end{aligned} \tag{1.28}$$

We define the tensors

$$h_{\mu\nu} = g_{\mu\nu} - A_\mu A_\nu \tag{1.29}$$

$$\mathcal{F}_{\mu\nu} = \partial_\mu A_\nu - \partial_\nu A_\mu \tag{1.30}$$

and use the notation and conventions:

- κ and K are (respectively) the coupling constants for the scalar and vector fields.

- ℓ is a scale length (related to a_0).
- μ is a non-dynamical scalar field.
- λ is a Lagrange multiplier implementing $g^{\mu\nu}A_\mu A_\nu = -1$ as a constraint.
- $F(\mu)$ is a free function (chosen to give different behaviour depending on the regime in question, implementing the MONDian solutions and others).
- Covariant derivatives denoted by $|$ are taken with respect to $\tilde{g}_{\mu\nu}$.
- Indices are **always** raised & lowered using the metric $g_{\mu\nu}$.

The equations of motion for the metric take the form

$$G_{\mu\nu} + g_{\mu\nu}\Lambda = 8\pi G\left[\tilde{T}_{\mu\nu} + (1-e^{-4\phi})A^\alpha \tilde{T}_{\alpha(\mu}A_{\nu)} + \tau_{\mu\nu}\right] + \Theta_{\mu\nu} \tag{1.31}$$

where as usual

$$\tilde{T}_{\mu\nu} = \frac{2}{\sqrt{-\tilde{g}}}\frac{\delta(\sqrt{-\tilde{g}}\mathcal{L}_m)}{\delta\tilde{g}^{\mu\nu}} \tag{1.32}$$

but also we have stress energy contributions from the scalar and vector fields of the form

$$\tau_{\mu\nu} = \frac{\mu}{\kappa G}\left[\partial_\mu\phi\partial_\nu\phi - \frac{1}{2}g_{\mu\nu}g^{\alpha\beta}\partial_\alpha\phi\partial_\beta\phi - A^\alpha\partial_\alpha\phi\left(A_\mu\partial_\nu\phi - \frac{1}{2}g_{\mu\nu}A^\alpha\partial_\beta\phi\right)\right] - \frac{1}{4}\frac{\mu^2}{\kappa^2\ell^2 G}F(\mu)\,g_{\mu\nu} \tag{1.33}$$

$$\Theta_{\mu\nu} = K\left(g^{\alpha\beta}\mathcal{F}_{\alpha\mu}\mathcal{F}_{\beta\nu} - \frac{1}{4}g_{\mu\nu}\mathcal{F}^{\alpha\beta}\mathcal{F}_{\alpha\beta}\right) - \lambda A_\mu A_\nu \tag{1.34}$$

Variation wrt to the scalar field ϕ gives:

$$\nabla_\beta\left(\mu\, h^{\alpha\beta}\,\partial_\alpha\phi\right) = \kappa G\left[g^{\alpha\beta} + (1+e^{-4\phi})A^\alpha A^\beta\right]\tilde{T}_{\alpha\beta} \tag{1.35}$$

and similarly for the μ field

$$-\mu F(\mu) - \frac{1}{2}\mu^2\frac{dF(\mu)}{d\mu} = \kappa\ell^2 h^{\mu\nu}\partial_\mu\phi\partial_\nu\phi \tag{1.36}$$

Finally variation wrt to the vector field A_μ gives:

$$KA^{[\alpha;\beta]}{}_{;\beta} + \lambda A^\alpha + \frac{8\pi\mu}{\kappa} A^\beta g^{\alpha\gamma}\phi_{,\beta}\phi_{,\gamma} = 8\pi G(1-e^{-4\phi})g^{\alpha\nu}A^\beta \tilde{T}_{\nu\beta} \tag{1.37}$$

and since λ is simply a lagrange multiplier, we can solve for by contracting with A_α and substitute back in to find

$$K\left(A^{[\alpha;\beta]}{}_{;\beta} + A^\alpha A_\gamma A^{[\gamma;\beta]}{}_{;\beta}\right) + \frac{8\pi\mu}{\kappa}\left[A^\alpha\phi_{,\beta}\phi_{,\gamma}g^{\alpha\gamma} + A^\alpha(A^\beta\phi_{,\beta})^2\right] = 8\pi G(1-e^{-4\phi})\left[g^{\alpha\nu}A^\beta\tilde{T}_{\alpha\nu} + A^\alpha A^\beta A^\gamma\tilde{T}_{\beta\gamma}\right] \tag{1.38}$$

We label the argument of (1.36) as $y \equiv \kappa\ell^2 h^{\mu\nu}\partial_\mu\phi\partial_\nu\phi$ and so we can solve as ODE for $\mu(y)$. Bekenstein

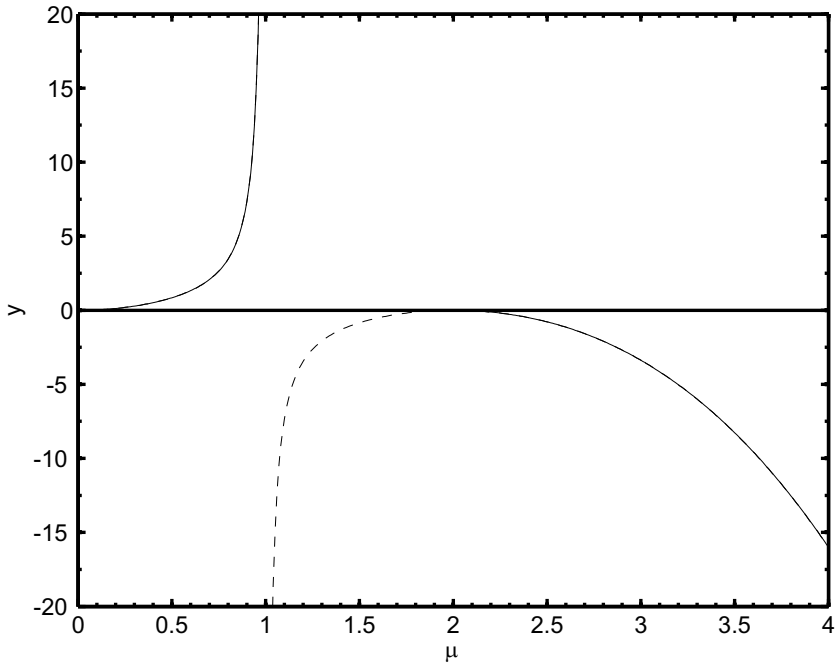

Figure 1.2: The function $y(\mu)$ as relevant for quasi-stationary systems ($0 < \mu < 1$) and cosmology ($\mu > 2$).

suggested a toy model of F of the form

$$F = \frac{3}{8}\frac{\mu(4+2\mu-4\mu^2+\mu^3)+4\ln(1-\mu)}{\mu^2} \tag{1.39}$$

upon solving for $\mu(y)$ results in

$$y = \frac{3}{4}\frac{\mu^2(\mu-2)^2}{1-\mu} \tag{1.40}$$

Bekenstein argues that in the limit $0 < \mu < 1$, we have solutions relevant for quasi-static systems and for $\mu > 2$ relevant for cosmology (with the rest of the domain excised), as illustrated Figure 1.2. By picking a perfect fluid form for the SET, our setup allows us to align the timelike vector field A_μ with the four velocity $\tilde{u}_\mu$, such that $A_\alpha = e^{-\phi}\tilde{u}_\alpha$. Substituting into (1.35) with appropriate contractions gives us the result

$$\nabla_\beta \left(\mu(y) h^{\alpha\beta}\partial_\alpha \phi\right) = \kappa G(\tilde{\rho} + 3\tilde{p})e^{-2\phi} \tag{1.41}$$

In the quasi-static limit, we neglect time derivatives, such that

$$h^{\mu\nu}\partial_\mu\phi \to g^{\mu\nu}\partial_\mu\phi \tag{1.42}$$

as well as just assuming

$$g^{\mu\nu} \quad \to \quad \eta^{\mu\nu} \tag{1.43}$$

$$|\phi| \ll 1 \Rightarrow e^{-2\phi} \quad \to \quad 1 \tag{1.44}$$

Finally for non-relativistic matter, we assume the pressure is negligible compared to the density, allowing us to find a modified Poisson equation for the scalar field ϕ

$$\nabla \cdot (\mu(y)\nabla\phi) = \kappa G\rho \tag{1.45}$$

The next obvious question is what force do massive particles feel? We begin by linearising our Einstein equations, with the potential $V = \Xi\Phi_N$ and so we have

$$g_{00} = -(1 + 2V) \tag{1.46}$$

similarly the vector field satisfies

$$A^\mu = N\xi^\mu = N\delta^\mu{}_0 \tag{1.47}$$

where ξ^μ is a Killing vector field[4] and $N = \sqrt{-g_{\mu\nu}\xi^\mu\xi^\nu}$, which is just a unit normalisation. We can see by substitution this is a solution to Equation (1.38) (see section IV of [14] for more details), meaning the vector field takes the form

$$A_\mu = -(1+V)\delta_{\mu 0} \tag{1.48}$$

From the definition of $\tilde{g}_{\mu\nu}$, we find

$$\tilde{g}_{\mu\nu} = -(1+2V+2\phi) \tag{1.49}$$

which compared with the form $\tilde{g}_{\mu\nu} = -(1+\ 2\Phi)$ means we can we interpret the total potential felt by particles (in the weak field) as $\Phi = V + \phi$. We find the value of Ξ is given by careful analysis of the field equations, the final result being

$$\Xi = 1 + \frac{K}{2} - 2\phi_c \approx 1 \tag{1.50}$$

where ϕ_c is the value of ϕ at spatial infinity, governed by the cosmological model in which our localised system is embedded. Thus in TeVeS, we find

$$\Phi = \Xi\Phi_N + \phi \tag{1.51}$$

where $\Xi \simeq 1$. Constraints on the couplings K and κ are found though analysis of the cosmology and perturbations of the theory (see [44, 45, 46]).

[4] A Killing vector field is a vector field on a Riemannian or pseudo-Riemannian manifold that preserves the metric. It is easy to assign some physical meaning here, for instance if none of the metric coefficients are a function of time, the manifold must automatically have a time-like Killing vector, as we see here.

1.2.3 Einstein Æther theories and Generalisations

Mattingly and Jacobson [15] considered an action with a derivative expansion in metric $g_{\mu\nu}$ and æther field A^a, the most general action that is diffeomorphism-invariant and quadratic in derivatives is simply,

$$S = \int \left[\frac{1}{16\pi G} \left(R - 2\Lambda + M^2 \mathcal{K} + \lambda(A^\mu A_\mu + 1) \right) + \mathcal{L}_m(g_{\mu\nu}, f^\alpha, \dots) \right] \sqrt{-g}\, d^4x \quad (1.52)$$

$$\mathcal{K} = M^{-2} \mathcal{K}^{\mu\nu}{}_{\alpha\beta}\, \nabla_\mu A^\alpha\, \nabla_\nu A^\beta \quad (1.53)$$

$$\mathcal{K}^{\mu\nu}{}_{\alpha\beta} = c_1\, g^{\mu\nu}\, g_{\alpha\beta} + c_2\, \delta^\mu{}_\alpha\, \delta^\nu{}_\beta + c_3\, \delta^\mu{}_\beta\, \delta^\nu{}_\alpha + c_4\, A^\mu\, A^\nu\, g_{\alpha\beta} \quad (1.54)$$

where c_i are just dimensionless constants, λ once again is just a Lagrange multiplier and M has units of mass. Their motivation being to consider a theory of gravity with a dynamical preferred frame (which we can contrast with the cosmological frame which is preferred, as setup from the perfect fluid). Later this was generalised to a theory with a general function of the scalar, $\mathcal{K} \to \mathcal{F}(\mathcal{K})$ [17, 18], allowing for the prospect of MONDian behaviour in the resulting modified Poisson equation. Interestingly by careful choice of extended $\mathcal{K}$, we can write a generalised Einstein Æther (GEA) theory equivalent to TeVeS [16] (with the caveat of an extended $\mathcal{K}$ and an exotic mechanism for a non-zero vacuum expectation value (vev) in A_μ). We find equations of motion for the metric

$$G_{\mu\nu} = 8\pi G\, T_{\mu\nu} + T^{\mathbf{A}}_{\mu\nu} \quad (1.55)$$

where $T_{\mu\nu}$ is just the usual stress-energy and $T^{\mathbf{A}}_{\mu\nu}$ is the contribution from the vector field A_μ:

$$T^{\mathbf{A}}_{\mu\nu} = \frac{1}{2}\nabla_\sigma \left(\mathcal{F}' \left(J_{(\mu}{}^\sigma A_{\nu)} - J^\sigma{}_{(\mu} A_{\nu)} - J_{(\mu\nu)} A^\sigma \right) \right) - \mathcal{F}'\, Y_{(\mu\nu)} + \frac{1}{2} g_{\mu\nu} M^2 \mathcal{F} + \lambda A_\mu A_\nu \quad (1.56)$$

and we use the notation

$$\begin{aligned} \mathcal{F}' &= \frac{d\mathcal{F}}{d\mathcal{K}} \\ Y_{\alpha\beta} &= \nabla_\sigma A^\eta \nabla_\gamma A^\xi \frac{\delta(\mathcal{K}^{\sigma\gamma}{}_{\eta\xi})}{\delta g^{\alpha\beta}} \qquad (1.57) \\ J^\alpha{}_\sigma &= \left(\mathcal{K}^{\alpha\beta}{}_{\sigma\gamma} + \mathcal{K}^{\beta\alpha}{}_{\gamma\sigma}\right) \nabla_\beta A^\gamma \qquad (1.58) \end{aligned}$$

For the vector field, the equations of motion take the form

$$\nabla_\alpha \left(\mathcal{F}' J^\alpha{}_\beta\right) + \mathcal{F}' y_\beta = 2\lambda A_\beta \qquad (1.59)$$

where we define

$$y_\beta = \nabla_\sigma A^\eta \nabla_\gamma A^\xi \frac{\delta(\mathcal{K}^{\sigma\gamma}{}_{\eta\xi})}{\delta A^\beta} \qquad (1.60)$$

For our choice of $\mathcal{K}$ we find

$$\begin{aligned} Y_{\alpha\beta} &= c_1 \left[(\nabla_\alpha A_\nu)(\nabla_\beta A^\nu) - (\nabla_\nu A_\alpha)(\nabla^\nu A_\beta)\right] + c_4 (A^\sigma \nabla_\sigma A_\alpha)(A^\gamma \nabla_\gamma A_\beta) \qquad (1.61) \\ y_\beta &= 2c_4 A^\sigma (\nabla_\sigma A_\nu)(\nabla_\beta A^\nu) \qquad (1.62) \end{aligned}$$

Consider linear perturbations in the metric and vector field around a flat static background

$$\begin{aligned} g_{\mu\nu} &= \eta_{\mu\nu} + \epsilon\, h_{\mu\nu} \qquad (1.63) \\ A^\alpha &= \bar{A}^\alpha + \epsilon B^\alpha \qquad (1.64) \end{aligned}$$

where $\bar{A}^\alpha = \delta^\alpha{}_0$. Next we need to compute the form of $\nabla_\alpha A_\beta$ and so need expressions for $\Gamma^\alpha{}_{\mu\nu}$ and A_α to first order. Recall (1.14) and similarly we know $A_\alpha = A^\beta g_{\mu\nu}$ and so to first order

$$A_\mu = \eta_{\mu\nu}\bar{A}^\nu + \epsilon(\bar{A}^\nu h_{\mu\nu} + B^\nu \eta_{\mu\nu}) + \mathcal{O}(\epsilon^2) \qquad (1.65)$$

Given the background equation $\bar{A}^\nu \eta_{\mu\nu} = \bar{A}_\mu = -\delta_{\mu 0}$, we interpret the term linear in ϵ as B_μ, giving

$$\begin{aligned} B_\mu = h_{\mu 0} + B^\nu \eta_{\mu\nu} \Rightarrow B_0 &= h_{00} - B^0 \quad (1.66) \\ B_i &= \delta_{ij} B^j \quad (1.67) \end{aligned}$$

One additional fact here is that the vector field is enforced to be time-like $A^\mu A_\mu = -1$ and so

$$A^\mu A^\nu g_{\mu\nu} = -1 = \underbrace{\bar{A}^\mu \bar{A}^\nu \eta_{\mu\nu}}_{-1} + \epsilon(\underbrace{\bar{A}^\mu \bar{A}^\nu h_{\mu\nu}}_{h_{00}} + \underbrace{2\bar{A}^\mu B^\nu \eta_{\mu\nu})}_{-2B^0} + \mathcal{O}(\epsilon^2) \quad (1.68)$$

Meaning that at linear order, we have $h_{00} = 2B^0$, so finally we will find

$$\nabla_\alpha A_\beta = \epsilon \partial_\alpha B_\beta - \underbrace{\Gamma^\sigma{}_{\alpha\beta} \bar{A}_\sigma}_{-\Gamma^0{}_{\alpha\beta}} = \epsilon \Sigma_{\alpha\beta} \quad (1.69)$$

giving the components of $\Sigma_{\mu\nu}$ as:

$$\begin{aligned} \Sigma_{00} &= -2\partial_0 \Phi \\ \Sigma_{0i} &= \partial_0 B_i + \partial_i \Phi \\ \Sigma_{i0} &= -\partial_i (\Phi + B^0) \\ \Sigma_{ij} &= \partial_i B_j - \delta_{ij} \partial_0 \Psi \quad (1.70) \end{aligned}$$

additionally we consider the B_i terms to be of order ϵ and time derivatives of the fields can be ignored (unless we are interested in time varying phenomena such as gravitational waves), giving

$$\begin{aligned} \Sigma_{00} &= 0 \\ \Sigma_{0i} &= \partial_i \Phi \\ \Sigma_{i0} &= -\partial_i (B^0 + \Phi) \\ \Sigma_{ij} &= 0 \quad (1.71) \end{aligned}$$

Using our linear perturbation scheme and assuming $c_4 = 0$ to simplify proceedings, we find the Einstein and vector equations take the form

$$2\nabla^2\Phi + (c_3 - c_1)\nabla \cdot (\mathcal{F}'\nabla B^0) - \lambda = 8\pi G\rho \tag{1.72}$$

$$2c_1\nabla \cdot (\mathcal{F}'\nabla(\Phi + B^0)) + 2c_3\nabla \cdot (\mathcal{F}'\nabla\Phi) = -2\lambda \tag{1.73}$$

and through some manipulations, we find an equation in just Φ,

$$\nabla \cdot ((2 + c_1\mathcal{F}')\nabla\Phi) = 8\pi G\rho \tag{1.74}$$

We see from the construction of $\mathcal{K}$, it takes the form:

$$\mathcal{K} = -c_1\frac{|\nabla\Phi|^2}{M^2} \tag{1.75}$$

If we can find $(2 + c_1\mathcal{F}') \propto |\nabla\Phi|$ (in some limit) and we associate $M \sim a_0$, then we have a modified Poisson equation with some MONDian limit. So we take $c_1 < 0$ (to ensure $\mathcal{K}$ remains positive) and seek the behaviour

$$\lim_{|\nabla\Phi| \leq a_0} (2 + c_1\mathcal{F}') \propto \mathcal{K}^{1/2} \tag{1.76}$$

which integrated out gives

$$\mathcal{F} = a_1\mathcal{K} + a_2\mathcal{K}^{3/2} \tag{1.77}$$

where a_i are constants. Notice that we need the full contribution from both terms, the α_1 term cancels out the constant term in (1.74) and we recover our MONDian limit. We will therefore make the association $\tilde{\mu} = 1 + \frac{c_1}{2}\mathcal{F}'$ (leaving the exact form of $\mathcal{F}$ to be decided later), resulting in the familiar expression

$$\nabla \cdot (\tilde{\mu}(\mathcal{K})\nabla\Phi) = 4\pi G\rho \tag{1.78}$$

Further constraints on these theories will arise from studying the perturbative regime and ensuring the propagation of the different spin components happens sub-luminally and non-tachyonically - these are issues in the underlying EA theory, which in the GEA's can be remedied [17].

1.2.4 Bimetric MOND

Milgrom later suggested that another way to connect with the MONDian paradigm is to consider a quasi-linear theory [47, 21, 48], rather than a manifestly non-linear one (as we saw in the previous two theories). Let's consider a manifestly bimetric theory, composed of two metrics $g_{\mu\nu}$ and $\hat{g}_{\mu\nu}$ (where each metric is an independent degree of freedom), each contributing their own Einstein-Hilbert action terms and matter frames. Additionally we will have some interaction term built from the two metrics

$$S = \frac{1}{16\pi G}\int \left(\beta R\sqrt{-g} + \alpha\hat{R}\sqrt{-\hat{g}} - 2(g\hat{g})^{1/4} f(\kappa)\ell^{-2}\mathcal{M}(\ell^m \Upsilon_i^{(M)})\right) d^4x + S_m(g_{\mu\nu},\psi_i) + \hat{S}_m(\hat{g}_{\mu\nu},\chi_i) \tag{1.79}$$

where $\ell = 1/a_0$, $\kappa = (g/\hat{g})^{1/4}$, $f(\kappa)$ is defined such that $f(1) = 1$. Additionally $\mathcal{M}$ is a free function and $\Upsilon_i^{(m)}$ is an object composed of (m even) contractions of a tensor $C^\alpha_{\beta\gamma}$, which is defined as the difference between two Levi-Civita symbols (and so will be a tensor)

$$C^\alpha_{\beta\gamma} \quad = \quad \Gamma^\alpha_{\beta\gamma} - \hat{\Gamma}^\alpha_{\beta\gamma} \tag{1.80}$$

and Milgrom considered a $\Upsilon_{\mu\nu}$ taking the simple form

$$\Upsilon_{\mu\nu} = C^\gamma_{\lambda\mu}C^\lambda_{\gamma\nu} - C^\gamma_{\mu\nu}C^\lambda_{\gamma\lambda} \tag{1.81}$$

We see that the parameters α, β relate to the renormalisation of G in each sector of the theory (at least at the level of the action). To simplify matters, let's take the argument of $\mathcal{M}$ to be of the form $-\Upsilon/2a_0^2$, where

$$\Upsilon \equiv g^{\mu\nu}\Upsilon_{\mu\nu} \tag{1.82}$$

and have the particular case $\alpha + \beta = 1$ and $\beta = 1$ to ensure $G = G_N$. Varying over $g_{\mu\nu}$ and $\hat{g}_{\mu\nu}$, we get the field equations

$$G_{\mu\nu} + S_{\mu\nu} = 8\pi G \mathcal{T}_{\mu\nu} \tag{1.83}$$

$$\hat{G}_{\mu\nu} + \hat{S}_{\mu\nu} = 8\pi G \hat{\mathcal{T}}_{\mu\nu} \tag{1.84}$$

where $G_{\mu\nu}$ are just the Einstein tensor for each metric, $\mathcal{T}_{\mu\nu}$ are the stress energy tensor defined by appropriate variation wrt to the metric in question. In this theory, we have the presence of matter in the $g_{\mu\nu}$ frame and so called "twin matter" in the $\hat{g}_{\mu\nu}$ frame (see [49] for further details). Each of $S_{\mu\nu}$, $\hat{S}_{\mu\nu}$ is constructed by variation of the interaction term

$$\delta \int 2(g\hat{g})^{1/4} f(\kappa) a_0^2 \mathcal{M}(-\Upsilon/2a_0^2) d^4x = \int \left(\delta g^{\mu\nu} S_{\mu\nu} \sqrt{-g} - \delta \hat{g}^{\mu\nu} \hat{S}_{\mu\nu} \sqrt{-\hat{g}} \right) d^4x \tag{1.85}$$

Using the symmetries of this system, we can also write (1.83) in the form,

$$R_{\mu\nu} + \kappa^{-1} f(\kappa) \mathcal{M}' \left(\Upsilon_{\mu\nu} - \frac{1}{2} g_{\mu\nu} \Upsilon \right) - \left[\kappa^{-1} \mathcal{M}' (\delta^{\lambda}_{(\mu} C_{\lambda)} - C^{\lambda}_{\mu\nu}) \right]_{;\lambda} + \Lambda_m g_{\mu\nu} = 8\pi G \left(\mathcal{T}_{\mu\nu} - \frac{1}{2} g_{\mu\nu} \mathcal{T} \right) \tag{1.86}$$

We investigate the non-relativistic limit here, examining perturbations of the form

$$g_{\mu\nu} = \eta_{\mu\nu} - 2\,\epsilon\,\phi \delta_{\mu\nu} \tag{1.87}$$

$$\hat{g}_{\mu\nu} = \eta_{\mu\nu} - 2\,\epsilon\,\hat{\phi} \delta_{\mu\nu} \tag{1.88}$$

and a relevant quantity is

$$\phi^* = \phi - \hat{\phi} \tag{1.89}$$

which will enter through the interaction tensor and so through the argument of $\mathcal{M}$. We will denote objects constructed from the difference between the $g_{\mu\nu}$ and $\hat{g}_{\mu\nu}$ objects similarly with an asterisk. Following the

same processes as before, we find

$$C^i_{00} = C^0_{0i} = C^0_{i0} = \epsilon \partial_i \phi^* \tag{1.90}$$

$$C^i_{jk} = \epsilon(\partial_i \phi^* \delta_{jk} + \partial_j \phi^* \delta_{ik} + \partial_k \phi^* \delta_{ij}) \tag{1.91}$$

Given that $S_{\mu\nu}$ and $\hat{S}_{\mu\nu}$ are symmetric in the two metrics, when we subtract these two quantities, they vanish and so the Einstein equations take the form

$$G^*_{\mu\nu} = 8\pi G \mathcal{T}^*_{\mu\nu} \tag{1.92}$$

furthermore only the (00) component of $G^*_{\mu\nu}$ is non-zero, which put together gives us

$$\nabla^2 \phi^* = 4\pi G \mathcal{T}^*_{00} \tag{1.93}$$

We can take the usual assumptions detailed in Section 1.1.1, and without the presence of twin-matter, meaning that $\mathcal{T}^*_{00} = \mathcal{T}_{00} = \epsilon\, \rho$, giving the Poisson equation

$$\nabla^2 \phi^* = 4\pi G \rho \tag{1.94}$$

Given that we have two field equations and have only used one of them, let's go back to the $g_{\mu\nu}$ equations, using the form presented in (1.86). Careful calculation gives us

$$R_{\mu\nu} - \left[\mathcal{M}'(\bar{S}^i_{\mu\nu} - \frac{1}{2}\bar{S}\eta_{\mu\nu})\right]_{,k} = 4\pi G \epsilon\, \rho \delta_{\mu\nu} \tag{1.95}$$

and given $\bar{S}^i_{00} = 2\epsilon\, \partial_i \phi^*$, the time-time components yield another Poisson equation of the form

$$\nabla^2 \phi = 4\pi G \rho + \nabla \cdot \left[\mathcal{M}'\left(\frac{|\nabla \phi^*|^2}{a_0^2}\right) \nabla \phi^*\right] \tag{1.96}$$

In light of (1.94), we can recast this simply as

$$\nabla^2\hat{\phi} = \nabla\cdot\left[\mathcal{M}'\left(\frac{|\nabla\phi^*|^2}{a_0^2}\right)\nabla\phi^*\right] \tag{1.97}$$

and so it seems clear to associate $\phi^* \to \Phi_N$ and also $\hat{\phi} \to \phi$, such that using (1.89):

$$\phi = \hat{\phi} + \phi^* \to \Phi = \phi + \Phi^N \tag{1.98}$$

Thus we have a sourced Poisson equation

$$\nabla^2\phi = \nabla\cdot(\mathcal{M}'(|\nabla\Phi_N|/a_0)\nabla\Phi_N) \tag{1.99}$$

We will require $\mathcal{M}'(v) \to v^{-1/2}$ for $v \ll 1$ (for a candidate MOND theory) and $\mathcal{M}'(v) \to C$ for $v \gg 1$, where C is some constant that will play a role in G renormalisation later. Obviously we can also treat (1.96) as being a single field theory, with free function $\tilde{\mu} \to 1 + \mathcal{M}'$ and the Newtonian field as being auxiliary - we will return to these issues in the next Section. One final mention should be given to the choice of argument for $\mathcal{M}$. Here a simple example was picked, motivated by the particular quasi-linear form of MONDian equations it produces in the non-relativistic limit, but obvsiously other examples will exist. It is in fact also possible to reduce to the modified Poisson equation seen in Section 1.2.2 using this setup [47].

1.2.5 Classifying MONDian theories

In the wider modified gravity literature, one can find a large number of relativistic modified gravity theories. Their complexity and differences arise from the requirement that they should explain relativistic phenomena (such as lensing and structure formation) without appealing to dark matter, whilst in the non-relativistic regime have some MONDian and Newtonian limit. In general, the large profusion of relativistic MONDian theories reduce to just three different non-relativistic limits:

- **Type I Theories**, where the non-relativistic dynamics results from the joint action of the usual Newtonian potential Φ_N (derived from the gravity frame metric, via $g_{00} \approx -(1 + 2\Phi_N)$) and a fifth force field, ϕ, responsible for MONDian effects. The total potential acting on non-relativistic particles in the matter frame $\tilde{g}_{00}$, is simply the sum of the two potentials:

$$\Phi = \Phi_N + \phi \tag{1.100}$$

The Newtonian potential satisfies the usual Poisson equation:

$$\nabla^2 \Phi_N = 4\pi G\rho \tag{1.101}$$

whilst the field ϕ is ruled by a non-linear Poisson equation:

$$\nabla \cdot (\mu(z)\nabla\phi) = \kappa G\rho \tag{1.102}$$

for convenience, we will pick the argument of the free function μ as:

$$z = \frac{\kappa}{4\pi}\frac{|\nabla\phi|}{a_0} \tag{1.103}$$

where κ is a dimensionless constant and a_0 is the usual MOND acceleration. In general we require that $\mu \to 1$ when $z \gg 1$ and $\mu \sim z$ for $z \ll 1$. One additional point to be made is often $\Phi = \Xi\Phi_N + \phi$ where $\Xi \simeq 1$, such as in the case of TeVeS. Throughout this work, we will take the case of $\Xi = 1$, but we will make the point that such an additional constant will play a role in G renormalisation.

- **Type II Theories**, have a similar setup to type I, with physical potential $\Phi = \Phi_N + \phi$. The field ϕ is ruled by a driven linear Poisson equation, whose source depends on the Newtonian potential Φ_N. In order to facilitate comparison with Type I theories, we write the equation of motion for ϕ in the form

$$\nabla^2\phi = \frac{\kappa}{4\pi}\nabla \cdot (\nu(w)\nabla\Phi_N) \tag{1.104}$$

where the argument of free function ν is given by

$$w = \left(\frac{\kappa}{4\pi}\right)^2 \frac{|\nabla\Phi_N|}{a_0} \tag{1.105}$$

and we require that $\nu \to 1$ when $w \gg 1$ and $\nu \sim 1/\sqrt{w}$ for $w \ll 1$. However, it is possible in some models that $\nu \to 0$ in the same limit, with qualitatively very different implications. To distinguish these two cases we call the $\nu \to 0$ case type IIA theories and the $\nu \to 1$ case type IIB theories.

- **Type III theories**, are the original non-relativistic MONDian proposal, derived from a non-relativistic action principle (the so-called AQUAL [13]). Crucially, here non-relativistic particles are sensitive to a single field Φ which satisfies a non-linear Poisson equation:

$$\nabla \cdot (\tilde{\mu}(x)\nabla\Phi) = 4\pi G\rho \tag{1.106}$$

where again, $\tilde{\mu}$ is a free function with a suitably chosen argument:

$$x = \frac{|\nabla\Phi|}{a_0} \tag{1.107}$$

so that $\tilde{\mu} \to 1$ when $x \gg 1$ and $\tilde{\mu} \sim x$ for $x \ll 1$.

A scan of the relativistic MONDian theories proposed in the literature suggests that they fall into these categories. Bekenstein's TeVeS [14] as well as Sanders' stratified theory [22] have type I limits. Milgrom's Bimetric theory [48, 49] can be either type I or type II, depending on details. GEA theories [16, 17] and Galileon k-mouflage [50] have a non-relativistic limit of type III. Often authors have attended to different considerations and constraints, so the parameter κ has been taken to be different. However, as we will point out, if in each case the same considerations have been employed, the value of κ would have to be comparable.

The most significant distinction between the non-relativistic limits listed above bundles together type I and IIB theories in opposition to type IIA and type III theories. In the former, non-relativistic particles

are sensitive to two fields, which mimic each other in the Newtonian regime and so the the gravitational constant is effectively renormalised. In the Newtonian regime (non-relativistic limit, with large total Newtonian force), we have $\mu \approx 1$ or $\nu \approx 1$, and so ϕ becomes proportional to Φ_N:

$$\phi \approx \frac{\kappa}{4\pi}\Phi_N \tag{1.108}$$

which has the effect of renormalising the observed gravitational constant

$$G_{Ren} \approx G\Big(1 + \frac{\kappa}{4\pi}\Big) \tag{1.109}$$

and G_{Ren} is the gravitational constant measured, say, by the Cavendish experiment. Nevertheless cosmology is sensitive to the bare G (for example the Friedmann equations) and constraints arising from Big Bang nucleosynthesis and the cosmic microwave background (CMB) [51, 52] fix κ to be of the order of 10^{-2} or smaller and structure formation considerations may further fix it (see [44] and references therein). The conclusion being that in the non-relativistic regime, the field ϕ must be suppressed when $a_N = |\nabla\Phi_N|$ is much larger than a_0.

A remark to make here is that the two equations ruling type II theories may be rewritten as a single equation, ruled by a redefined ν. A real concern here is whether G is renormalized, this is encoded in the limiting behaviour of the free function ruling the non-relativistic equations and in particular whether they're written as a single field or two fields system. It has been argued that in some relativistic formulations of type II theories, the bare G (appearing in cosmology) and the total G (ruling the non-relativistic equation) are the same. We will denote such theories type IIA, and for them $\nu \to 0$ in the Newtonian limit. Otherwise let's call the rest type IIB, with a G renormalisation, and $\nu \to 1$. As we will see, this has crucial phenomenological implications.

Another important difference stems from the fact that we have a curl term (often called a magnetic field) in type I and III theories. This is easiest seen when one attempts to linearize the non-linear Poisson equations present by introducing an auxiliary vector field (e.g. $\mu\nabla\phi$ for type I theories) - such a field has non-zero curl. The same is not true for type II theories, being already linear in ϕ and driven by a

function of the Newtonian field, $\nu\nabla\Phi_N$, (a quantity which has a curl). This turns out to have a significant quantitative effect upon the magnitude of the saddle tidal stresses, as the magnetic field is known to soften the anomalous tidal stresses around the saddle points in type I theories, as explained in section 2.2. We will expand upon this point in our discussion of type II theories in Section 3.5.

With these results in mind, we organise the investigations of this thesis as follows; in Chapter 2 we move onto techniques to characterise a saddle point test. We will consider on both analytical (Section 2.2) and numerical (Section 2.3) investigations into type I theories. Section 2.4 introduces the LISA Pathfinder spacecraft and Section 3.1 shows how methods from experimental gravitational wave searches can be applied to characterise such a test. In Section 3.2 we look at specifics - how different noise models, trajectories approaching the saddle and systematics would affect such an experimental test. In Section 3.3, we explore different free functions μ and show how they could impinge on our results - allowing us to place some preliminary constraints on μ from a null result. Section 3.5 explores how these predictions could vary in type II theories and Chapter 4 attempts to explore the wider parameter space of these theories, varying both constants such as κ, a_0 as well of the free function itself. Section 4.7 concerns itself with constraining μ from data. We conclude with some future thoughts and directions in this field.

Chapter 2

Techniques

In this chapter we will introduce the techniques we will need later to characterise theoretical and experimental ideas in MONDian tests. We will follow the notation and formalism first developed in [41], as well as numerical ideas presented in [5].

2.1 Saddle Points in the Solar System

Obviously to test MONDian theories, we will need a regime where the *total* acceleration on test masses will be small enough to be approaching galactic acceleration scales, which we will take as a_0. Such regions do in fact exist in the solar system, our own cosmic backyard. Before we continue, we will need to understand where these regions are located and solve our MONDian equations of motion in these regimes, before examining how we can test these ideas concretely.

We start by considering a two body gravitational system, with masses m and M, such that $M \gg m$, separated by some distance R along the $\mathbf{e}_z$ axes linking them. We centre the coordinates on mass M and look at the resultant acceleration along $\mathbf{e}_z$,

$$\mathbf{F}_N = -\nabla\Phi_N = \left(-\frac{GM}{r^2} + \frac{Gm}{(R-r)^2}\right)\mathbf{e}_z \tag{2.1}$$

The stationary point of this force is thus located at

$$r_s = \frac{R}{1+\sqrt{m/M}} \simeq R\left(1-\sqrt{\frac{m}{M}}\right) \tag{2.2}$$

The form of the force shows that moving along $\mathbf{e}_z$ towards either mass results in an attractive force, however moving perpendicular to the axes results in a restoring force towards the stationary point - we have a gravitational saddle point (SP). We should be clear to distinguish these points from the well known Lagrange points, which exist *only* in a system of rotating bodies, whereas this saddle always exists (the effect of two attractive forces along the line linking them, in opposite directions). We find that the Newtonian force is linearised about the saddle, taking the form

$$\mathbf{F}_N = -\nabla\Phi_N = A\,(r-r_s)\,\mathbf{e}_z \tag{2.3}$$

where A is the Newtonian tidal stress at the saddle, defined as the derivative of the force

$$S^N_{ij} = \frac{\partial^2\Phi_N}{\partial x_i \partial x_j} \tag{2.4}$$

Here S^N_{ij} is simply a constant, found when we compute the Taylor expansion coefficients in the linear expression (2.3) from the full two body expression (2.1)

$$A = 2\frac{GM}{r_s^3}\left(1+\sqrt{\frac{M}{m}}\right) \tag{2.5}$$

We can make two observations, one being that since $F_N \to 0$, it will indeed pass through the acceleration barrier of a_0, suggesting MONDian effects should be visible around saddles. For the Earth-Sun SP, such a low acceleration region is located at $r \leq 2.2$m around the saddle - a poor prospect for a satellite target. If however we consider the rule of thumb for MONDian systems, i.e.

$$F \leq a_0 \quad \Rightarrow \quad F \to \sqrt{F_N a_0} \tag{2.6}$$

then the (previously linear) force near the SP is now of the form

$$F \to \sqrt{Aa_0|r - r_s|} \tag{2.7}$$

(taking the form of a so called Nortons Dome [53]) and the tidal stresses would appear to diverge as we approach the saddle! Clearly we need to investigate the calculation using a fully relativistic theory, but this simple calculation provides at least a proof-of-concept for a tidal stress based MOND saddle test.

A second relevant point to make concerns the other contributions to the Newtonian tidal stresses at the saddle, surely the other objects in the solar system, as well as the galaxy will play a role here? At leading order, only the Earth and Sun play a role in this calculation, as (2.5) shows. The effect of the moon, providing a truly 3-body system, can be computed using a numerical treatment of the saddle system, as we will shortly show in Section 2.3. One conclusion of that work is that the position of the Earth-Sun saddle is shifted with respect to the phase of the Moon (and hence at different times of the month the saddle is shifted to a known, but differing location), on the order of a few tens of km. Taking the effect of most of the mass of the solar system (from Saturn and Jupiter) into account shifts the saddle a few more km. Taking the contribution from the galaxy into account shifts it a tiny bit more. Given this, we can consider the total Newtonian tidal stress at the saddle taking the form

$$A_{SP} \simeq A_{ES} + A_M + A_{SS} + A_G + \dots \tag{2.8}$$

where ES denotes Earth-Sun, M denotes Moon, SS denotes Solar System and G denotes the galactic contribution. The ordering here is such that each contribution is smaller in magnitude than the one previous. Given that each contribution to the saddle is an attractive force component, there will always be a saddle (and at a location close to the 2-body case) and hence an observable for a tidal stress experiment.

2.2 Analytical Solutions - U Formalism

We move to a system of spherical polar coordinates, centered on the saddle. Clearly here $\nabla^2\Phi_N = 0$, so we can consider a multipole expansion for $\nabla\Phi_N$, truncated at linear order:

$$-\nabla\Phi_N = \mathbf{F}_N = A\,r\,\mathbf{N} \tag{2.9}$$

$$\mathbf{N} = N_r\mathbf{e}_r + N_\psi\mathbf{e}_\psi \tag{2.10}$$

$$N_r = \frac{1}{4}(1+3\cos 2\psi) \tag{2.11}$$

$$N_\psi = -\frac{3}{4}\sin 2\psi \tag{2.12}$$

Notice due to the symmetries of this two body system, the polar angle φ does not appear (but would be important if a three body system, such as including the moon, was considered).

Recall the non-linear modified Poisson equation (1.102) for the MONDian field ϕ, let's move to a linear system of variables by defining

$$\mathbf{U} = -\frac{\kappa}{4\pi}\frac{\nabla\phi}{a_0}\mu \tag{2.13}$$

meaning $U = \mu z$. Since our free functions here are $\mu = \mu(z)$, we can similarly write them solely as $\mu = \mu(U)$. This change of variable allows us to write dimensionless vacuum equations

$$\nabla\cdot\mathbf{U} = -\frac{\kappa^2}{4\pi}\frac{G\rho}{a_0} = 0 \tag{2.14}$$

$$\nabla\wedge\left(\frac{\mathbf{U}}{\mu}\right) = -\frac{\kappa}{4\pi a_0}\nabla\wedge\nabla\phi = 0 \tag{2.15}$$

$$\Rightarrow \frac{1}{\mu}\nabla\wedge\mathbf{U} + \nabla\left(\frac{1}{\mu}\right)\wedge\mathbf{U} = 0 \tag{2.16}$$

Which we can simplify and tidy up into the two expressions

$$\nabla\cdot\mathbf{U} = 0 \tag{2.17}$$

$$4\,m\,U^2\nabla\wedge\mathbf{U} + \mathbf{U}\wedge\nabla U^2 = 0 \tag{2.18}$$

where $4m$ has the form

$$4m = \frac{d \ln U^2}{d \ln \mu} \tag{2.19}$$

and we have dropped sources (as would be the case at the SP). We can reconnect with the MONDian force from the expression

$$-\nabla\phi = \delta\mathbf{F} = \frac{4\pi a_0}{\kappa}\frac{\mathbf{U}}{\mu(U)} \tag{2.20}$$

Next comes the choice of free function μ, we will start with the case considered previously in analytical [41] and numerical work [5], namely

$$z = \frac{\mu}{\sqrt{1-\mu^4}} \Longleftrightarrow \mu = \sqrt{\frac{\sqrt{1+z^4}-1}{2z^2}} \tag{2.21}$$

which we will hereafter refer to as $\mu_{fiducial}$. This makes the analytical work considerably easier, since here $4m = 4(1+U^2)$, meaning Equation (2.18) becomes solely one in U and by solving for these dynamics, we can find the behaviour in F_ϕ. In general, though one can not write $4m(U)$ explicitly, but as we will show later it is still possible to find asymptotic solutions for these systems, whatever the choice of μ. Here the MONDian force explicitly is given by

$$\delta\mathbf{F} = \frac{4\pi a_0}{\kappa}\mathbf{U}\left(1+\frac{1}{U^2}\right)^{1/4} \tag{2.22}$$

It is clear from $U = \mu z$ and the behaviour of μ that each limit satisfies

$$z \gg 1 \quad \Rightarrow \quad U \gg 1 \quad \text{(Quasi-Newtonian)}$$

$$z \ll 1 \quad \Rightarrow \quad U \ll 1 \quad \text{(Deep-Mondian)}$$

Between these two regions, we have a boundary located at $|\mathbf{U}|^2 \simeq 1$. To locate these regions, we assume

$$\mu \to 1 \Rightarrow \nabla\phi \simeq \frac{\kappa}{4\pi}\nabla\Phi_N \tag{2.23}$$

which will clearly be true at zeroth order and as we will show later, leading order corrections are negligible at the boundary. Using expression (2.12), this becomes

$$|\mathbf{U}|^2 = \left(\frac{\kappa}{4\pi}\frac{|\nabla\phi|}{a_0}\right)^2 \simeq \left(\left(\frac{\kappa}{4\pi}\right)^2\frac{|\nabla\Phi_N|}{a_0}\right)^2 = \left(\left(\frac{\kappa}{4\pi}\right)^2\frac{Ar|\mathbf{N}|}{a_0}\right)^2 \simeq 1 \tag{2.24}$$

this takes the form (after rearrangement)

$$r^2\left(\cos^2\psi + \frac{1}{4}\sin^2\psi\right)^2 = \left(\frac{16\pi^2}{\kappa^2}\frac{a_0}{A}\right)^2 = r_0^2 \tag{2.25}$$

which is just the equation for an ellipsoid with a size we will denote r_0. These results show that in general the functional forms of the inner and outer ellipsoid (hereafter bubble) solutions should be quite different.

2.2.1 Quasi-Newtonian (QN) Regime

Given this system of vector equations, we need to specify boundary conditions. For $r/r_0 \gg 1$, we expect $\mu \to 1$ and so the MONDian potential to mimic the Newtonian $\phi \approx \frac{\kappa}{4\pi}\Phi_N$. Let's pick our ansatz to be of the form

$$\mathbf{U} = \mathbf{U}_0 + \mathbf{U}_2 \tag{2.26}$$

$$\mathbf{U}_0 = \frac{r}{r_0}\mathbf{N}(\psi) \tag{2.27}$$

and $\mathbf{U}_2$ will be some subdominant contribution as we move far from the saddle, but a very relevant one closer to the bubble. Additionally although $\mathbf{U}_0$ is curl free, the form of Equation (2.18) suggests $\mathbf{U}_2$ will in general have a curl, automatically satisfying

$$\nabla\cdot\mathbf{U}_2 = 0 \tag{2.28}$$

and from rearrangement of (2.18) we see that at leading order, $\mathbf{U}_2$ is sourced by $\mathbf{U}_0$

$$\nabla \wedge \mathbf{U}_2 = -\frac{\mathbf{U}_0 \wedge \nabla |\mathbf{U}_0|^2}{4m\,|\mathbf{U}_0|^2} \tag{2.29}$$

Using our choice for $\mu_{fiducial}$ and $U = \mu z$, we can write this solely in terms of U as

$$\mu_{fiducial} = \frac{U^{1/2}}{(1+U^2)^{1/4}} \tag{2.30}$$

and hence

$$4m \equiv \frac{d\ln U^2}{d\ln \mu} = 4(1+U^2) \tag{2.31}$$

and so in this $U \gg 1$ regime, $4m \to U^2$. Using the notation

$$\mathbf{U}_2 = U_r \mathbf{e}_r + U_\psi \mathbf{e}_\psi \tag{2.32}$$

Equations (2.28) and (2.29) take the form

$$\frac{1}{r^2}\frac{\partial}{\partial r}(r^2 U_r) + \frac{1}{r\sin\psi}\frac{\partial}{\partial \psi}(\sin\psi\, U_\psi) = 0 \tag{2.33}$$

$$\frac{1}{r}\left[\frac{\partial}{\partial r}(rU_\psi) - \frac{\partial U_r}{\partial \psi}\right] = \frac{s(\psi)}{r^2} \tag{2.34}$$

$$s(\psi) \equiv -\frac{12\sin 2\psi}{(5+3\cos 2\psi)^2} \tag{2.35}$$

The form of (2.33) and (2.34) strongly suggest that $U_2 \propto 1/r$ and so we can write

$$\mathbf{U}_2 = \frac{r_0}{r}\mathbf{B}(\psi) = \frac{r_0}{r}\left(F(\psi)\mathbf{e}_r + G(\psi)\mathbf{e}_\psi\right) \tag{2.36}$$

In this case, (2.34) collapses and we simply integrate to find

$$F = \frac{2}{5+3\cos 2\psi} + A \tag{2.37}$$

where A is some constant and we can insert into (2.33) to find

$$G\sin\psi = \frac{\tan^{-1}(\sqrt{3}-2\tan\frac{\psi}{2})+\tan^{-1}(\sqrt{3}+2\tan\frac{\psi}{2})}{\sqrt{3}} + A\cos\psi + B \tag{2.38}$$

with B another constant. After imposing the conditions of homogeneity and continuity and that at the boundaries of the bubbles, $G(\psi=0)=G(\psi=\pi)=0$ (akin to the Newtonian), we find:

$$A = B = -\frac{\pi}{3\sqrt{3}}$$

Expanding (2.22) in this limit gives us

$$\delta\mathbf{F} = -\nabla\phi = \frac{4\pi a_0}{\kappa}\left(\mathbf{U}_0 + \frac{\mathbf{U}_0}{4U_0^2} + \mathbf{U}_2 + \dots\right) \tag{2.39}$$

we see that the first term (which we denote $\delta\mathbf{F}_0$) is simply a rescaled Newtonian contribution, here serving the role of renormalising the gravitational constant

$$G_{eff} = G_N\left(1+\frac{\kappa}{4\pi}\right) \tag{2.40}$$

such a contribution is relevant as it will obviously be constrained by limits on G_N variation (e.g. cosmological constraints [52]), however it is of little use as a MONDian observable. If we consider the second and third terms however (denoted $\delta\mathbf{F}_1$ and $\delta\mathbf{F}_2$ respectively), which result from a rescaled Newtonian vector and curl field, these are the leading order MONDian observables at order r^{-1}

$$\delta\mathbf{F}_1 = \frac{8\pi a_0}{\kappa}\frac{r_0}{r}\frac{\mathbf{N}(\psi)}{5+3\cos 2\psi} \tag{2.41}$$

$$\delta\mathbf{F}_2 = \frac{4\pi a_0}{\kappa}\frac{r_0}{r}\mathbf{B}(\psi) \tag{2.42}$$

We can recast this in terms of the **N** and **B** fields to see explicitly the effects here

$$\delta\mathbf{F} = -\nabla\phi = \frac{4\pi a_0}{\kappa}\frac{\mathbf{U}}{\mu} \simeq \frac{4\pi a_0}{\kappa}\left(\underbrace{\frac{r}{r_0}\mathbf{N}}_{G_N\ renorm} + \underbrace{\frac{r_0}{r}\left(\frac{\mathbf{N}}{4N^2}+\mathbf{B}\right)}_{main\ observable} + \dots\right) \tag{2.43}$$

Additionally, we can justify our prior assumption of $\mathbf{U} = \mathbf{U}_0$ when estimating the bubble boundary. Given $|\mathbf{B}| \sim |\mathbf{N}| \sim \mathcal{O}(1)$, our naive first order correction would be

$$\frac{|\mathbf{U}_2|}{|\mathbf{U}_0|} \simeq \left(\frac{r_0}{r}\right)^2$$

however this is only strictly true in the $r/r_0 \gg 1$ limit, so we must think more carefully about our assumption at $r \simeq r_0$. We assumed $\mu \to 1, \nabla\phi \to \frac{\kappa}{4\pi}\nabla\Phi_N$, however in reality we have $\mu = 1 - \delta\mu$ in this limit and so the fractional correction is of order

$$\frac{F_\phi}{F_N} \simeq \frac{\kappa}{4\pi}\left(1 + \frac{1}{4z^2} + \dots\right) \tag{2.44}$$

Expanding to first order gives

$$\mathbf{F}_\phi = \frac{\kappa}{4\pi}\mathbf{F}_N + \mathbf{F}_\phi^{(1)} \tag{2.45}$$

and so

$$\frac{\delta F}{F_N} \sim \frac{\kappa}{4\pi}\left(\frac{r_0}{r}\right)^2 \tag{2.46}$$

meaning that even close to the boundary, taking $\mathbf{U} \sim \mathbf{U}_0$ is a good approximation as long as $\kappa \ll 4\pi$ is true. In circumstances when this is not the case, our approximation will break down. The bubble however will also be much smaller (remember $r_0 \sim 1/\kappa^2$) and so after a few r_0, we will clearly be in the QN regime anyway. For the solar system at least, it is doubtful that assuming such will result in an order of magnitude correction in r_0.

2.2.2 Deep-MONDian (DM) Regime

Our previous intuition with boundary conditions does not help us here, since we expect a very different signal compared to the linear Newtonian falling to zero at the saddle. We can write Equations (2.17) and (2.18) here as

$$\frac{1}{r^2}\frac{\partial}{\partial r}\left(r^2\, U_r\right) + \frac{1}{r\sin\psi}\frac{\partial}{\partial\psi}(\sin\psi\, U_\psi) = 0 \tag{2.47}$$

$$\left[\frac{4m}{r}\left(\frac{\partial(rU_r)}{\partial r} - \frac{\partial U_\psi}{\partial\psi}\right) + \left(\frac{U_r}{r}\frac{\partial}{\partial\psi} - U_\psi\frac{\partial}{\partial r}\right)\right] U^2 = 0 \tag{2.48}$$

which given the scaling symmetries of these equations

$$\begin{aligned} \mathbf{U} &\to \mathbf{U} \\ r &\to \lambda\, r \end{aligned} \tag{2.49}$$

suggests an ansatz for the potential as

$$\mathbf{U} = C\left(\frac{r}{r_0}\right)^{\alpha-2}(F(\psi)\mathbf{e}_r + G(\psi)\mathbf{e}_\psi) \tag{2.50}$$

where $\alpha-2$ is used for notational convenience later and C is a constant required for matching between the two regimes. We will look for solutions which keep U small but have tidal stresses become increasingly divergent as $r/r_0 \ll 1$ and since $U \ll 1$ in this regime, $4m \to 4$. Using this ansatz gives a pair of coupled equations for F and G

$$G' + G\,\cot(\psi) + \alpha F = 0 \tag{2.51}$$

$$F\frac{d(F^2+G^2)}{d\psi} + 2[\alpha G - 2F'](F^2+G^2) = 0 \tag{2.52}$$

Given

$$\delta\mathbf{F} = -\nabla\phi \approx \frac{4\pi a_0}{\kappa}\frac{\mathbf{U}}{U^{1/2}} \tag{2.53}$$

which we rewrite in a separable form as

$$\delta\mathbf{F} \approx \frac{4\pi a_0}{\kappa} C^{1/2} \left(\frac{r}{r_0}\right)^{\frac{\alpha-2}{2}} \frac{\mathbf{D}(\psi)}{D^{1/2}} \tag{2.54}$$

where $\mathbf{D}$ is the angular profile in the DM regime. Also requiring $U \ll 1$ means $\alpha > 2$ in all cases (a point realised but not explicitly spelt out in [41]), whilst $\alpha < 4$ is needed for a divergent tidal stress solution. These bounds are helpful for picking out the particular α we require from the sequence which satisfy these equations and permits regular solutions. We write the ansatz profile functions as Fourier series

$$\begin{aligned} F &= f_0 + f_2 \cos 2\psi + \dots \\ G &= g_2 \sin 2\psi + \dots \end{aligned} \tag{2.55}$$

and use Equation (2.51) to find algebraic relations between the Fourier coefficients f_i and g_i. Equation (2.52) then yields quadratic and higher order equations in these coefficients (depending at which order we truncate our series), which are soluble for certain roots in α. Since we have no restriction on our scaling C, without loss of generality we set $F(\psi = 0) = F(\psi = \pi) = 1$ and again enforcing the condition $G(\psi = 0) = G(\psi = \pi) = 0$ gives us simple conditions to normalise each series. In doing so we find $\alpha \approx 3.528$, with profile functions

$$\begin{aligned} F &\approx 0.2442 + 0.7246 \cos 2\psi + 0.0472 \cos 4\psi + \dots \\ G &\approx -0.8334 \sin 2\psi - 0.0368 \sin 4\psi + \dots \end{aligned} \tag{2.56}$$

2.3 Computational Techniques

Whilst the applicability of these analytical solutions is wide, they remain only strictly valid in the asymptotic regimes of large and small U. In the intermediary regime, such as around the bubble boundary, very model dependent effects could be produced - suggesting we need a full numerical treatment of the

system. We rewrite (2.17 - 2.18) in the form

$$\nabla \cdot (\mu \mathbf{g}) = 0 \tag{2.57}$$

$$\nabla \wedge \mathbf{g} = 0 \tag{2.58}$$

where $\mathbf{g} = -\nabla\phi$. We aim to simultaneously solve these on a non-uniform lattice around the saddle, as Figure 2.1 illustrates. We make our numerical boxes large enough to allow us to use rescaled Newtonian boundary conditions at the edges, i.e. $\mu \to 1$, $\mathbf{F}_\phi \to \frac{\kappa}{4\pi}\mathbf{F}_N$.

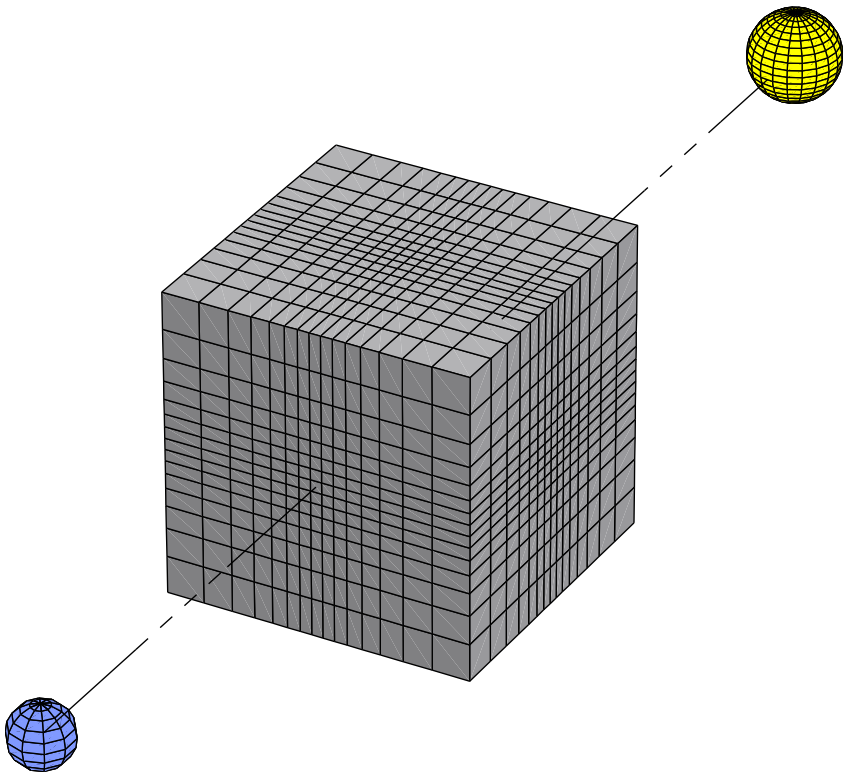

Figure 2.1: An illustration of the lattice used when calculating solutions for the Earth-Sun saddle region - surrounding the saddle, without enclosing any of the nearby gravitating bodies. We also show the non-uniform nature of coordinates, employed to increase the simulations resolution near the SP. (Not to scale). Reproduced from [5].

Additionally, since we are only concerned with the near saddle dynamics, we neglect sources inside the grid, our initial conditions at each site are simply the Newtonian solution, rescaled appropriately by $\frac{\kappa}{4\pi}$. A relaxation algorithm then cycles over each lattice site $\mathbf{x}$ and changes the values of $\mathbf{g}$ at $\mathbf{x}$ and the

neighboring sites so that the discrete divergence equation (2.57) is solved *locally*, that is:

$$D_{\mathbf{x}} = \sum_j \frac{\mu_{\mathbf{x}} g^j_{\mathbf{x}} - \mu_{\mathbf{x}-\mathbf{j}} g^j_{\mathbf{x}-\mathbf{j}}}{r^j_{\mathbf{x}} - r^j_{\mathbf{x}-\mathbf{j}}} = 0 \tag{2.59}$$

We then move to the next site and change the field values so that the condition is valid there, using the newly updated values as we proceed. However, when enforcing the above condition at these subsequent sites, the value of $D_{\mathbf{x}}$ at the first site will be slightly changed. We therefore require many cycles over the whole lattice before we achieve convergence towards a solution which satisfies the systems' equations globally. This technique requires that we define all the components of $\mathbf{g}$ and μ at the each location, that is:

$$\mu_{\mathbf{x}} = \mu\left(\kappa \mathbf{g}_{\mathbf{x}}/a_0\right)$$

The presence of this non-linear free function μ is also a notable complication, so our system is set up to solve it for some arbitrary function (a feature we will make good use of later).

We see that the algorithm solves the divergence equation to first order in $\delta\mathbf{g}$ and $\delta\mu$ (where δ denotes the change from one step to the next) and then as the system converges to the solution, the terms of order δ^2 become negligible very rapidly. We contrast this method to that of Ref. [54], which solved the curl equation for $\mathbf{U}$ locally, while keeping the μ values fixed at their old values. Once the μ values are updated using the new $\mathbf{U}$, the curl equation would no longer be matched, and this slows the convergence of solutions. Under such a scheme the calculation of u^i/μ at any position in a 3D calculation would require knowledge of 33 values of u^j, whereas to determine $\mu_{\mathbf{x}} g^j_{\mathbf{x}}$ here, we require merely the knowledge of the three components of $\mathbf{g}_{\mathbf{x}}$.

Crucial in the above method is that as we update the field configuration, the curl of $\mathbf{g}$ remains zero, we define our discrete curl,

$$(\nabla \times \mathbf{g})^k_{\mathbf{x}} = \frac{g^j_{\mathbf{x}+\mathbf{i}} - g^j_{\mathbf{x}}}{r^i_{\mathbf{x}+\mathbf{i}} - r^i_{\mathbf{x}}} - \frac{g^i_{\mathbf{x}+\mathbf{j}} - g^i_{\mathbf{x}}}{r^j_{\mathbf{x}+\mathbf{j}} - r^j_{\mathbf{x}}} \tag{2.60}$$

where $\mathbf{r}_{\mathbf{x}}$ is the position vector site $\mathbf{x}$. The aim being to preserve this condition and so at each step of

the relaxation, it is necessary to change the fields according to:

$$\begin{aligned} \delta g^j_{\mathbf{x}} &= \frac{+C_{\mathbf{x}}}{r^j_{\mathbf{x}+\mathbf{j}} - r^j_{\mathbf{x}}} \\ \delta g^j_{\mathbf{x}-\mathbf{j}} &= \frac{-C_{\mathbf{x}}}{r^j_{\mathbf{x}} - r^j_{\mathbf{x}-\mathbf{j}}} \end{aligned} \tag{2.61}$$

where the value of $C_{\mathbf{x}}$ is chosen to yield (2.59) to first order. Expanding $\delta D_{\mathbf{x}}$ to first order in $\delta\mathbf{g}$ and $\delta\mu$, we find

$$\delta D_{\mathbf{x}} \approx \sum_j \frac{\mu_{\mathbf{x}}\delta g^j_{\mathbf{x}} + g^j_{\mathbf{x}}\delta\mu_{\mathbf{x}} - \mu_{\mathbf{x}-\mathbf{j}}\delta g^j_{\mathbf{x}-\mathbf{j}} - g^j_{\mathbf{x}-\mathbf{j}}\delta\mu_{\mathbf{x}-\mathbf{j}}}{r^j_{\mathbf{x}} - r^j_{\mathbf{x}-\mathbf{j}}} \tag{2.62}$$

and similarly writing $\delta\mu$ in terms of δg^2 and substituting the above values for $\delta\mathbf{g}$ then yields,

$$\frac{\delta D_{\mathbf{x}}}{C_{\mathbf{x}}} \approx \sum_j \left[\frac{\mu_{\mathbf{x}}}{\Delta^j_- \Delta^j_+} + 2\sum_i \frac{g^i_{\mathbf{x}}}{\Delta^i_+}\frac{g^j_{\mathbf{x}}}{\Delta^j_-}\frac{\mathrm{d}\mu_{\mathbf{x}}}{\mathrm{d}g^2_{\mathbf{x}}} + \frac{\mu_{\mathbf{x}-\mathbf{j}}}{(\Delta^j_-)^2} + 2\left(\frac{g^j_{\mathbf{x}-\mathbf{j}}}{\Delta^j_-}\right)^2 \frac{\mathrm{d}\mu_{\mathbf{x}-\mathbf{j}}}{\mathrm{d}g^2_{\mathbf{x}-\mathbf{j}}} \right] \tag{2.63}$$

for brevity, we use the notation

$$\begin{aligned} \Delta^j_+ &= r^j_{\mathbf{x}+\mathbf{j}} - r^j_{\mathbf{x}} \\ \Delta^j_- &= r^j_{\mathbf{x}} - r^j_{\mathbf{x}-\mathbf{j}} \end{aligned} \tag{2.64}$$

Finally, since we want $D_{\mathbf{x}}$ to be zero after each change, we set:

$$\delta D_{\mathbf{x}} = -D_{\mathbf{x}} \tag{2.65}$$

giving us the $C_{\mathbf{x}}$ required to obtain $D_{\mathbf{x}} = 0$ (If μ had not changed during this step, the above procedure would have set $D_{\mathbf{x}}$ to be exactly zero, i.e. to all orders in $\delta\mathbf{g}$).

In practice, cycling over the lattice and solving the discrete equation locally does not lead to rapid enough convergence to the solution. As D_x is (approximately) zeroed at later sites, D_x at earlier sites is moved slightly away from its desired value and a large number of iterations of this procedure are required

before each $\mathbf{g_x}$ has converged to a good approximation. We therefore preempt the changes to the field that will occur at other points in the cycle using the fact that these very changes are (largely) responsible for $D_{\mathbf{x}}$ being non-zero. This is achieved by a method known as successive over-relaxation (SOR, e.g. [55]) in which $\delta g^j \to \lambda \delta g^j$, where λ is the over-relaxation parameter and is larger than unity. We begin with $\lambda = 1$ and increase it once the system has begun to settle down, since high values of λ can initially result in the RMS value of D_x increasing, contrary to our goal. This algorithm was first presented in [5] and was coded using the LATfield library [56].

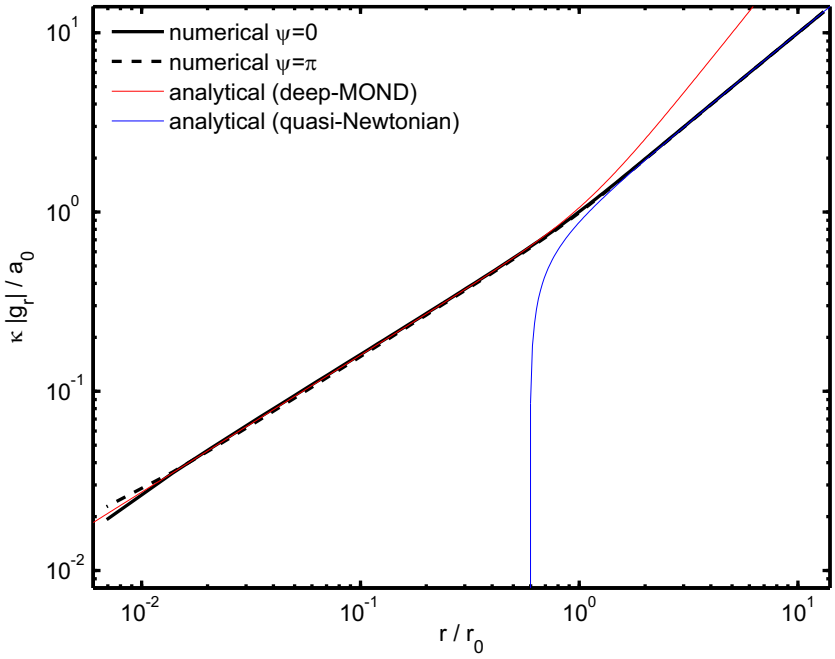

Figure 2.2: A comparison between the numerical and analytical results for components of $g = -\nabla\phi$ for the Earth-Sun SP. Results are plotted as function of r for $\psi = 0$ and π (similar results are found for other values of ψ, see Figure 2 [5]). As we see, the analytical symmetry between the g-component values (up to a sign) is also seen in the numerical case (except at low r, where the discretisation starts to become noticeable, giving us an estimate of the errors). We used $C = 0.839$ for the DM scaling of the analytical results here. Reproduced from data presented in [5].

2.3.1 Numerical Results

Using this code, we can compute numerical solutions for the MONDian system, initially for the Earth-Sun SP case, as so to compare with the two-body analytical results. Typically with the use of the SOR techniques, we computed results on a 273^3 lattice for a few days (using an MPI code running on 64

cores). These long run times were need for the solutions to achieve a decent level of convergence. If we re-ran the code, using a 2D setup, similar convergence could be achieved but for a much smaller runtime (easily within say eight hours, the standard allowed runtime on the COSMOS supercomputer used). We see a good agreement in the respective domains between the analytical and numerical results as well as providing a good interpolation between them, as seen in Figure 2.2. Additionally we can use this data to "measure" the DM scaling, which other than being an $\mathcal{O}(1)$ contribution, remains poorly constrained from analytics. C is determined by converting g into our variable U, using (2.22) and then computing the ratio of the numerical results to the analytical solutions with C set to unity for all lattice sites within bounds of $r/r_0 = 0.05 \to 0.5$, such that we are "comfortably" in the DM regime. We find a ratio of $C = 0.839 \pm 0.016$, the central value from which we have used for all comparisons against the DM solution.

The observables here are however the tidal stresses rather than force. In defining the anomalous tidal stress, we need to take into account the rescaled Newtonian contribution from the MONDian field ϕ, giving:

$$S_{ij} = -\frac{\partial^2 \phi}{\partial x_i \partial x_j} + \frac{\kappa}{4\pi}\frac{\partial^2 \Phi^N}{\partial x_i \partial x_j} \tag{2.66}$$

The results we find from this tell us what the observable effect on measured tidal stresses in the presence of a fifth-force field ϕ. We subtract off the rescaled Φ_N contribution, which although plays the role of renormalising G_N does not provide a real experimental observable. A distinctive signal from the $\mathbf{F}_\phi \to S^\phi_{ij}$ should however provide a very good observable. Using our numerical results, we plot the predicted tidal stresses along a given trajectory past the SP in Figure 2.3, along with the introduction of the Moon in the dynamics. As we see, the effect is only a perturbing one, the main dynamics still coming from the Earth and Sun.

2.4 LISA Pathfinder

LISA Pathfinder (LPF) presents the next generation of low frequency gravitational wave interferometry instrumentation [57, 6, 58]. It is a technology validation mission for the Laser Interferometry Space Array

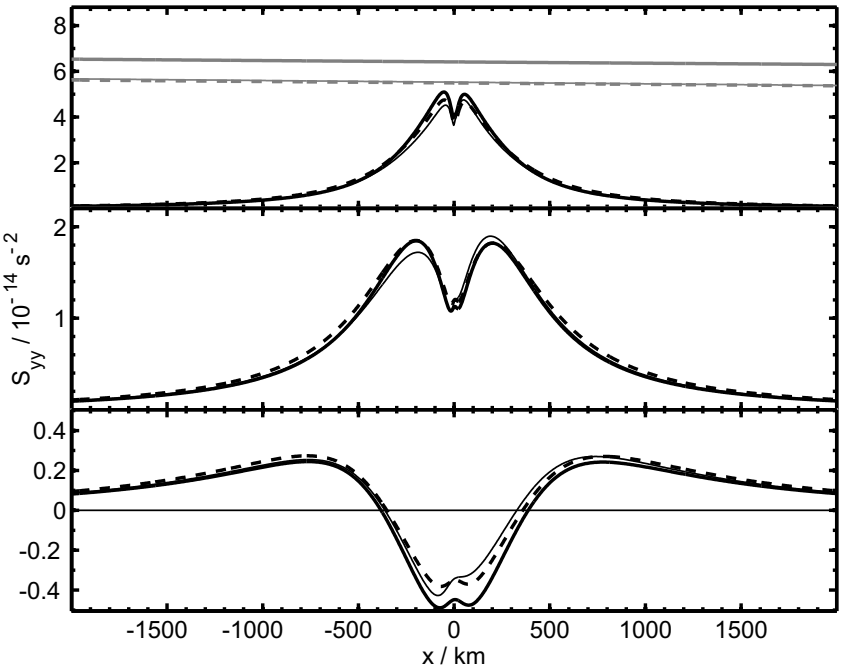

Figure 2.3: The transverse MOND stress signal S_{yy} along $b = 25$, 100 and 400 km (top to bottom), for the Sun-Earth SP taking into account the effect of the Moon. The different lines represent lunar phases: new Moon (thick, black, solid), full Moon (thick, black, dashed) and the Moon appearing 18° away from the Sun, towards positive y (thin, black, solid). In the $b = 25$ km case, the Newtonian stresses (grey) rescaled by $\kappa/4\pi$ are shown for comparison. Reproduced from data presented in [5].

(LISA) experiment [59]. LISA's goal is to accurately detect gravitational waves (GW) from astrophysical sources using a space based laser interferometry. Passing GWs induce oscillations along the laser beams between the spacecraft (arranged in a triangle with an inter-spacecraft distance of 5×10^6 km) and by monitoring these, we should be able to precisely measure GWs from, say, massive black hole mergers and other extreme gravitational events. The idea behind LPF is to emulate one of the arms of LISA by putting two test masses in gravitational free-fall, control and then measure their motion with unrivalled accuracy. In the process it will use and test a drag-free control system, a laser metrology system, inertial sensors and an ultra-precise micro-propulsion system. Additionally the sensitivity of LPF is aimed at being more than two orders of magnitude better than any current experiment. The nominal requirements of the mission are to:

- Test feasibility of laser interferometry with resolution approaching 10^{-12} m $Hz^{-1/2}$ in the low frequency band of 1-30 mHz.
- Demonstrate drag-free and attitude control in a spacecraft with two free proof masses.
- Test the feasibility and endurance of the instruments in space.

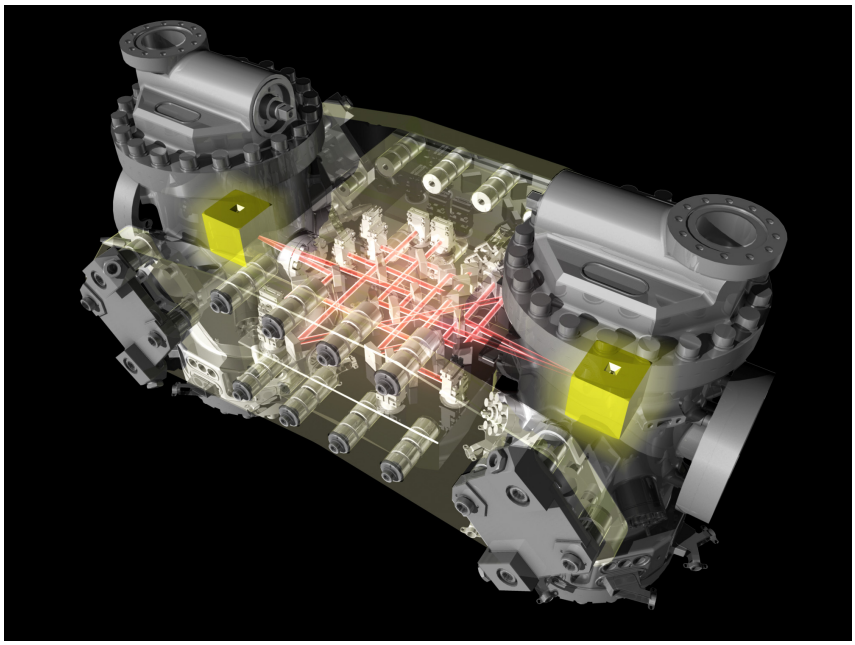

Figure 2.4: The LTP demonstrating the laser interferometry between the two test masses. Reproduced from http://sci.esa.int/lisapf.

The onboard instruments in the LISA technology package (LTP) are sensitive to the test mass motions relative to the spacecraft of up to 10^{-9}m and the relative test mass motion of up to 10^{-12} m. The LTP will carry two identical proof masses, in the form of 46 mm cubes, made of gold-platinum each suspended in a vacuum can, as seen in Figure 2.4. The idea being to scale down an arm of LISA, from millions of kilometres to just centimetres. The onboard disturbance reduction system includes a set of micro-rockets that aim to control the spacecraft's position to within 10^{-9}m. The drag-free control system consists of an inertial sensor, a proportional micro-propulsion system and a control system. The inertial sensors will monitor the micro motions of the two test masses and if they move away from their null positions, a signal is sent to the control system which is used to command the micro-propulsion thrusters, which in turn enable the spacecraft to remain centred on the test mass.

The LPF launch is planned for 2015, where it will head to the L1 Lagrange point with the operational phase lasting six months, with the possibility of extension up to one year. After this, the remaining fuel could be used to make manoeuvres towards an Earth-Sun SP fly-by. It may also be possible to include a second approach towards the SP and perhaps approaching the Moon-Earth-Sun saddle is an additional possibility.

2.5 Gravitational Wave Techniques

Predictions are cast in the form of tidal stresses, because this is what will be measured by the instrument. LPF measures the relative acceleration between the masses (or its Fourier transform (FT) in time) and up to a factor dependent on the proof mass separation, the measurement is therefore one of tidal stress along the direction linking the two masses (with further masses, other tidal stress components would become accessible). In line with this statement, noise evaluations and forecasts are expressed in terms of tidal stress or relative accelerations; one should use the inter-mass separation (approximately 0.38m) to convert between the two.

The data analysis task in hand is therefore to detect a waveform of this type with the instrument aboard LPF. As a first hack at the problem, we evaluate the performance of noise matched filters. Matched filtering is a well-known data analysis technique used for efficiently digging a signal with a known shape out of noisy data [60, 61]. The technique is extensively used in the search for gravitational waves. The idea is to correlate a time series $x(t)$ with an optimized template designed to provide maximal signal to noise ratio (SNR), given the signal shape $h(t)$ and the noise properties of the instrument. The signal $h(t)$ here, as measured by LPF, will be the relative acceleration between the two test masses. This can then be converted into a tidal stress signal (as a function of $\mathbf{x} = \mathbf{v}t$), although we will leave the exact details and form of the stress signal we want to characterise to Section 3.1. Generally we have $x(t) = h(t - t_a) + n(t)$, where t_a is the signal "arrival time" and $n(t)$ is a noise realisation. We want to

correlate $x(t)$ and an optimal template $q(t)$, yet to be defined, according to:

$$c(\tau) = \int_{-\infty}^{\infty} x(t)q(t+\tau)dt \tag{2.67}$$

where τ is a lag parameter, giving us essential leverage if we don't know t_a a priori. The average of c over noise realizations is the expected signal, S, and its variance is the square of the noise in the correlator, N^2; the forecast signal to noise ratio is therefore $\rho = S/N$. A straightforward calculation (under general assumptions, namely the Gaussianity of the noise—more on this later) shows that ρ is maximized by choosing a template with Fourier transform:

$$\tilde{q}(f) = \int_{-\infty}^{\infty} q(t)e^{2\pi i f t}dt = \frac{\tilde{h}(f)e^{2\pi i f(\tau - t_a)}}{S_h(f)} \tag{2.68}$$

and setting the lag τ to the arrival time, $\tau = t_a$. Here $S_h(f)$ is the power spectral density (PSD) of the noise, conventionally defined from

$$\langle \tilde{n}(f)\tilde{n}^{\star}(f')\rangle = \frac{1}{2}S_h(f)\delta(f - f') \tag{2.69}$$

(the factor of $1/2$ hails from the tradition of taking one-sided FTs of the noise auto-correlation—-i.e. with $f > 0$ only). The maximal SNR, realized by the optimal template, is then:

$$\rho = \rho_{\text{opt}} = 2\left[\int_0^{\infty} df \frac{\left|\tilde{h}(f)\right|^2}{S_h(f)}\right]^{1/2} \tag{2.70}$$

Notice that the optimal template, $q(t)$, defined by (2.68) is a filtered version of the signal $h(t)$, with a pass where the noise is low and a cut where the noise in high. Additionally see that the optimal SNR given by (2.70) is not the energy in the signal but an integrated signal power weighted down by the noise PSD.

These techniques are run of the mill in gravitational wave detection, where the arrival time of a signal

is often not known[1]. Take for example a chirping signal, even if we have a fair idea of the shape of the signal, we can't know when a binary coalescence is to take place. We therefore have to shift the template Fourier transforms, $\tilde{h}(f)$, by all possible phases, until the maximal SNR is obtained, should there be indeed a signal. This adds an extra parameter to the fit and may also be the source of spurious detections. It affects the management of $1/f$ noise and increases the false alarm rates (as effectively we have a number of trials equal to the total observation time divided by the duration of the template). This problem is absent in the context of our test, since we know where the saddle is and therefore where the signal starts in the time-ordered series and so t_a is known[2]. A natural truncation in integration time T is also present, simplifying $1/f$ dealings.

It has been estimated that the saddle can be pin pointed to about a kilometer and the spacecraft location determined to about 10 km even with most basic tracking methods - given that the computational grids have this sort of resolution, the effect on the SNRs should be negligible. We should add that these uncertainties are of a practical, experimental nature rather than a theoretical one, it has been liberally estimated that the MOND saddle will not be shifted with respect to the Newtonian saddle by more than a meter. Thus, we can simply set $t_a = 0$ with an appropriate choice of conventions and set to zero the time lag τ in the correlator c, to achieve optimal results. This means that for all practical purposes, the starting time is indeed known and to the same degree of approximation so is the spacecraft trajectory and velocity with respect to the saddle.

[1] There are exceptions, for example if the signal comes from a supernova or any other source for which there is an extrinsic method, typically in the optical domain, for flagging the source of gravity waves.

[2] Although there will also be some intrinsic experimental variation in t_a, shifts in it (even on the scale of km) should not produce large deviations in SNR as the signals here are typically on the scale of 10^2 km.

Chapter 3

Solar System Tests

3.1 Characterising a test using SNR

The quantitative predictions for type I theories have been extensively studied using both analytical methods resorting to simplifying assumptions and numerical techniques [5], including complications from the perturbing effect of the Moon and planets, as illustrated in Figure 2.3. We adopt a coordinate system with x aligned along the Sun-Earth axis and centered at the saddle and considered trajectories parallel to x ($y = b$ lines, where b is the impact parameter), but other trajectories are easy to implement. Due to a number of practical issues [43], only transverse tidal stresses can be measured, say the S_{yy} component. Recall the observable MONDian stress

$$S_{ij} = -\frac{\partial^2 \phi}{\partial x_i \partial x_j} + \frac{\kappa}{4\pi} \frac{\partial^2 \Phi^N}{\partial x_i \partial x_j}$$

remembering that the field ϕ produces both a MONDian effect and a rescaled Newtonian pattern, associated with a rescaling of G in the Newtonian limit. It is paramount that ϕ and Φ^N are found to the same degree of accuracy and in Section 3.2.3, we will discuss the impact of an imperfect subtraction of the Newtonian component. Given a spacecraft trajectory, the conversion of tidal stresses (such as those depicted in Figure 2.3) into a template in time, $h(t)$, is then trivial. For a setup such as the one described

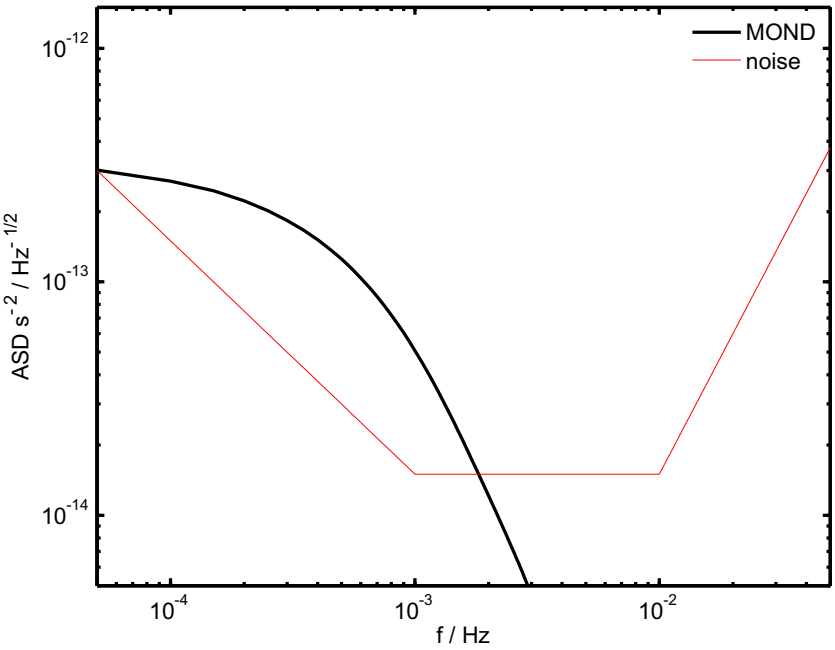

Figure 3.1: The amplitude spectral density (ASD) of the MOND tidal stress signal for a trajectory with $b = 50$ km and $v = 1.5$ km s^{-1}, compared to the ASD of the basic noise model described in the text, assuming a baseline of 1.5×10^{-14} s$^{-2}/\sqrt{\text{Hz}}$. This scenario generates a SNR of 28.

above we have $h(t) = S_{yy}(vt, b, 0)$, where v is the velocity of the spacecraft and $t = 0$ corresponds to the point of closest saddle approach. In a more general setup, for an approximately constant velocity $\mathbf{v}$ with a closest approach vector $\mathbf{b}$, and masses aligned along unit vector $\mathbf{n}$, we have:

$$h(t) = n^i n^j S_{ij}(\mathbf{b} + \mathbf{v}t) \tag{3.1}$$

This template should be Fourier transformed and using a given noise model, used to produce an optimal template (using our noise matched filter techniques) so that finally its SNR can be evaluated.

To gain some intuition on the nature of the signal, we plot in Figure 3.1 the amplitude spectral density (ASD) of the signal, i.e.

$$P(f) = \frac{2}{T}\left|\int_{-T/2}^{+T/2} \mathrm{d}t\; h(t)\; e^{-2\pi i f t}\right|^2 \tag{3.2}$$

where f is the frequency, t is the time and T is the integration period (here taken conservatively to be $T = 2 \times 10^4$ s). This can be directly compared to the noise ASD, the form usually quoted by

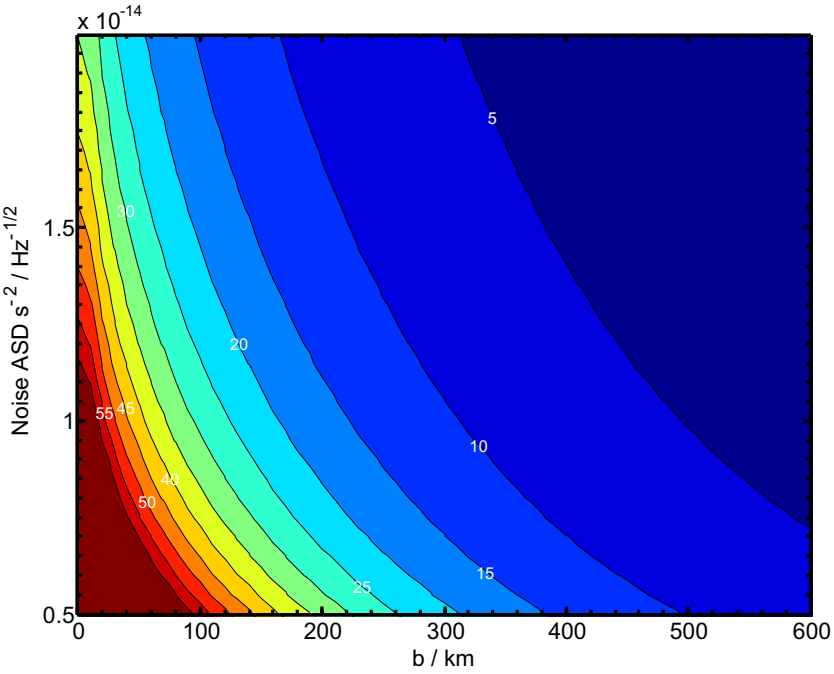

Figure 3.2: Signal to Noise ratio contours, for various impact parameters up to 600km and base noise ASD. We set the spacecraft velocity at 1.5km s^{-1}. Calamitous assumptions would still lead to SNR of 5. More optimistic ones ($b \sim 50$km with noise half way up the scale) would lead to SNRs easily around 50.

experimentalists. As a simplified LPF noise model (for more details, see [43]), we assume that the noise is white in the frequency range between 1 and 10 mHz, i.e. we assume a constant baseline with ASD around 1.5×10^{-14} $s^{-2}/\sqrt{Hz}$. For lower frequencies we assume $1/f$ noise and for higher frequencies that the noise degrades as f^2. With these assumptions the noise and signal ASDs are plotted in Figure 3.1, for typical parameters. As we can see, there's signal to noise of order 10 over a couple of decades, making it not surprising that the integrated SNR is in double figures (in this case around 28).

We can now run through the parameter space of the experiment and evaluate the expected SNRs. For example, let's assume $v = 1.5$ km s^{-1} and explore impact parameters up to 600 km. We also considered the effect of changing the base line ASD of our noise model, with the results plotted in Figure 3.2. We see that we would need to miss the saddle by more than 300 km to enter single figures in SNR, with typical noise levels. For $b \sim 50$ km a SNR of 30-40 is not unrealistic and recent work has suggested an the impact parameter around $b \leq 10$ km within easy reach. In combination with the expectations for the noise, this makes the test very promising indeed. However we should now look at this preliminary

analysis in more detail.

3.2 Systematics

There is considerable uncertainty regarding the details of the flyby trajectory, chief among them its speed. In Section 3.2.1 we show that the effect of the speed is minimal, within the range of speeds expected from any trajectory in the Moon-Earth system. In Section 3.2.2 we present improved, more realistic noise models, repeating the analysis with a best and worst case scenario for instrument performance as understood at the time of writing. We also outline work in progress, improving on noise matched filters and on estimates of false alarm rates. In Section 3.2.3, issues related to the background tidal stresses, namely the the Newtonian background and the spacecraft self-gravity are discussed.

3.2.1 The impact of the spacecraft velocity

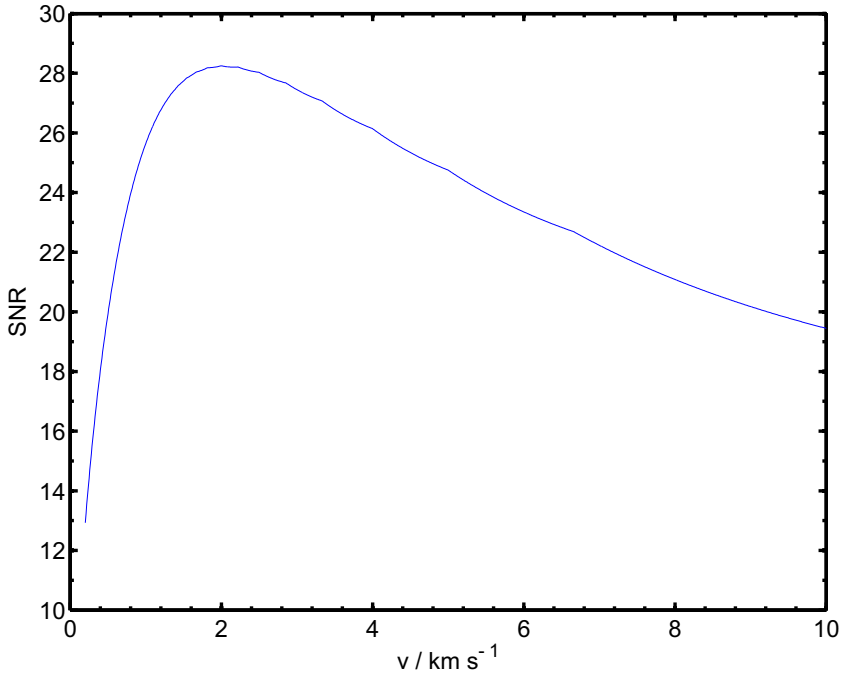

Figure 3.3: Plot of SNR against satellite velocity for an impact parameter of 50 km and a baseline noise of 1.5×10^{-14} s$^{-2}/\sqrt{\text{Hz}}$. We note a broad peak around $v = 2$ km s^{-1}. Higher speeds shift the signal to higher temporal frequencies; however the rough speeds of all trajectories in the Earth-Moon system are already optimal, given the noise properties of the instrument.

A relevant question to ask is what is the effect of the spacecraft velocity on the SNRs presented previously? The question is relevant as it can assist the strategy in designing flyby trajectories. Within the range of realistic speeds, the SNRs do not vary substantially. The good news is that due to a remarkable coincidence, these speeds are already near optimal.

As Equation (3.1) shows, the spacecraft velocity is the conversion factor between the spatial scale of the tidal stress and the time scale at which the instrument measures them. Of course, *in detail*, this has an effect on expected SNRs. Higher/lower speeds mean a faster/slower scanning of these spatial features and so a shift of the template $\tilde{h}(f)$ to higher/lower frequencies, whilst keeping the noise ASD fixed - we see therefore the SNR has to change. This is ilustrated in Figure 3.3, for a $b = 50$ km run and a baseline noise of 1.5×10^{-14} s$^{-2}/\sqrt{\text{Hz}}$ - the SNR has a peak at $v = 2$ km s^{-1}. However this peak is very broad with respect to the type of variations that might be expected from different trajectories leading from L1 to the saddle [43]. For the rough range $v = 1.5 - 2.5$ km s^{-1}, the SNR approximately varies in the range 27-28. For $v = 1 - 3$ km s^{-1} (which is probably at the limits of what are possible from real orbits) the variations would be in the approximate range 25-28. The priority therefore should be getting as close as possible to the SP, the speed will never be far from optimal.

This result can be understood qualitatively - as a crude estimate, anything moving in the Earth-Moon system has a typical speed of the order of 1 km s^{-1}. The MONDian tidal stress for the Earth-Sun saddle displays variations on a length scale of the order of 100 km. Therefore the MONDian signal will always be felt by LPF on a time scale of minutes, i.e. in the mHz range. This is just where the instrument noise is lowest, a remarkable coincidence considering that the instrument was built to these specifications for entirely different reasons (astrophysically motivated gravitational wave templates have these time scales). And yet the typical speeds and length scales of the problem combine to make the instrument already optimal for a MONDian saddle test.

3.2.2 Improved noise models

A number of improvements to the noise model used previously are possible. One obviously being it is unlikely there will be a frequency region with white noise. Instead, the noise is likely to be higher than

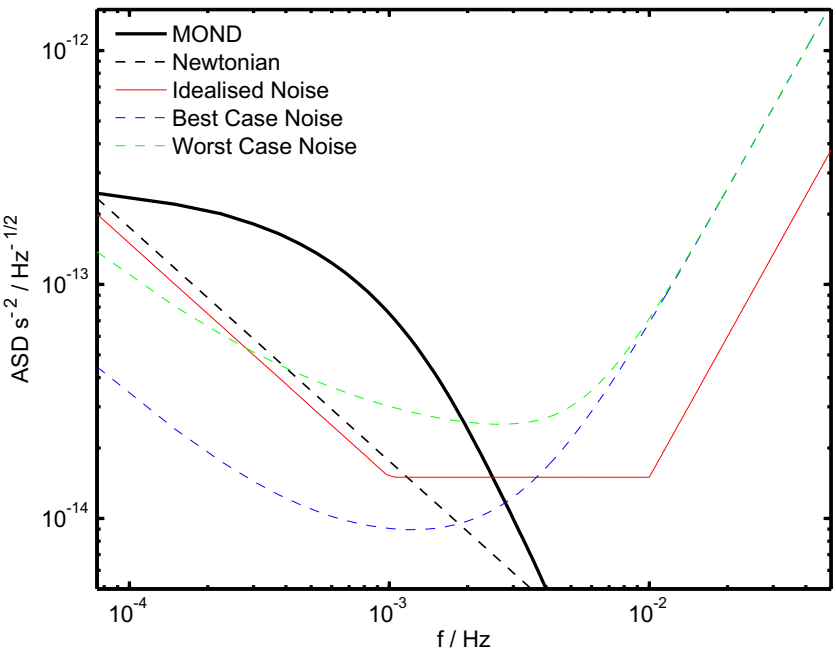

Figure 3.4: Here we replot Figure 3.1, adding on the best and worst case scenarios for more realistic noise models (as at the time of writing). We have assumed a trajectory with the geometry described in the main text, with impact parameter of $b = 50$ km and velocity $v = 1.5$ km s^{-1} and have additionally plotted the contribution of ϕ to the Newtonian background.

modeled in Section 3.1 at high frequencies but lower than expected at low frequencies. The turnover between the two regimes is smooth, as depicted in Figure 3.4, where we superimposed the simplified noise model used in Section 3.1 with the more realistic estimates for ASD for a best and worst case scenario. It has been argued that the worst case scenario might be too pessimistic and the best case scenario too optimistic, so we will take these two models as extremes. The nominal noise requirements were set out in [62], typical parameter values from simulations for each source of noise are detailed in [63] and simulations have been done to fully understand the total instrument response in [64]. In Figure 3.5, we depict the nominal noise requirements for LPF as well as that for the worst case noise, as an illustration of the high and low frequency behaviour of different noise sources.

In Figure 3.6 we plot the SNR as a function of impact parameter with $v = 1.5$ km s^{-1}, assuming the two extreme scenarios. As we can see, in the best case scenario we'd need to miss the saddle by more than 650 km for the SNR to drop below 5. In the worst case noise scenario, however, that figure would shrink to about 250 km. For $b \sim 50$ km the SNR would be in the range $13 - 44$. In spite of

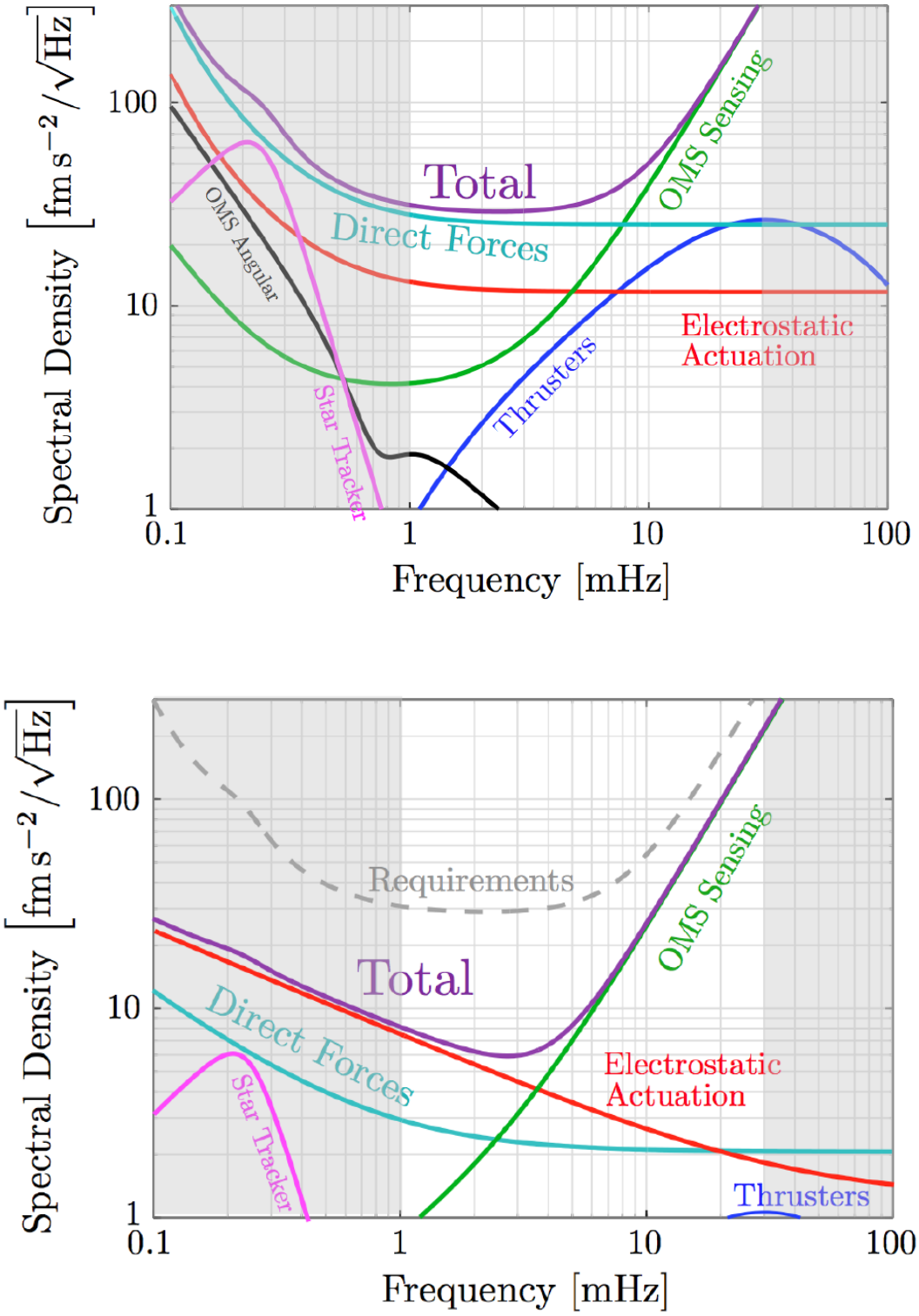

Figure 3.5: Here we show the requirement **(top plot)** and actual worst case **(bottom plot)** noise budgets, as a depiction of how the different sources of noise will affect the spacecraft noise ASD. The different low and high frequency noise contributions are detailed, showing a wide spread in behaviour depending on the source. These suggest that actually with even the most pessimistic estimates for the real noise, there should still be a decent SNR. Reproduced from [6].

the uncertainties, all scenarios lead to optimistic prospects for detection. We stress that we will know what the noise is, *in situ* (while at L1). These forecasts are useful, but should become concrete, fixed numbers once the mission goes ahead. We should add that even if the noise ASD is known, further issues

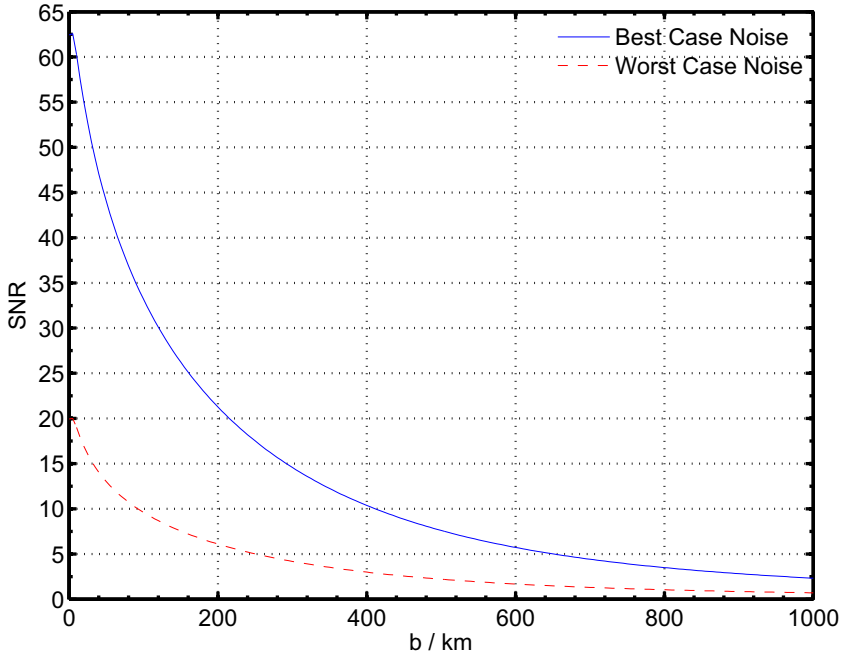

Figure 3.6: The SNR for the improved noise models (best and worst case scenario) assuming $v = 1.5$ km s^{-1} for a variety of impact parameters b.

complicate the simple data analysis procedures presented. Most notably, if the real noise is non-Gaussian and non-stationary, then this *may* increase the probability of a false alarm. Putting a realistic figure to the probability of a false detection requires having the instrument switched on before and after a saddle flyby, characterizing the noise *in situ*, and evaluating the false alarm rates with real noise (and no prior modeling can be a substitute for this). Nonetheless more realistic simulations of the instrument response and noise are possible and in progress, but the issue of false alarm rates is obviously central, should there be a detection. But even just planning the experiment, it raises important questions - *given these rates, is it better to sacrifice b at the expense of multiple flybys or should all effort be put into a single flyby with a b as low as possible?* Assuming the noise is approximately Gaussian and stationary, the probability of a false detection is simply [61]:

$$\mathcal{F} = N\mathrm{erfc}(\rho) \tag{3.3}$$

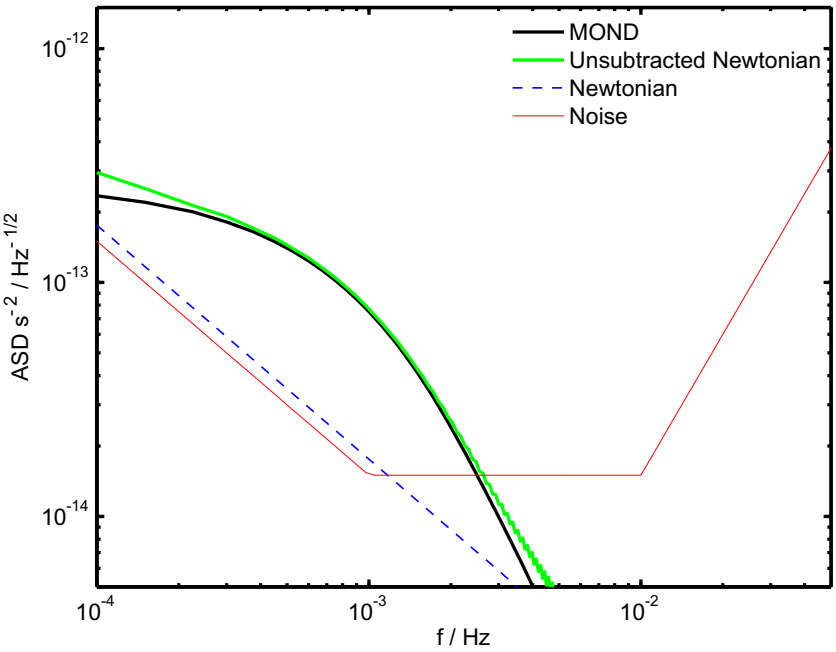

Figure 3.7: ASD plot of the MONDian and scaled Newtonian signal (ie multiplied by $\kappa/4\pi$) compared to the noise profile. We consider the effect of subtracting the Newtonian component in ϕ and see this becomes considerable at very small and very large frequencies.

where ρ is the optimal SNR, and N is the number of trials. In gravitational wave detection $N = O/T$, where O is the total observation time and T the useful duration of the filtered template. The factor N can be very large, so that even substantial SNRs (say 8 or 9) can produce non-negligible rates $\mathcal{F}$. In gravitational wave detection this nuisance can be mitigated by coincident observations. *We stress that no such problem is present here.* We do know where the saddle is for all practical purposes, so $N = 1$, removing the extra factor enhancing the false alarm rate. The high SNRs we have obtained for low b suggests that it would be inadvisable to sacrifice b for the sake of multiple flybys, in order to reduce false alarm rate. This statement should be further scrutinized using real noise. But even if it is true, there is an important sociological element - the reliability of any scientific claim rests on reproducibility. Should there be a positive detection, more than one flyby would go some way towards establishing the case for reproducibility.

3.2.3 The Newtonian background and self-gravity

We finish by examining two possible systematics that could plague a saddle test: the Newtonian background and the spacecraft self-gravity. These are natural concerns, but as we will see, their impact is negligible. In establishing this fact, it is important not to confuse force and tidal stress. It is also essential to examine the Fourier components of the stress signal and distinguish between a DC component from a signal peaking at frequencies to which the experiment is sensitive.

The DM saddle signal has a spatial scale $r_0 \approx 383$ km. In this region, as we recall from Section 1.2.5, would probe the regime $a_0 < a_N < a_N^{trig}$, with $a_N^{trig} \approx 10^{-5}$ m s^{-2}. The Newtonian tidal stress is therefore dominant in this regime (with an intensity of the order $A \sim 10^{-11}$ s^{-2}). Crucially however, it is approximately a DC component, as we see in Figure 3.7. This is to be contrasted with the distinctively varying MONDian signal (see Fig. 2.3) which, translates into a signal peaking at frequencies where the noise is low. A DC component, on the other hand, is well buried in the $1/f$ noise. It is true that *in detail* the Newtonian tidal stress is not exactly constant on the scale of r_0. But it is a known, well understood quantity and to the same accuracy as we know the saddle location and trajectory, and can subtract it off. An imperfect subtraction can be easily seen from this analysis, as shown in Figure 3.7.

A related matter (flagged in Section 3.1) relates to subtracting off from ϕ its effect on the renormalisation of the gravitational constant. As we know, there is a contribution to the Newtonian background from the ϕ field and should not be included in the MONDian predictions. The impact of not subtracting the component of ϕ contributing to the Newtonian measurement can be appreciated in Figure 3.8. This also gives us an idea of the level of impact an imperfect Newtonian subtraction might have. We considered the transverse tidal stresses felt in trajectories with impact parameters $b = 100, 500, 1000$ km. In the top plot, we subtract only the DC component (using the linear Newtonian approximation), in the bottom plot we use the full contribution of ϕ to the Newtonian tidal stresses. As we can see an imperfect subtraction would produce a spurious ramp in the stresses.

Another potential issue is self-gravity of the spacecraft. The mission requirement is that the differential acceleration of the test masses should be balanced at the level of $a \sim 10^{-9}$ m s^{-2}, but actual performance may beat the nominal requirements by a factor of 10. Yet again this is a DC component and does

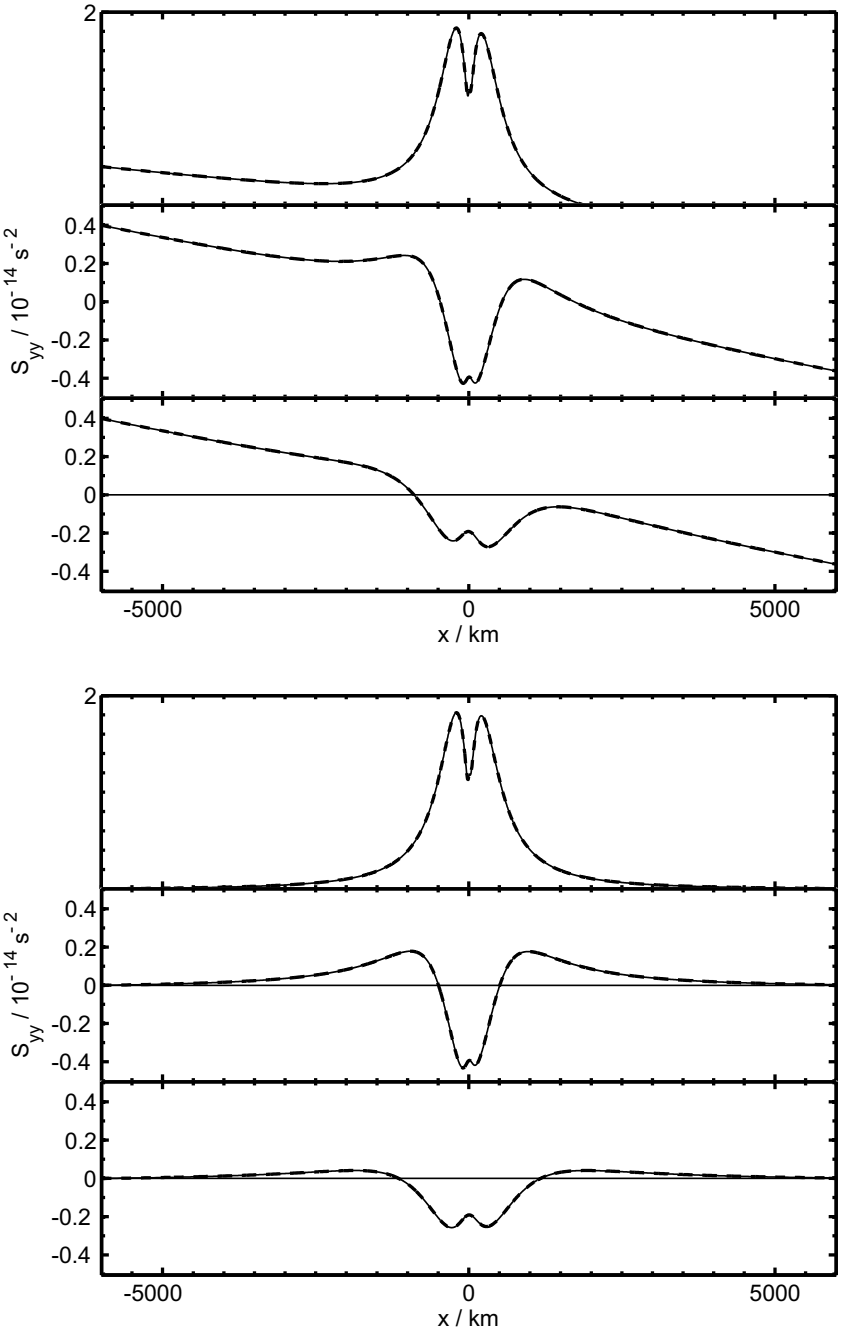

Figure 3.8: This plot illustrates the systematic effects that might result from an incorrect Newtonian subtraction. We consider the transverse tidal stresses felt in trajectories with impact parameters $b = 100, 500, 1000$ km. We then subtract the DC constant Newtonian tidal stress contributions from ϕ (top) and its full contribution (bottom). As we can see an imperfect subtraction produces a spurious ramp in the stress.

not affect the measurement in tidal stresses with the distinctive temporal variations we have posited. There are, of course, time-varying uncertainties in the self-gravity balancing but these are mainly due to thermoelastic effects and are much smaller, on the level of 3×10^{-16} m s$^{-2}/\sqrt{\text{Hz}}$ at least down to 1mHz. A related issue concerns the position of the saddle, as naively one might think that with a self-gravity of the order of 10^{-9} m s^{-2} the position of the saddle would be perturbed by the spacecraft. The two test masses could even generate distinct saddle points due to their gravity, however this ignores the fact that with *realistic* impact parameters, we are *not* testing the regime $a_N \sim a_0$, but rather $a_0 < a_N < a_N^{trig}$ with much larger Newtonian accelerations. We would need to approach the saddle much closer than around 400 meters before self-gravity becomes an issue and the spacecraft itself must be included in the computation of the SP location.

3.3 MONDian free-functions

Let us now examine the generality of our predictions, so far we have focused on type I theories with a specific free function (our $\mu_{fiducial}$). But even if we restrict ourselves to just these theories, there remains a whole series of free functions $\mu(z)$ to play with. Would theorists be able to wriggle out of a negative result availing themselves of this freedom?

As a start, we see that astrophysical applications of type I and IIB theories require that when $a_N < a_0$, the *total* Φ must have MONDian behaviour. This requires *simultaneously* that the ϕ field be in the MONDian regime and it be the dominant contribution. This suggests that the MONDian behaviour in ϕ is switched on at Newtonian accelerations a_N larger than a_0. Assuming the free function turns from 1 to a single power-law (and ignoring the MONDian magnetic field where appropriate), we have $F_\phi/F_N \propto 1/\sqrt{F_N}$ once MONDian behavior in ϕ has been triggered. Given the limit of (1.108), we should be triggering MONDian behaviour in ϕ at

$$a_N < a_N^{trig} \approx \left(\frac{4\pi}{\kappa}\right)^2 a_0 \tag{3.4}$$

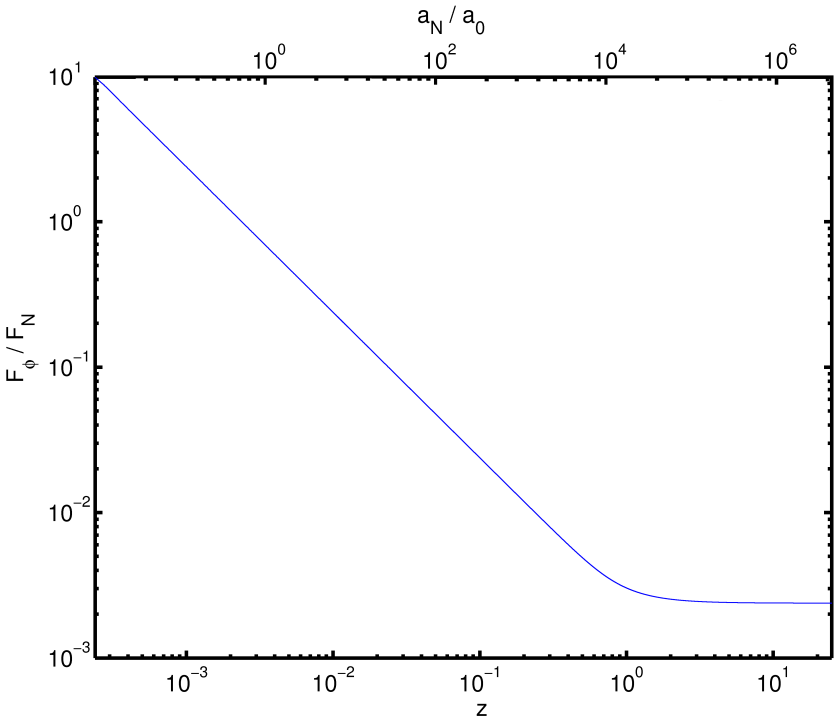

Figure 3.9: Log plot of ratio between the MONDian and Newtonian forces, F_ϕ/F_N, against $z = (k/4\pi)|F_\phi|/a_0$ (bottom axis) and F_N/a_0 (top axis), using $\mu = \mu_{fiducial}$. So that $F_N \sim F_\phi$ when $F_\phi \sim a_0$ (and so $z = \kappa/4\pi$; also $F_N \sim a_0$) and at the same time have $F_\phi/F_N \sim \kappa/4\pi \ll 1$ in the Newtonian regime ($z \gg 1$, $F_N \to \infty$), we must trigger MONDian behaviour in ϕ at accelerations much larger than a_0 (when $z \sim 1$).

(with $a_N^{trig} \sim 10^{-5}$ ms^{-2} for typical κ) or equivalently

$$|\nabla\phi| < a_\phi^{trig} = \frac{4\pi}{\kappa} a_0 \tag{3.5}$$

as we illustrate in Figure 3.9. This simple argument fails if μ becomes divergent (with part of its domain excised). Then, F_ϕ goes to a constant as $F_N \to \infty$, and so $G_{Ren} = G$ (see [30, 65] for more details). Consequently, it is possible to have $a_N^{trig} \approx a_0$, without fine-tuning the free-function or inducing unduly different G_{Ren}, in such theories. Such functions, however, *may* have other problems, rendering them non-viable (we will return to this issue later). For the same reasons, this simple argument also fails for type IIA theories (for which G is not renormalized). In Section 1.2.5, we parameterised the type IIB free-function ν to allow for simple comparison to type I theories, consequently the same value of κ will renormalise the gravitational constant by the same amount in both types of theory. These features explain the large

size of the bubbles around the saddle (inside which type I and IIB theories have these anomalous tidal stresses). They represent the region where the field ϕ has started to behave in a MONDian fashion, such that $a_N < a_N^{trig}$, *not* $a_N < a_0$ as might be naively expected. It is this regime that a LPF saddle test will be probing. Despite of the dominance of Φ_N in such a regime, the signal in ϕ can be detected because it has a distinctive spatial variation, whereas the Newtonian tidal stress is just a (known) DC component. The experiment is sensitive to the time Fourier transform of the signal with a sensitivity that peaks at the MOND frequency (and is very poor for a DC component, due to $1/f$ noise). Contrastingly, type IIA and III theories MONDian effects are only triggered for $a_N \sim a_0 \sim 10^{-10}$ m s^{-2}, resulting in bubbles with $r_0 = a_0/A \sim 2.2$ m across. We will show later, that under some quite general conditions, pretty much only type I and IIB theories with fine-tuned μ-functions would survive a negative result (with some of notable exceptions). Type IIA and III theories on the other hand turn out to be the only ones which would to evade a LPF saddle test, due to their small saddle bubbles.

3.3.1 Notation and previous proposals

As explained in Section 1.2.5, for type I theories two potentials act on non-relativistic test masses: the Newtonian potential Φ_N and a fifth force ϕ. Thus, the total potential is $\Phi = \Phi_N + \phi$ and recall that both contributions satisfy Poisson type equations:

$$\begin{aligned} \nabla^2 \Phi_N &= 4\pi G\rho \\ \nabla \cdot (\mu \nabla \phi) &= \kappa G\rho \end{aligned}$$

where we use $\mu = \mu(z)$, with $z = \frac{\kappa}{4\pi}\frac{|\nabla\phi|}{a_0}$. We will take note that

$$z = \sqrt{\frac{y}{3}} \tag{3.6}$$

where y is the original variable employed by Bekenstein (as derived in Section 1.1) - much confusion has arisen from different notations in the literature in this respect. We will take care not to confuse $\mu(z)$ with

the function $\tilde{\mu}(x)$ used in type III theories. In types I and II theories, we can loosely define an effective $\tilde{\mu}(x)$, obtained from adding the modified and Newton Poisson equations and comparing with the Type III equation

$$\nabla \cdot (\tilde{\mu}(x)\nabla\Phi) = 4\pi G\rho$$

The resulting effective $\tilde{\mu}(x)$ function is frequently used when connecting with galactic phenomenology. However the two functions $\tilde{\mu}(x)$ and $\mu(z)$ can only be easily related if the MONDian curl term can be neglected (such a proviso is often incorrectly ignored). If the curl term is non-negligible, then type I theories don't properly have a $\tilde{\mu}(x)$ function, and there is no substitute for integrating the equations on a case by case basis. In such a case when it can be ignored, then it's easy to relate functions $\mu(z)$ and $\tilde{\mu}(x)$ (as was considered in [44]), their definitions can be rewritten as $\mathbf{F} = \frac{\mathbf{F}_N}{\tilde{\mu}}$ and $\mathbf{F}_\phi = \frac{\kappa}{4\pi\mu}\mathbf{F}_N$, so that $\mathbf{F} = \mathbf{F}_N + \mathbf{F}_\phi$ implies:

$$\tilde{\mu} = \frac{1}{1 + \frac{\kappa}{4\pi\mu}} \tag{3.7}$$

In addition, we can write the argument $x = \frac{F}{a_0}$, in terms of $z = \frac{\kappa}{4\pi}\frac{F_\phi}{a_0}$, by deriving:

$$x = \frac{4\pi}{\kappa} z \left(1 + \frac{4\pi\mu(z)}{\kappa}\right) \tag{3.8}$$

These two equations provide a parametric expression for $\tilde{\mu}(x)$ with the former suggesting that in the Newtonian regime ($\mu \to 1$), there is a renormalising effect on Newton's constant G

$$G_{Ren} = \frac{G}{\tilde{\mu}} \approx G\Big(1 + \frac{\kappa}{4\pi}\Big) \tag{3.9}$$

as we saw in Section 1.2.5. Different μ functions are presented in the literature, for instance Bekenstein's toy model, as well as our $\mu_{fiducial}$, used to originally study 2-body analytical solutions [41, 5]. A proposal quite distinct from these two has also been put forward in the form of:

$$\mu(z) = \frac{z}{1 - \frac{4\pi\alpha}{\kappa} z} \tag{3.10}$$

with the case $\alpha = 1$ first suggested in [25]. To bridge our notation with the $\mu_s(s)$ used in [30], we define a dictionary (obtained from direct comparison of the Type I and III equations and their counterparts in the literature):

$$\mu = \frac{\kappa}{4\pi}\mu_s \tag{3.11}$$

$$z = \frac{\kappa}{4\pi}s \tag{3.12}$$

We stress that this function diverges, a property that sets it apart from all those functions which tend to a constant as $z \to \infty$. Underlying this statement is the postulate that the domain of the function should be excised after the divergence is reached, meaning that we should impose $s < 1/\alpha$. The distinction between bounded and divergent μ has received significant attention (for instance in [65]) and is indeed central to this discussion. On notational grounds, we note that for convergent free-functions, we define μ such that $\mu \to 1$ as $z \to \infty$, whilst in [65] one has $\mu_s \to \mu_0$, so that in effect we get the dictionary $\mu_0 = 4\pi/\kappa$. A hybrid possibility, incorporating the behaviour of (3.10) on galactic scales into a bounded function, can be adapted from the proposal in [25], as we will examine later. There remains debate over which $\tilde{\mu}$ functions best fit astrophysical data, examples include [26]:

$$\tilde{\mu}(x) = \frac{x}{1+x} \tag{3.13}$$

$$\tilde{\mu}(x) = \frac{x}{\sqrt{1+x^2}} \tag{3.14}$$

or even, as suggested by [25, 30]:

$$\tilde{\mu}(x) = \frac{2x}{1+(2-\alpha)x+\sqrt{(1-\alpha x)^2+4x}} \tag{3.15}$$

Another notational issue here is that our $\tilde{\mu}$ tends to G/G_{Ren} (or in the notation of [65], to $1/\nu_0$). The Milgrom-like proposals considered above all tend to 1. Thus these can only be approximately true with $G_{Ren} \approx G$ and so will denote them $\mu^{Milg}(x)$, with $\tilde{\mu} = \frac{G}{G_{Ren}}\mu^{Milg}$. With the proviso of the non-invertibility of a $\mu(z)$, in terms of a $\tilde{\mu}(x)$ in the presence of a curl field, we find (3.15) can be derived from

(3.10). Likewise (1.40) and (2.21) lead to:

$$\begin{aligned}\tilde{\mu}(x) &\approx 1+\frac{1-\sqrt{1+4x}}{2x}\\ &= \frac{\sqrt{1+4x}-1}{\sqrt{1+4x}+1}\\ &= \frac{2x}{1+2x+\sqrt{1+4x}}\end{aligned} \tag{3.16}$$

where we have written three algebraically equivalent expressions to facilitate comparison with the literature. Note that although (3.16) follows from (3.15) for $\alpha = 0$, the same doesn't happen with their μ functions, and Bekenstein's proposal (1.40) is strictly not covered by (3.10). The claim has been made previously [25, 65] that galactic observations favour $\alpha = 1$.

3.3.2 Permissible μ functions

Putting aside detailed predictions for galaxy rotation curves (which may well have been combined with inconsistent approximations, e.g. regarding the curl field), the following criteria are reasonable for what we will term physically permissible (if you like non-fine tuned) μ functions, defining type I theories:

- A. The cosmologically measured G cannot differ significantly from that measured, say, by the Cavendish experiment. That is: $G_{ren} \approx G$.
- B. When the total Newtonian acceleration a_N drops below a_0 the full potential Φ must be in the MONDian regime, that is, we need ϕ to be in the MONDian regime *and* to dominate Φ_N.
- C. Function μ should only have one scale, below which ϕ is MONDian, and above which it is near Newtonian. The detailed form of the transition is left undefined, but μ should have a single transition from 1 to z.

Items A and B have already been discussed in Section 1.2.5 - item B is the most basic requirement for the theory to be of astrophysical use, *regardless of the details*. Item C has been spelled out to illustrate just how finely tuned μ would have to be to evade a negative saddle result.

As explained in Section 1.2.5, these requirements imply that ϕ must enter the MONDian regime at a much higher acceleration than a_0, leading to an intermediate regime $a_0 < a_N < a_N^{trig}$ where ϕ displays MONDian behaviour but is still sub-dominant to Φ_N. This implies that for *any* μ satisfying these constraints, when $a_N \sim a_0$ (i.e. for astrophysical applications) we must necessarily have

$$F_\phi \approx \sqrt{F_N a_0} \tag{3.17}$$

This statement is independent of κ and only relies on the fact that $\mu \approx z = \frac{\kappa}{4\pi}\frac{|F_\phi|}{a_0}$ in the MONDian regime. *If the curl term can be ignored* we therefore have $zF_\phi = \frac{\kappa}{4\pi}F_N$, and thus (3.17) follows. Recalling $x = F/a_0$ we must conclude that:

$$\tilde{\mu}(x) \approx \frac{F_N}{F} \approx 1 + \frac{1-\sqrt{1+4x}}{2x} \tag{3.18}$$

The exception to this rule is obtained with a divergent μ, where we find the interesting behaviour [30, 65] that F_ϕ goes to a constant as F_N grows to infinity, instead of becoming proportional to F_N (c.f. Eq.(1.108)). Specifically, taking model (3.10), we find that:

$$F_\phi \approx \frac{a_0}{\alpha} \tag{3.19}$$

so that asymptotically no renormalisation of G takes place: $G_{Ren} = G$. Such a functions would lead to a different $\tilde{\mu}$, as we have seen and the MONDian behaviour driven by these functions would also be rendered invisible to LPF.

3.3.3 SNRs and μ dependence

If we take the whole class of μ satisfying our aforementioned requirements, we conclude that they have the same a_N^{trig} and consequently the same r_0. Alterations to the μ therefore do no change the spatial scale of the effect for type I theories (and similarly for type IIB). The predictions for $h(t)$ for $r < r_0$ are also model independent, since they rely on $\mu \approx z$, for $z < 1$. However the predictions referring to regions

with $r > r_0$ depend on the exact form of the transient from $\mu \approx z$ to $\mu \approx 1$, because they depend on $\delta\mu$ rather than μ itself, as we will show in Chapter 4. For example, we could consider

$$\mu = \frac{z}{1+z} \approx 1 - \frac{1}{z} \tag{3.20}$$

$$\mu = \frac{z}{\sqrt{1+z^2}} \approx 1 - \frac{1}{2z^2} \tag{3.21}$$

which clearly have different fall offs in the large z regime. Missing the saddle by more than r_0 would therefore leave us at the mercy of model dependence, and μ functions satisfying A, B, C could be found bypassing a negative result, for example we could consider the function

$$\mu = \frac{z}{(1+z^\beta)^{\frac{1}{\beta}}} \approx 1 - \frac{1}{\beta z^\beta} \tag{3.22}$$

with a large β. However, for trajectories hitting the region $r < r_0$, the peak of the signal is actually model independent (a result we will show in detail later) and therefore the SNRs predicted are not expected to depend on the details of the theory.

As an extreme illustration of the model (in)dependence of our SNR predictions we have excised the signal outside the MOND bubble from our templates, imposing an exponential fall off of the form:

$$\begin{aligned} S_{ij}(r < r_0) &\longrightarrow S_{ij}(r < r_0) \\ S_{ij}(r \geq r_0) &\longrightarrow S_{ij}(r \geq r_0)\, e^{1-\left(\frac{r}{r_0}\right)^2} \end{aligned} \tag{3.23}$$

Although artificial, such a model demonstrates the worst case results, as we see in Figure 3.10 (which should be contrasted with Figure 3.2). We see broadly that for $b < 400$ km our conclusions remain substantially the same and for $b > 400$ km, the SNRs drop much more sharply. One important point however is the behaviour of the fall off on the deep MOND scaling C, which should change depending on the details of the large z regime. In Section 4.5, we will consider techniques to constrain the C in the event of changing the fall off. Any changes in C however will likely be within an order magnitude.

Impact parameters of 50 km or less are within easy reach for LPF and so in order to bypass a negative

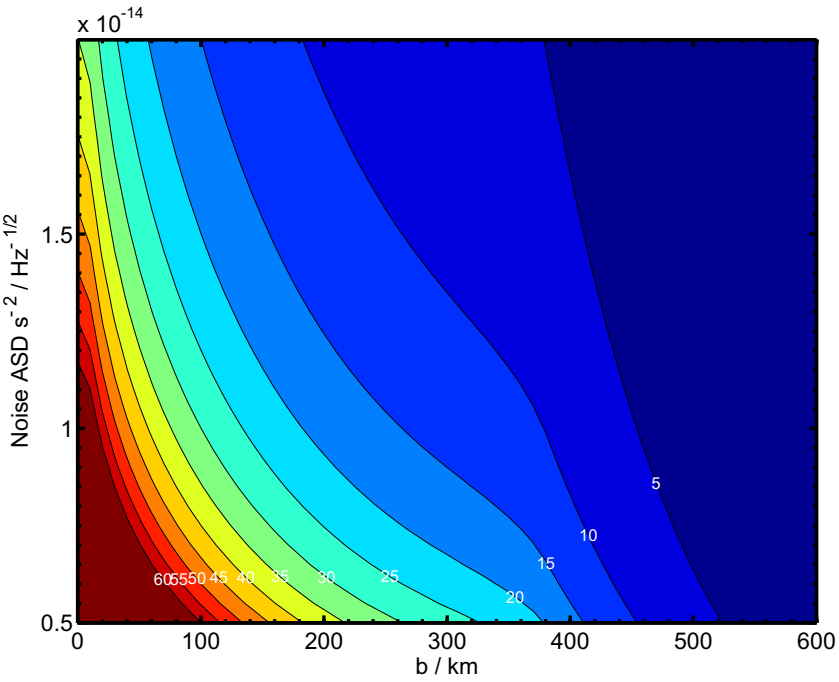

Figure 3.10: Signal to Noise ratio contours, for various impact parameters up to 600km and base noise ASD, using the same templates as in Fig. 3.2 but with an exponential fall off in the model-dependent region $r > r_0$. As we can see, for impact parameters $b > 400$ km the SNR drops more sharply, but nothing changes very much for $b < 400$ km.

result, we would have to shrink the bubble size (set by r_0). This would require breaking condition C and for us to consider "contrived" μ functions with two scales, which we now proceed to do in order to appreciate the full implication of a negative result.

3.4 A null result and designer μ functions

It is often difficult to falsify a theory containing free parameters - all that can be readily done is to constrain its parameters. However the constraints may be such that the theory becomes contrived beyond some definition of "reasonable". In what follows, we imagine a scenario where no anomalies are found with respect to the Newtonian expectation of the gravitational field (up to $b < 400$ km). Obviously all the theories considered so far would be ruled out to a degree of significance of the same order as their expected SNR. The issue would then become to determine which "designer" functions μ predicts a SNR of order 1, such that they will survive a no anomaly result. The more contrived the required μ, the more blatantly

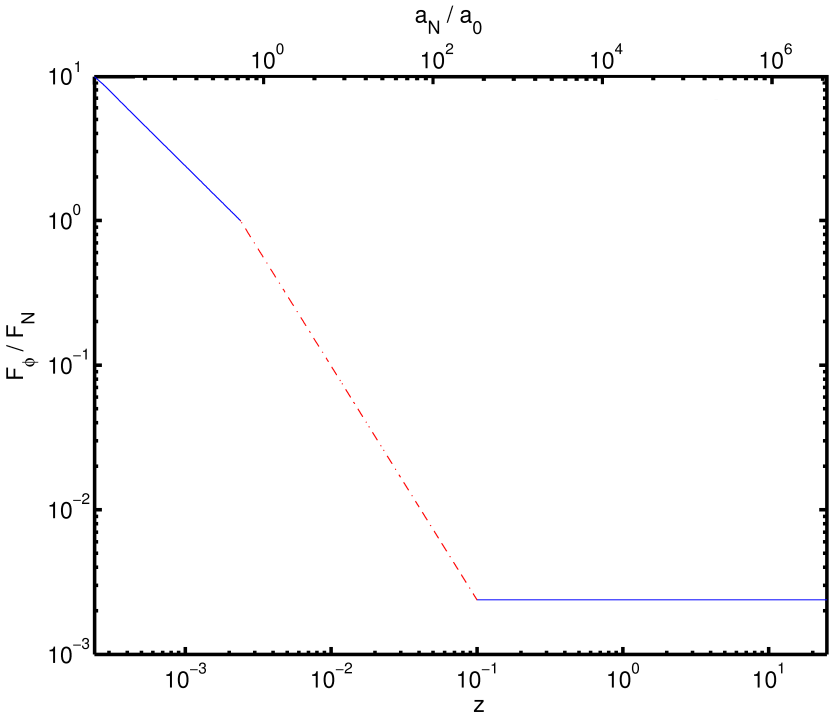

Figure 3.11: Log plot of ratio between the MONDian and Newtonian forces, F_ϕ/F_N, against $z = (k/4\pi)|F_\phi|/a_0$ (bottom axis) and F_N/a_0 (top axis). So that $F_N \sim F_\phi$ when $F_\phi \sim a_0$ (and so $z = \kappa/4\pi$; also $F_N \sim a_0$) and at the same time have $F_\phi/F_N \sim \kappa/4\pi \ll 1$ in the Newtonian regime ($z \gg 1$, $F_N \to \infty$), we must trigger MONDian behaviour in ϕ at accelerations much larger than a_0. However, by allowing a sharper intermediate power-law in μ, the trigger acceleration a_N^{trig} may be smaller (in this illustration by a factor of 10).

one should give up hope on such a theory.

In proposing a designer μ we shall impose that it satisfies requirements A and B to the same extent as the functions we've been considering. The theory should still be of astrophysical use and not conflict with observations on very general grounds. However we drop requirement C allowing the function to have two independent scales (and we notice that a_N^{trig} is not independent for the models considered so far). Specifically consider endowing μ with an intermediate power $n \neq 1$ linking the Newtonian regime ($\mu \approx 1$), with the astrophysically relevant MONDian regime ($\mu \approx z$).

Requirement B demands that $\mu \approx z$ for $z < \kappa/4\pi$, as before, so that $F_\phi \approx F_N$ when $F_N \approx a_0$, and $F_\phi \approx \sqrt{F_N a_0}$ for $a_N < a_0$. Requirement A imposes $\mu \to 1$ for large z, so that G_{ren} is the same as for the single power-law μ considered before (c.f. Equation (3.9)). If we are to shrink the size of the MOND bubble so as to accommodate a negative outcome from a saddle test, then we need a sharper power,

$n > 1$, bridging these two regimes. Thus F_ϕ/F_N could increase faster, with decreasing a_N, from its small value $\kappa/4\pi$ in the Newtonian regime, to 1 at $a_N = a_0$. This would reduce a_N^{trig} and thus r_0, as illustrated in Figure (3.11).

These considerations fully specify the function μ, up to details on the transition regions. Consider the function:

$$\mu \approx z \qquad \text{for} \qquad z < \frac{\kappa}{4\pi} \tag{3.24}$$

$$\mu \approx \left(\frac{z}{z^{trig}}\right)^n \qquad \text{for} \qquad \frac{\kappa}{4\pi} < z < z^{trig} \tag{3.25}$$

$$\mu \approx 1 \qquad \text{for} \qquad z > z^{trig} \tag{3.26}$$

such that the point where non-Newtonian behaviour in ϕ is triggered can be interchangeably pinpointed by:

$$z^{trig} = \left(\frac{\kappa}{4\pi}\right)^{1-\frac{1}{n}} \tag{3.27}$$

$$a_\phi^{trig} = a_0 \left(\frac{\kappa}{4\pi}\right)^{-\frac{1}{n}} \tag{3.28}$$

$$a_N^{trig} = a_0 \left(\frac{\kappa}{4\pi}\right)^{-1-\frac{1}{n}} \tag{3.29}$$

Notice that a_N^{trig} is a now a truly independent parameter of the theory (which can be traded for n). We still have that when $a_N < a_0$, the field ϕ dominates Φ_N as per requirement B, but now the intermediate region, where ϕ hasn't yet dominated but is already non-Newtonian, is in a narrower band of accelerations $a_0 < a_N < a_N^{trig}$. As a result here, the MOND bubble will shrink by

$$r_0 \approx 383 \left(\frac{\kappa}{4\pi}\right)^{\frac{n-1}{n}} \text{ km} \tag{3.30}$$

plotted in Figure 3.12. As can be seen, it is easy to change r_0 by an order of magnitude with n not much different from 2. To reduce r_0 by more than that however would require a very extreme intermediate power[1].

[1] Notice that with this particular model the MOND bubble can never shrink smaller than $\frac{\kappa}{4\pi}383$ km.

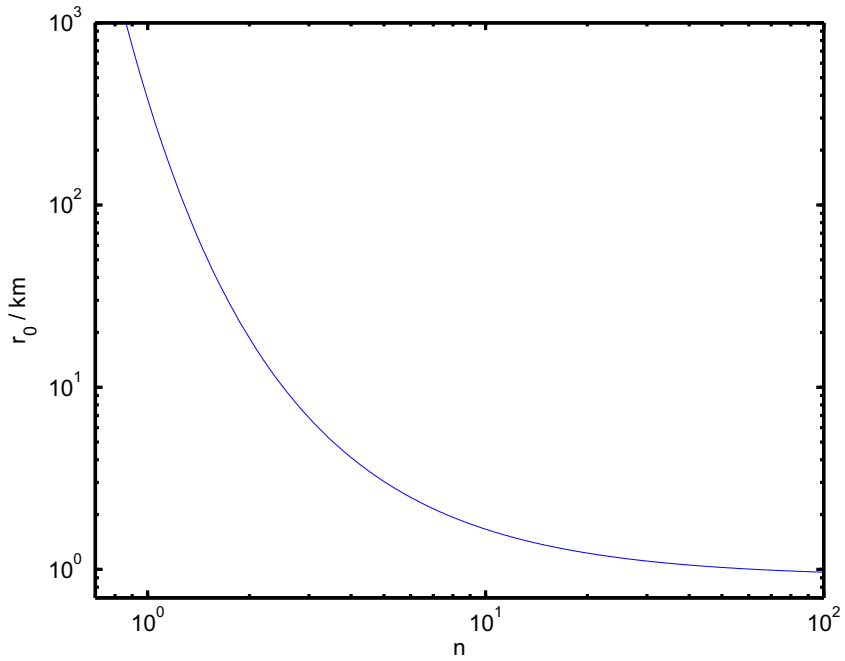

Figure 3.12: The size of the MOND bubble as a function of the intermediate power n. It is easy to collapse to bubble by an order of magnitude (say to around 20 km) with $n \sim 2$. However, to make the bubble much smaller (say, on the order of a few kilometers), very dramatic intermediate powers would be required.

Regrettably we can never make a model independent statement on what n is needed for a SNR of order 1. If nothing is observed, then by the nature of the problem, we must be making observations in the regime $b \gg r_0(n)$. Therefore we are necessarily probing the transient from $\mu \propto z^n$ to $\mu \sim 1$, dependent on the exact form of the function μ. Nonetheless it is interesting to perform this exercise, assuming a specific function, say:

$$\mu(z) = \frac{\left(\frac{z}{z^{trig}}\right)^n}{1 + \left(\frac{z}{z^{trig}}\right)^n} \tag{3.31}$$

In the $z \gg z^{trig}$ regime, this can be expanded as:

$$\mu \approx 1 + \delta\mu = 1 - \left(\frac{z^{trig}}{z}\right)^n \tag{3.32}$$

Since for $b \gg r_0(n)$, the curl field can be neglected, here we can write:

$$\mu \mathbf{F}_\phi = \frac{\kappa}{4\pi} \mathbf{F}_N \tag{3.33}$$

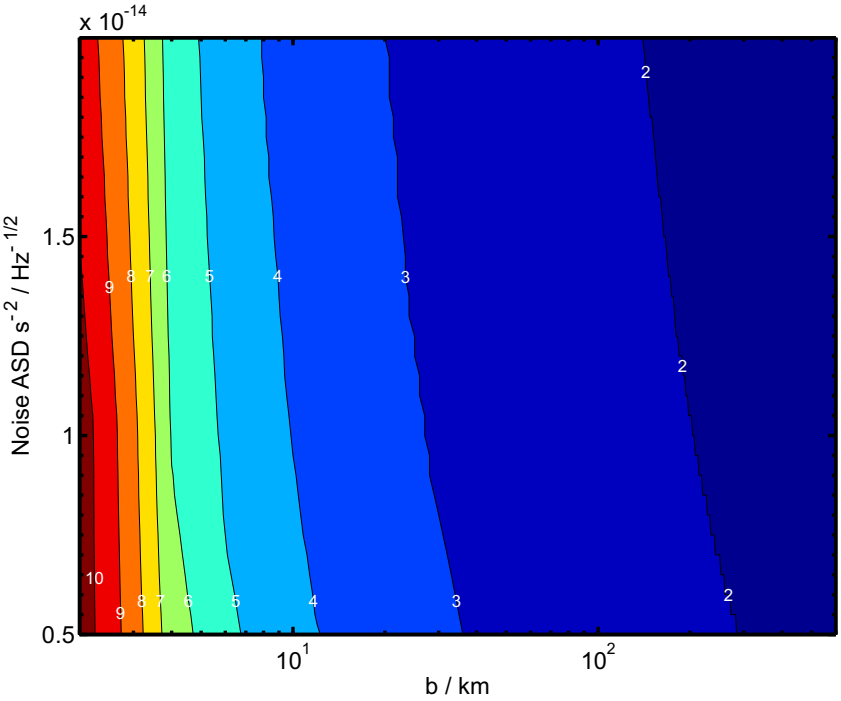

Figure 3.13: Contours of the power n needed to obtain SNR= 1, for different noise levels and impact parameters up to $b = 400$ km, noting that these values of n are an upper bound. For $n \neq 1$ the function is "unnatural". We see that as soon as we plunge deep into the MOND bubble, a rather unnatural designer μ becomes necessary to accommodate a negative result.

and consider perturbative solutions, expanding $\mathbf{F}_\phi = {}^0\mathbf{F}_\phi + \delta\mathbf{F}_\phi$, giving at zero order ${}^0\mathbf{F}_\phi = \frac{\kappa}{4\pi}\mathbf{F}_N$. At first order we find:

$$\delta\mathbf{F}_\phi \approx -\frac{\kappa}{4\pi}(\delta\mu)\mathbf{F}_N \approx \left(\frac{4\pi}{\kappa}\frac{a_0}{|\mathbf{F}_N|}\right)^n \mathbf{F}_N \tag{3.34}$$

from which the tidal stresses can be inferred. The results are condensed in Figure 3.13, depicting the value of n needed for a given b and noise level in order for a SNR of one to be obtained (and so a negative result be acceptable). We see that the value of n produced here is merely an upper bound, from the condition on the SNR, larger values of n would be acceptable too, we would just consider them unnecessary. As we can see as soon as we plunge deep into the MOND bubble, a rather unnatural designer μ becomes necessary to accommodate a negative result.

3.4.1 Motivated functions with features

So far we have attempted not to mix galaxy rotation fits with our considerations. The simple reason being that it is not clear how these fits would stand if performed together with the need to fit Solar system data and a saddle test: the performance of goodness of fit statistics under *joint* constraints might be very different. Penalisation for extra parameters (such as α) has probably not been properly enforced and they would almost certainly behave very differently in a joint fit, where the number of degrees of freedom would be much larger (we can consider the behaviour of the Bayesian information criterion, as seen in [66]). However it may well be that these two-scale models are precisely what are required for such a joint fit. We therefore examine how functions with such motivation fare in terms of SNR for a saddle test.

One type of function which evades a saddle test are those μ which diverge (e.g. Equation (3.10), see [30]), such that the asymptotic G is not renormalised, since F_ϕ tends to a constant,

$$\mathbf{F}_\phi \approx \frac{a_0}{\alpha}\frac{\mathbf{F}_N}{F_N} \tag{3.35}$$

as $F_N \to \infty$. Thus the profile of F_N/F_ϕ is merely changing from one power-law $(1/\sqrt{F_N})$ to another $(1/F_N)$, never leveling off into a constant, as we show in Figure 3.14 with the curve labelled $n = 0$. Since F_ϕ/F_N never levels off, $G_{Ren} = G$, with $a^{trig} \approx a_0$. Also since μ doesn't go to a constant, strictly speaking full MONDian effects are present for all accelerations and as such the curl field can never be neglected. Still we may expect the order of magnitude of the predicted effects to be small, and the associated saddle bubble to be invisible for LPF. In Section 4.6, we will consider more detailed predictions of these types of functions using different techniques.

Divergent μ functions *may* however fall foul of Solar System constraints (see discussions in [8, 24, 65, 67]), but we stress that this conclusion might not be fully general. A compromise can be struck by combining the functional form of the proposed unbounded μ with a curve flattening to a constant beyond the scales probed by galaxy rotation curves. With such constructions, we are plainly entering the realm of the designer or multiple functional form functions. These multiple regime, multi-scale, functions are

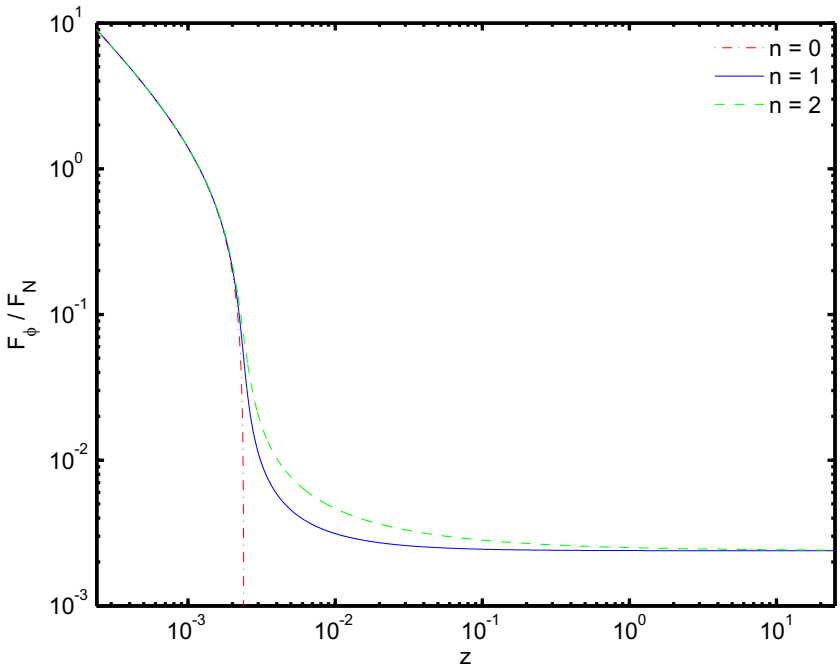

Figure 3.14: Log-log plot of ratio between the MONDian and Newtonian forces, F_ϕ/F_N, against $z = (k/4\pi)|F_\phi|/a_0$ for functions (3.36), with $n = 0, 1, 2$. For $n = 0$ we realize the divergent function (3.10) and as we can see there are only two regimes, corresponding to two power-laws, with the ratio never flattening to a constant. For all other cases we have a 3 piece function, with a fall off to the Newtonian regime which depends crucially on n.

implemented in one way or another, in all such proposals [25, 68, 69, 70]. We can consider the idea presented in [25] and translating into our variables leads to:

$$\frac{4\pi z}{\kappa} = \frac{\mu}{\frac{\kappa}{4\pi} + \alpha\mu}\frac{1}{(1-\mu)^n} \tag{3.36}$$

On galactic scales, this reduces to (3.10), however on Solar System scales we find

$$\mu \approx 1 - \left(\frac{a_0}{\alpha F_\phi}\right)^{\frac{1}{n}} \tag{3.37}$$

The F_ϕ/F_N profile for these models is plotted in Figure 3.14, which should be compared with the original proposal in Figure 3.9 and the more contrived toy model depicted in Fig. 3.11. These models can be constrained using the methods proposed here and in the face of a negative result we could assume being

in the QN regime and so after a similar argument we reach the counterpart of (3.34)

$$\delta\mathbf{F}_\phi \approx -\frac{\kappa}{4\pi}(\delta\mu)\mathbf{F}_N \approx \frac{\kappa}{4\pi}\left(\frac{4\pi}{\alpha\kappa}\frac{a_0}{|\mathbf{F}_N|}\right)^{\frac{1}{n}}\mathbf{F}_N \tag{3.38}$$

We can now constrain parameter n as before, with the result plotted in Figure 3.15. As in Figure 3.13, we have plotted the value of n (not to be confused with the parameter used there) for which the SNR = 1, for a given noise and impact parameter. A negative result from LPF would therefore require n to be smaller than this value, giving an upper bound.

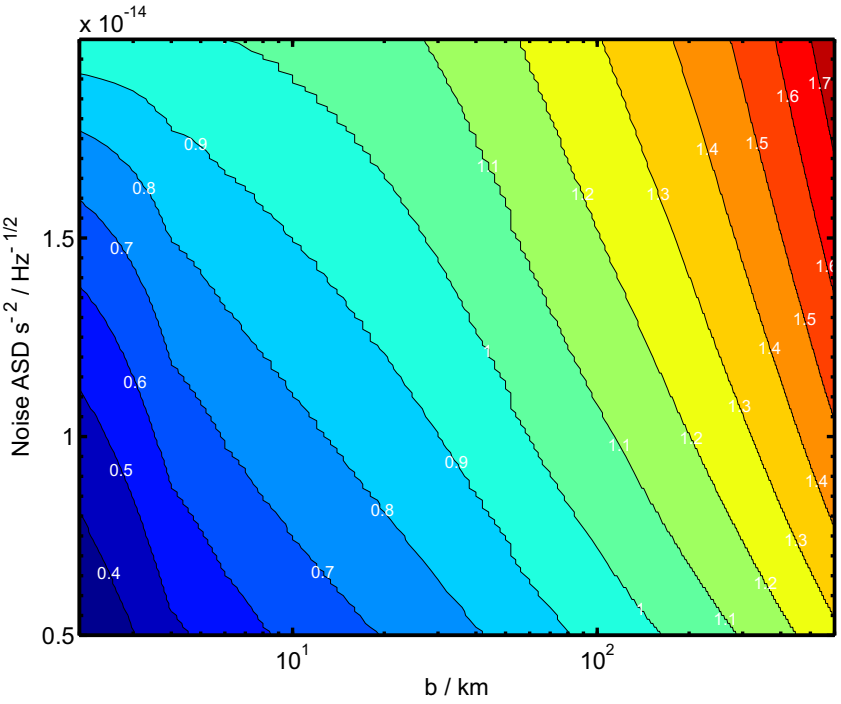

Figure 3.15: Contours of the power n in (3.36) required to obtain SNR = 1, for different noise levels and impact parameters, up to $b = 600$ km. These should be seen as an upper bound on n, should LPF find a negative result.

3.5 Type II Theories

So far we have concentrated on Type I non-relativistic MONDian theories, developing analytical and numerical predictions for the LPF saddle test. It is interesting, however, in light of the results presented

in Section 1.2.5 to consider whether the phenomenology associated with these theories are carried over into Type II theories and whether there are any easy ways of determining between different theories potentially from data.

As we pointed out in Section 1.2.5, we have two subclass of theory here, types IIA and IIB. In these theories, we have the driven Poisson equation

$$\nabla^2\phi = \frac{\kappa}{4\pi}\nabla\cdot(\nu(w)\nabla\Phi_N)$$

with argument

$$w = \left(\frac{\kappa}{4\pi}\right)^2 \frac{|\nabla\Phi_N|}{a_0}$$

such that $\nu \to 1/\sqrt{w}$ for $w \ll 1$ and $\nu \to$ constant for $w \gg 1$. The distinction between these ideas can be made clear if we consider the physical potential $\Phi = \Phi_N + \phi$ and consider:

$$\nabla^2\Phi = \nabla\cdot(\hat{\nu}(w)\nabla\Phi_N) \tag{3.39}$$

where $\hat{\nu} = 1 + \frac{\kappa}{4\pi}\nu$ and so crucially the difference lies in

$$\nu \to 0 \qquad \text{IIA} \tag{3.40}$$

$$\nu \to 1 \qquad \text{IIB} \tag{3.41}$$

In IIB theories, we see that in a similar fashion as in type I, we will have $G_{ren} = G(1+\kappa/4\pi)$. In IIA, we have a single field (like in type III), with physical potential Φ and Newtonian field Φ_N (which here plays an auxiliary role). This means that there is no G renormalisation, the triggering of MONDian effects happens at $a_{trig} = a_0$ and consequently a tiny bubble at the SP. Similar to type III, these theories would therefore escape the net of an LPF Earth-Sun SP test.

One noteworthy point in these theories is that because we are faced with a driven Poisson equation with a known and well understood right hand side, computing solutions here are far easier than with the

non-linear type I equation, as we see in Appendix A. We suggest using a free function ν inspired by the form of the $\mu_{fiducial}$, where we see in the $z \gg 1$ limit has the form

$$\mu \simeq 1 - \frac{1}{4z^2} + \dots \tag{3.42}$$

which suggests in the $w \gg 1$ limit, we need a function of the form

$$\nu \simeq 1 + \frac{1}{4w^2} + \dots \tag{3.43}$$

Whilst some effects are more precisely model dependent than others, we suggest the function

$$\nu = \left(1 + \frac{1}{w^2}\right)^{1/4} \tag{3.44}$$

and in Appendix A, we show such a derivation easily arises from spherical symmetry arguments. Here we will explore some of the ideas we presented earlier using type II theories and see how, if at all, they differ. We will only consider type IIB theories, the IIA case has been considered separately [71].

3.5.1 Analytical Results

Given Equation (1.104), let's expand

$$\nabla^2\phi = \nabla \cdot (\nu \nabla \Phi_N) = \nu \underbrace{\nabla^2 \Phi_N}_{=0|_{SP}} + \nabla\nu \cdot \nabla\Phi_N \tag{3.45}$$

and then use the linear Newtonian approximation, giving us the form of the source term

$$\nabla^2\phi = \frac{a_0}{2}\left(\frac{4\pi}{k}\right)\left(\frac{1}{r_0\, r}\right)^{1/2}\left(\frac{r_0^2}{r_0^2 + (rN)^2}\right)^{1/4}\left(\frac{N_r}{N^{1/2}} + \frac{N_\psi}{N^{3/2}}\frac{\partial N}{\partial \psi}\right) \tag{3.46}$$

The problem here is akin to electrostatics, solving the equations subject to the boundary conditions that $\delta \mathbf{F}_\psi$ vanishes (and $\delta \mathbf{F}_r$ equate) at $\psi = 0$ and π, such that we avoid a jump in the field at $\psi = \pi/2$.

DM Regime

For $r \ll r_0$, it's clear Equation (3.46) reduces to:

$$\nabla^2\phi = \frac{a_0}{2}\left(\frac{4\pi}{k}\right)\left(\frac{1}{r\,r_0}\right)^{1/2}\left(\frac{N_r}{N^{1/2}} + \frac{N_\psi}{N^{3/2}}\frac{\partial N}{\partial \psi}\right)\left\{1 - \frac{3}{4}w^2 + ...\right\} \tag{3.47}$$

where the angular functions of the leading order term neatly reduce to

$$\frac{7 + 9\cos 2\psi}{(2(5 + 3\cos 2\psi))^{5/4}} = g(\psi) \tag{3.48}$$

The separable form of the source suggests an ansatz for ϕ of

$$\phi = C_1\, r^a\, F(\psi) \tag{3.49}$$

where C_1 is some constant to be fixed from the source term above. This gives rise to a sourced second order ODE:

$$r^{a-2}\left(a(a+1)F + \cot(\psi)\,F' + F''\right) = r^{-1/2}\,g(\psi) \tag{3.50}$$

where $' = \partial/\partial\psi$ and

$$C_1 = \frac{4\pi}{k}\frac{a_0}{\sqrt{r_0}} \tag{3.51}$$

We find that the solutions of the homogenous equation are Legendre Polynomials of order a, with the form of (3.50) suggesting $a = 3/2$ and the inhomogeous solution is found to be

$$F \approx -0.0236 - 0.1886\,\cos(2\psi) + 0.0108\,\cos(4\psi) + ... \tag{3.52}$$

We can then compute the components of the MONDian force

$$\begin{aligned} -\nabla\phi &= \frac{4\pi a_0}{\kappa}\left(\frac{r}{r_0}\right)^{0.5}(F_r\mathbf{e}_r + F_\psi \mathbf{e}_\psi) \\ F_r &\approx 0.0354 + 0.2829\cos 2\psi - 0.0162\cos 4\psi + \ldots \\ F_\psi &\approx -0.3772\sin 2\psi - 0.0432\sin 4\psi + \ldots \end{aligned} \tag{3.53}$$

and we compare angular profile functions for type I and IIB solutions in Figure 3.16. We see from the form of the MONDian force,

$$\delta\mathbf{F} = -\nabla\phi = \frac{4\pi a_0}{\kappa}\left(\frac{r}{r_0}\right)^{p}\mathbf{S}(\psi) \Rightarrow S_{ij} \propto r^{p-1}$$

where in type I, $p \simeq 0.764$ and in type IIB, $p = 0.5$ - clearly the tidal stresses will have a sharper divergence as we approach the SP. This is due to the ϕ Poisson equation being linear and so with no curl forces present, the inner bubble solutions are not softened, unlike in type I.

In addition, at the saddle we have region where $|\mathbf{g}_N| = 0$ and so we need to consider solutions to the Laplace equation

$$\nabla^2\phi_L = 0 \tag{3.54}$$

which subject to smoothness and continuity conditions being satisfied and regularity at the origin, can be written in general by

$$\phi_L = a_0\left(\frac{4\pi}{k}\right)\sum_\ell A_\ell\, r^\ell\, P_{2\ell}(\cos\psi) \tag{3.55}$$

where $P_{2\ell}(\cos\psi)$ are Legendre polynomials,

$$A_\ell = \frac{a_\ell}{r_0^{\ell-1}} \tag{3.56}$$

and a_ℓ are dimensionless constants to be found by matching solutions at the intermediate MONDian regime (akin to the DM scaling C in type I theories). Our normalisation is picked to be of the same form as the sourced solutions, so that $\nabla\phi$ has units of acceleration. We only need to expand out a few terms

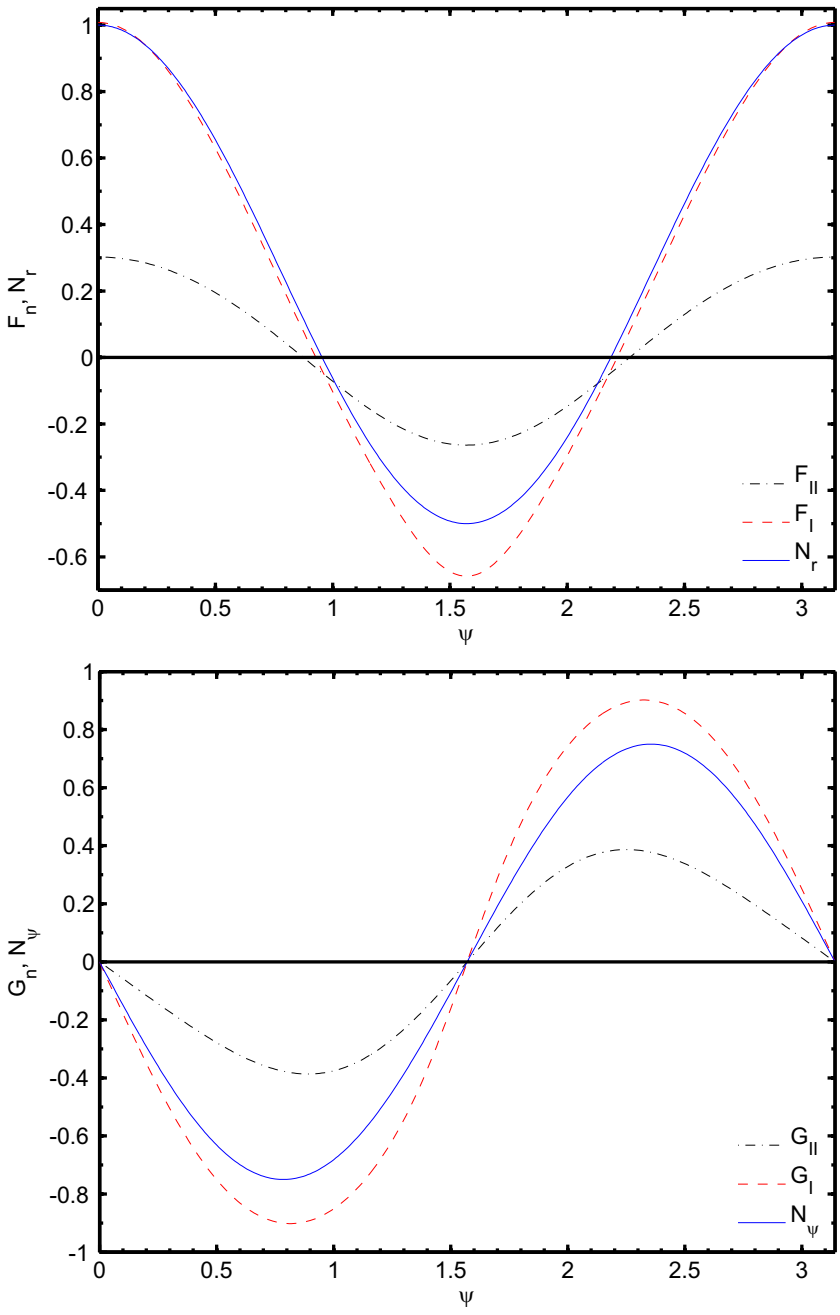

Figure 3.16: The angular profile functions F and G for the inner bubble forces in both type I and type IIB theories, alongside the linear Newtonian radial and azimuthal angular profiles.

from this contribution, since the region of validity of these solutions is small.

QN Regime

For $r \gg r_0$, it's clear that (3.46) reduces to:

$$\nabla^2\phi = a_0 \left(\frac{4\pi}{k}\right) \frac{r_0}{r^2} \frac{1}{2N^2} \left(N_r + \frac{\partial N}{\partial \psi}\frac{N_\psi}{N}\right) \left\{1 - \frac{3}{4}\frac{1}{w^2} + ...\right\} \tag{3.57}$$

where at leading order

$$\frac{2(7 + 9\cos 2\psi)}{(5 + 3\cos 2\psi)^2} = h(\psi) \tag{3.58}$$

In order to satisfy our boundaries conditions, our ansatz for the leading term needs to be of the form

$$\phi_2 = C_1\, H_2(\psi) + C_2 \ln\left(\frac{r}{r_0}\right) \tag{3.59}$$

Computing the Laplacian gives

$$\nabla^2\phi = \frac{C_1}{r^2}\frac{1}{\sin\psi}\frac{\partial}{\partial\psi}(\sin H_2') + \frac{C_2}{r^2} r_0 = a_0 \left(\frac{4\pi}{k}\right) \frac{r_0}{r^2} h(\psi) \tag{3.60}$$

allowing us to set

$$C_1 = C_2\, r_0 = \left(\frac{4\pi}{k}\right) a_0\, r_0 \tag{3.61}$$

Integrating out once then gives

$$\sin\psi\, \frac{\partial H_2}{\partial\psi} = \int (h-1)\sin\psi\, d\psi + A \tag{3.62}$$

and from the boundary conditions, we find

$$A = -\left(\frac{3}{2} + \frac{\pi}{3\sqrt{3}}\right) \tag{3.63}$$

meaning we solve (3.62) to find

$$H_2 \approx -0.2292 + 0.2876\,\cos 2\psi - 0.1163\,\cos 4\psi + ... \tag{3.64}$$

Expanding to higher terms will result in the series

$$\phi = \phi_2 + \frac{4\pi}{k} a_0 \sum_{n=2}^{\infty} C_n \left(\frac{r}{r_0}\right)^{2-2n} H_n(\psi) + \frac{\kappa}{4\pi}\Phi_N \tag{3.65}$$

where $H_n(\psi)$ satisfies the sourced ODE

$$n(n+1)H_n + \cot(\psi)H_n' + H_n'' = h_n \tag{3.66}$$

and h_n is given by

$$h_n(\psi) = \frac{2^{3n/2-2}(7+9\cos 2\psi)}{(5+3\cos 2\psi)^{n/2+1}} \tag{3.67}$$

We also always have the background rescaled Newtonian contribution

$$\frac{\kappa}{4\pi}\Phi_N = \frac{\kappa}{4\pi}\frac{Ar^2Nr}{2} = \frac{4\pi a_0}{\kappa}\frac{r^2}{8r_0}(1+3\cos 2\psi) \tag{3.68}$$

which obviously is the dominant contribution in the $r/r_0 \gg 1$ limit.

3.6 SNRs and motivating ν functions

Using a modification of our code (detailed in Appendix B), we can numerically solve the Poisson equation around the SP. Using the same system of non-uniform coordinates and computational parameters considered in Section 2.3, we can draw comparisons between these different ideas. We will note that although the fall offs from $\nu \to 1$ will vary between free functions, we expect the majority of the signal to come from the inner bubble. Using our SNR techniques, with the same parameters as before ($b = 50$km, $v = 1.5$km s^{-1}), we find SNR = 35 and we can compare the ASD plot for the MONDian signal in Figure

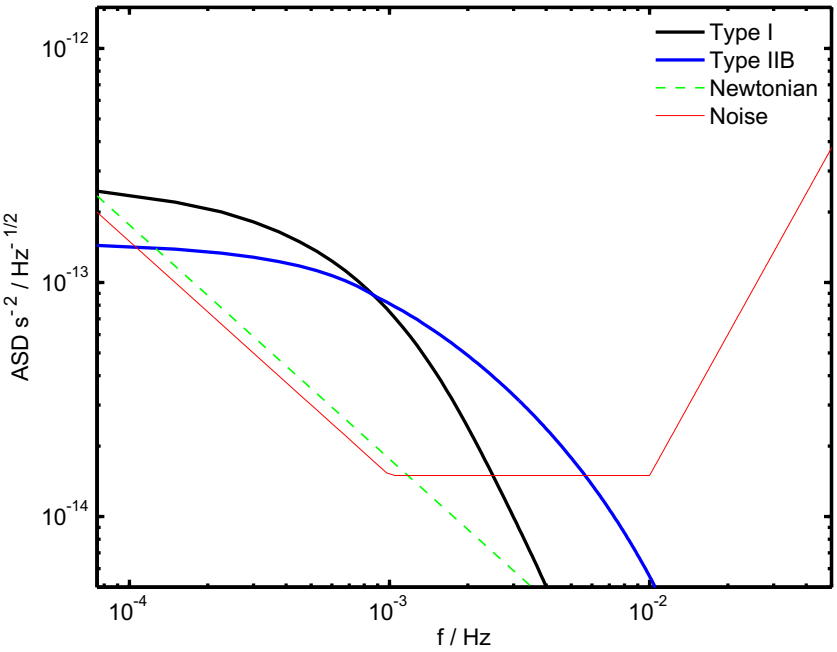

Figure 3.17: ASD plot of the MONDian and rescaled Newtonian signals, along with the noise profile. Using the same parameters ($b = 50$km fly-by and $v = 1.5$ ms^{-1}), we compare between type I and IIB theories, finding in this scenario SNRs of 28 and 35, respectively.

3.17 - as we see a marked difference at both lower and higher frequencies. By similar variation of the baseline of the noise and impact parameter, we produce the counterpart to the type I contour plot in Figure 3.18 and compare between I and IIB, suggesting in general larger SNRs.

3.6.1 Designer ν functions

It is very easy to construct free functions which mimic the galactic $\tilde{\mu}$ functions, such as

$$\nu = \frac{\sqrt{w}^{-1}}{1 + \frac{4\pi\alpha}{\kappa} w^{n-1/2}} \tag{3.69}$$

i.e. the usual $\nu \to 1/\sqrt{w}$ in the MONDian regime but moving to a different power law for larger accelerations $\nu \to 1/w^n$. So let's try and repeat the exercise of designing a free function, based on a null result (taking an upper bound from a SNR = 1 result) at some acceleration. We can then convert this into a restriction on the ν parameter space (akin to what we attempted in Section 3.4) - we will see the SP bubble clearly will have shrink, naively we would expect it to be smaller, given the stronger signed

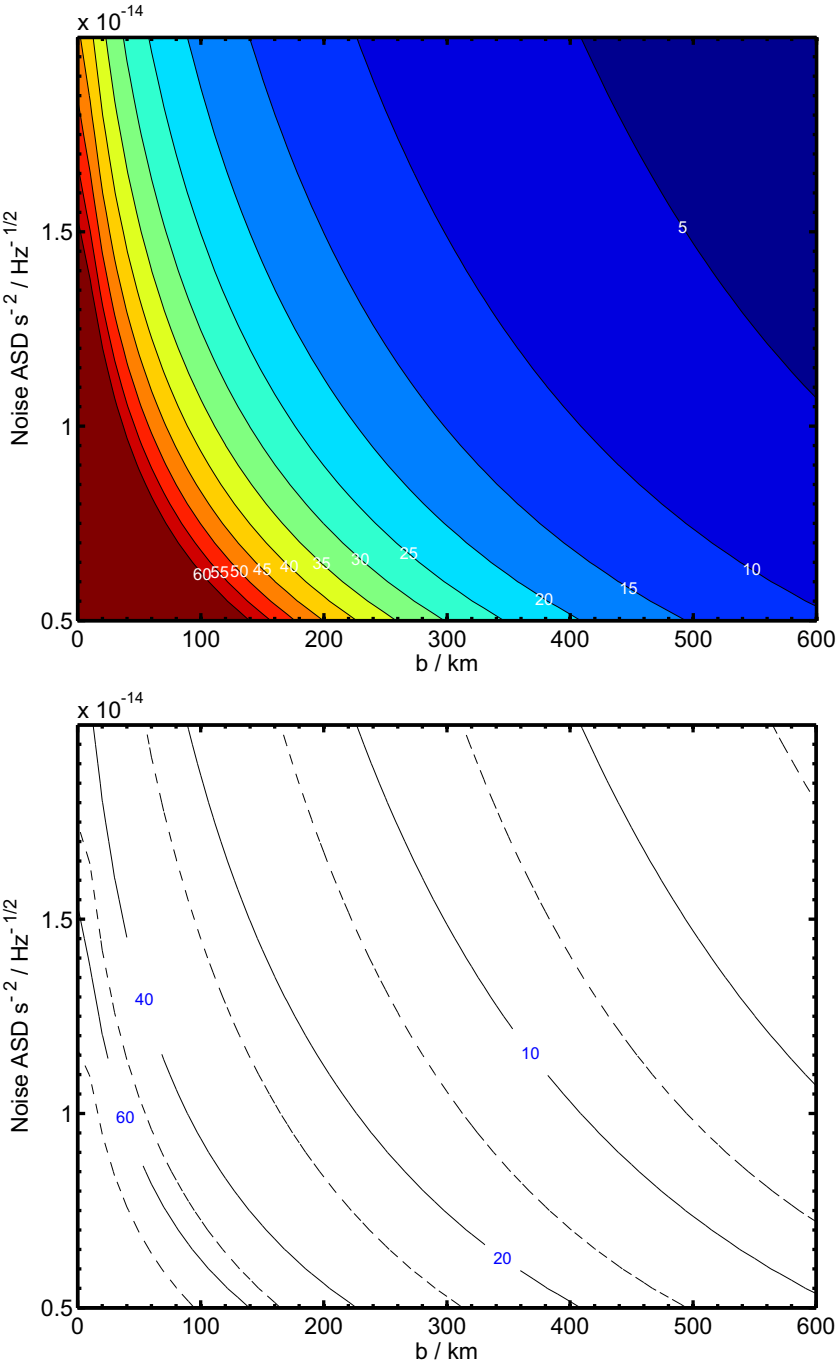

Figure 3.18: **Top panel**, SNR contours for various impact parameters and baseline ASD noise, for $v = 1.5$ kms^{-1}. Calamitous assumptions would still lead to SNR in excess of 5. More optimistic ones (b around 50km or less, noise half way up the scale) would lead to SNRs easily around 55. **Bottom panel**, a comparison of SNR contour lines between type I and IIB theories. The solid lines are the typical SNR to be obtained in IIB theories and the dashed lines to their immediate left the corresponding type I line - as we see IIB beats I.

expected. We start by fixing the asymptotica, the astrophysical regime gives us $\nu \approx 1/\sqrt{v}$ for $F_N \leq a_0$, ie $w \ll 1$. Far from the SP, we will have $\nu \approx 1$, but in the intermediate regime that we will be probing, we can suggest a model such as:

$$\nu \approx 1/\sqrt{w} \qquad \text{for} \qquad w < \left(\frac{k}{4\pi}\right)^2 \tag{3.70}$$

$$\nu \approx \left(\frac{w^{trig}}{w}\right)^n \qquad \text{for} \qquad \left(\frac{k}{4\pi}\right)^2 < w < w^{trig} \tag{3.71}$$

$$\nu \approx 1 \qquad \text{for} \qquad w > w^{trig} \tag{3.72}$$

where the point when non-Newtonian behaviour in ϕ is triggered can be interchangeably pinpointed by:

$$w^{trig} = \left(\frac{\kappa}{4\pi}\right)^{2-\frac{1}{n}} \tag{3.73}$$

$$a_\phi^{trig} = a_0 \left(\frac{\kappa}{4\pi}\right)^{1-\frac{1}{n}} \tag{3.74}$$

$$a_N^{trig} = a_0 \left(\frac{\kappa}{4\pi}\right)^{-\frac{1}{n}} \tag{3.75}$$

We still have that when $a_N < a_0$, the field ϕ dominates Φ_N - as per our requirements. Now the intermediate region where ϕ hasn't yet dominated but is already non-Newtonian is in a narrower band of accelerations $a_0 < a_N < a_N^{trig}$. As a result, the MOND bubble shrinks in this model according to

$$r_0 \approx 383 \left(\frac{\kappa}{4\pi}\right)^{\frac{2n-1}{n}} \text{ km} \tag{3.76}$$

This result shows that for a given null measurement up to some acceleration a_N^{trig}, using this general argument, our constraints between type I and IIB theories will be different. In this case, the bubble size would be expected to shrink more than in the type I case, given the sharper divergence in the tidal stress (and so larger signal) and this is exactly what (3.76) suggests.

The only problem that we come up against here is that given the different transients from $\nu \to 1$, making a model dependent statement is beyond our reach - quite simply because a null result only lets us probe the regime of $b \gg r_0(n)$. Performing a similar order of magnitude argument however is possible,

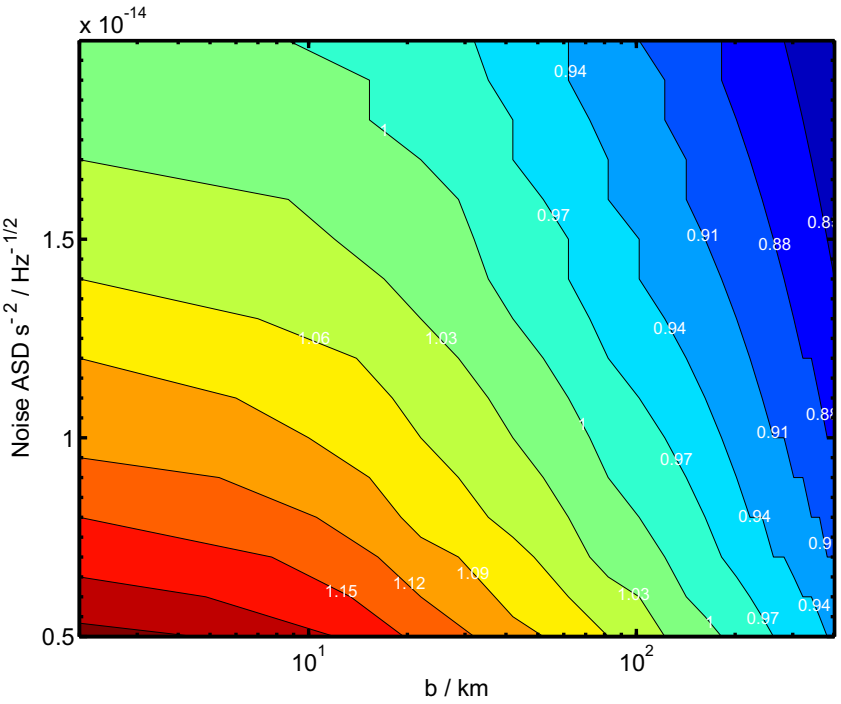

Figure 3.19: Contours of the power n needed to obtain SNR $= 1$ for different impact parameters and noise levels, upto $b = 400$ km using our designer free function.

using a designer function:

$$\nu(w) = 1 + \left(\frac{w^{trig}}{w}\right)^n \tag{3.77}$$

Assuming spherical symmetry means

$$\mathbf{F}_\phi = \frac{k}{4\pi}\,\nu\,\mathbf{F}_N \tag{3.78}$$

which we will break up into

$$\mathbf{F}_\phi = {}^0\mathbf{F}_\phi + \delta\mathbf{F}_\phi \tag{3.79}$$

with rescaled Newtonian component ${}^0\mathbf{F}_\phi = \frac{\kappa}{4\pi}\mathbf{F}_N$. Substituting in and solving gives:

$$\delta\mathbf{F}_\phi = \frac{k}{4\pi}\,(\nu - 1)\,\mathbf{F}_N \simeq \left(\frac{a_0}{|\mathbf{F}_N|}\right)^n \mathbf{F}_N \tag{3.80}$$

from which the tidal stresses can be inferred. We plot the resulting values of n required for a SNR $=$ 1 result in Figure 3.19 (which should be compared to Figure 3.13). As we see, the dynamics here are

somewhat different, which might allow us to differentiate between type I and IIB theories from an LPF result. This raises the interesting possibility that in one type of theory, a result could be unnatural, but possibly viable in another.

3.7 Conclusions

Our investigations have shown how a LPF saddle flyby could either detect MOND to a high SNR or rule it out (if not comprehensively then at least to a large extent). The former conclusion could be expected from back of the envelope calculations but here we have provided quantitative SNR estimates. This highlights an uncanny coincidence, given that the accelerometer aboard LPF has a non-white noise profile, dipping in the region of the mHz (on the rough time scale of minutes). The motivation for such a design lies in the gravitational wave signals to be targeted by LISA - it just happens that the MONDian bubbles of anomalous tidal stresses around the Earth-Sun-Moon saddles are of length scale $\sim 10^3$ km and free-falling bodies around this region have a typical speed of ~ 1 km s^{-1}. Put together, this suggests the time scale for crossing a MONDian bubble would be on the order of minutes - right where the instrument performance is optimal.

The question then arises as to how generic this conclusion is, or conversely, should a negative result be found, how thoroughly have we ruled out MOND. We examined some μ functions on offer in the literature and laid down criteria for reasonable μ based on astrophysical usefulness, viability in the face of constraints and in some sense *naturalness*. We found that once these criteria are taken into account, the size of the MOND bubble, (which we denoted r_0) is fixed. Predictions for what happens inside the bubble are also model independent; however the tidal stress anomalies outside the bubble depend on the transient from MONDian into Newtonian regime, with a fall-off which is indeed model dependent. Thus for impact parameters smaller than r_0 the predicted SNRs are robust, and do not change substantially with the model. For the currently expected $b < 50$ km (with $r_0 \sim 383$ km), this is indeed the case.

A way therefore for MONDian theories to wriggle out of a negative LPF result would be to change the bubble size r_0. This can only be accomplished with what we deemed designer μ-functions. If the free

function is allowed to have two scales and two power-laws away from its Newtonian value of 1, then it is possible to bypass a negative LPF result. Even for undemanding noise levels and impact parameters, the intermediate power becomes very contrived. In a similar vein, fine-tuned functions have been proposed in the literature and in Section 3.4.1, we showed how LPF could be used to constrain them. The point remains that one would have to bend backwards to accommodate a negative result, although there are also exceptions, such as diverging μ functions.

We reached the similar conclusions for type IIB (but not IIA) theories. If the G is renormalised and the free function ν is chosen to produce the same phenomenology as type I theories (in particular with regards to G_{Ren} and MONDian behaviour), then the MOND bubble has the same size, and the anomalous tidal stresses are of the same order. As explained in Section 1.2.5, in both types of theory MONDian behaviour is due to an extra field ϕ, and if one attends simultaneously to $G_{Ren} \approx G$ and $\phi \sim \Phi_N$ for $a_N \approx a_0$, then MONDian behavior in ϕ should be triggered at the same Newtonian acceleration (which we denoted $a_N = a_N^{trig} \gg a_0$). Furthermore the (also ν-independent) effects inside the bubble are different from type I predictions, but generically stronger. This stems from type II theories lack of curl field, a feature which softens the anomalous tidal stresses in type I theories. This results generically in larger SNRs between type I and IIB theories. As we see applying the same arguments between the two theories results in different constraints and the bubble size generically being smaller here compared to type I for a null result.

However, it may be that the relativistic "mother theory" is set up in such a way that the cosmological and non-relativistic G coincide (as is the case for type IIA theories). In this case, the MOND bubble around the saddle is very small. Likewise type III theories, such as those deriving from Generalised Einstein-Aether theories produce effects around saddles which are unobservable with current technology. In such theories, G is not renormalised (giving $a^{trig} = a_0$) such that the MOND bubble is just a few meters across. Remarkably, Solar System tests appear quite constraining upon type III theories, due to the so-called external field effect [38]. Solar System effects for type I and IIB theories are contrastingly suppressed by a factor of $\kappa/4\pi$ (the very same factor that boosts their MONDian bubble size). Thus saddle tests and planetary orbits seem to be complementary in constraining MONDian theories.

We could detach our considerations entirely from the MOND paradigm as an alternative to dark matter and regard these theories formally as a class on alternative theories of gravity (see [23] for an extensive review). As it appears only three classes of theories emerge in the non-relativistic regime of these theories, we can view the κ and a_0 in each case as free parameters, converting a LPF saddle flyby into a constraint or a detection in this space - an approach we will take in Section 4.3.

Chapter 4

Exploring the Parameter Space

4.1 Introduction

There is a ubiquitous acceleration scale in the universe, $a_0 \sim 10^{-10}$ ms^{-2}, which turns up variously in cosmology and astrophysics: the cosmic expansion rate, galactic rotation curves, etc. This observation has prompted the investigation of alternative theories of gravity endowed with a preferred acceleration. TeVeS [14] and other relativistic MONDian theories [16, 17, 22, 48, 49] provide a blueprint for such constructions. MONDian theories were first proposed with the motivation of bypassing the need for dark matter [12, 24]. However, they may also be considered independently from this application, and be seen simply as alternative theories of gravity [23] into which an acceleration scale has been embedded. In this guise they constitute prime targets for experimental gravitational tests inside the solar system.

If we consider for example a type I theory (such as from TeVeS), abstracting from aspects which do not affect the non-relativistic limit, the theory benefits from the leeway of a whole free-function μ. Its choice may be informed by minimalism and simplicity, for example building μ may be built to encode only 2, rather than 3 or more regimes (as we considered in Section 3.4.1). Putting aside details affecting the transition between the two regimes, we are then left with two free parameters: a_0 (the acceleration scale of the theory) and κ (controlling the renormalisation of the gravitational constant G). These are fixed by astrophysical and cosmological applications, if the theory is to act as a competitor to dark matter. But

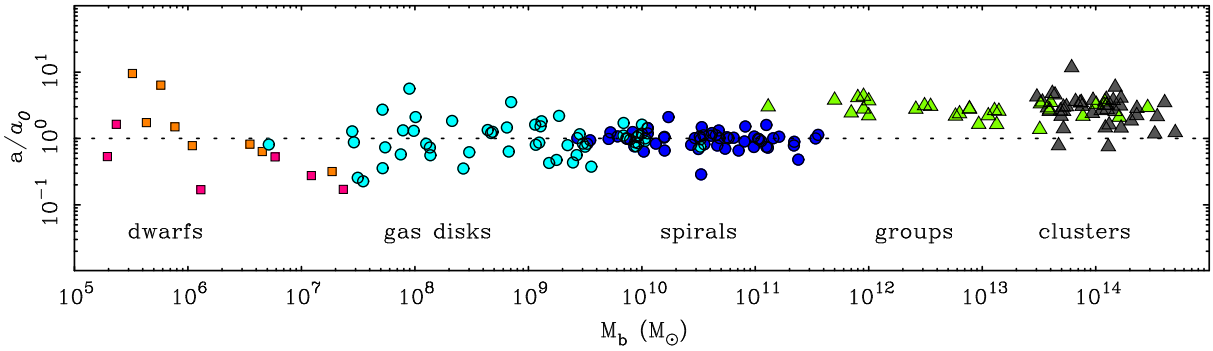

Figure 4.1: The anomalous acceleration parameter of extragalactic systems, spanning ten decades in baryonic mass. Reproduced from [7]

a_0 and κ can also be seen as fully free parameters in any Solar System test.

Predictions for minimal theories constrained by cosmological and astrophysical applications were studied in Section 3.4, where the general impact of a negative result was also examined. Detaching the target theory from its duties as dark matter alternative requires the generation of a large database of templates. However, re-running the adaptive-mesh code presented in Section 2.3 for each μ is simply not computationally feasible. Also, the "galactic" value of $a_0 = 10^{-10}\mathrm{ms}^{-2}$ should be taken with a pinch of salt, as Figure 4.1 shows, the value of a_0 could be subject to some variation.

In this chapter, we will demonstrate how this work can be partly alleviated. Changing only κ and a_0 requires a simple scaling argument, allowing for the generation of the whole set of required templates from those obtained with fiducial values for a_0 and κ (short cutting much tedious or downright impossible hard labour). Section 4.2 presents the analytical argument and its application to LPF is given in Section 4.3 and Section 4.3.1 shows a topical application, how the lunar saddle would fare were LPF to include it in a mission extension. Later in Section 4.4, we develop a full rescaling algorithm for changes to the free function as well and demonstrate how to constrain it, in the event of a positive detection. We end with some ideas towards extending the parameter space to more general free functions than those considered previously and their MONDian effects.

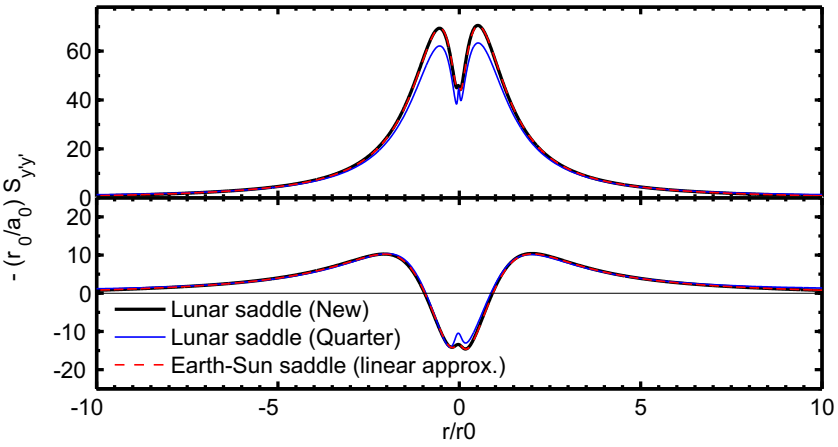

Figure 4.2: Stress signals for the lunar saddle, compared to the results from the Earth-Sun saddle (in the linear approximation). Lunar results are expressed in a new coordinate system (x', y', z), a rotated version of (x, y, z) such that the x'-axis is the line joining the Moon and the saddle, with $y' \approx 0.26r_0$ (**top panel**) and $1.05r_0$ (**bottom panel**). In the Earth-Sun case, the results are for $y = 100$ and $y = 400$ km, which correspond to the $0.26r_0$ and $1.05r_0$. At New moon $r_0 \approx 81$ km while at Quarter Moon $r_0 \approx 38$ km. Reproduced from [5].

4.2 Scaling behaviour around saddles

Scaling is an interesting tool for generating solutions to apparently intractable problems. For example imposing a self-similar ansatz leads to striking progress in the study of gravitational collapse, rendering what *a priori* are PDEs into simpler ODEs (e.g. [72, 73]). Scaling behaviour was observed in the MONDian tidal stresses around saddles, when comparing the profiles around the Moon saddle and the Earth-Sun saddle (as shown in Figure 4.2). It was noted that the tidal stresses are very approximately the same once they are spatially stretched and their amplitude scaled to account for the different Newtonian tidal stress A. In what follows we rigorously explain this empirical fact and extend its scope, deriving the scaling laws associated with varying a_0 and κ.

We recall that in type I theories, we have the total potential acting on non-relativistic particles $\Phi = \Phi_N + \phi$, from the joint action of the usual Newtonian potential Φ_N and a scalar field ϕ. Further to this, we have the non-linear Poisson equation driving the dynamics of ϕ in $\nabla \cdot (\mu(z)\nabla\phi) = \kappa G\rho$ with $z = \frac{\kappa}{4\pi}\frac{|\nabla\phi|}{a_0}$, κ is a dimensionless constant and a_0 is the MONDian preferred acceleration scale. In solving

this system, we defined the $\mathbf{U}$ variable:

$$\mathbf{U} = -\frac{\kappa}{4\pi a_0}\mu(z)\nabla\phi$$

such that we linearise the problem and our vacuum equations become:

$$\nabla \cdot \mathbf{U} = 0$$

$$4m\,U^2\,\nabla \wedge \mathbf{U} + \mathbf{U} \wedge \nabla U^2 = 0$$

with

$$4m = \frac{d\ln U^2}{d\ln \mu}$$

and notice the free parameters a_0 and κ drop out in these (universal) equations. Finally the MONDian force is obtained from $\mathbf{U}$ using:

$$\mathbf{F}_\phi = -\nabla\phi = \frac{4\pi a_0}{k}\frac{\mathbf{U}}{\mu(U)}$$

Notice that the vacuum equations are invariant under a rigid rescaling of the spatial variables:

$$\begin{aligned} \mathbf{U} &\rightarrow \mathbf{U} \\ \mathbf{x} &\rightarrow \lambda\mathbf{x} \end{aligned} \tag{4.1}$$

where λ is spatially constant. This means we can find homothetic solutions, such that

$$\mathbf{U} = \mathbf{F}(\lambda\mathbf{x}) \tag{4.2}$$

where $\mathbf{F}$ is a universal function. Next we need to supply our system with boundary conditions, which we do by going far enough from the saddle so that the field ϕ has entered the Newtonian regime, i.e. one

has $\mu \to 1$ (the renormalization in G is fully absorbed in κ), and so:

$$\phi \approx \frac{\kappa}{4\pi}\Phi_N$$

The appropriate boundary condition is then supplied from the Newtonian limit relation:

$$\mathbf{U} \approx \frac{\kappa}{4\pi a_0}\mathbf{F}_\phi \approx \left(\frac{\kappa}{4\pi}\right)^2 \frac{1}{a_0}\mathbf{F}_N \tag{4.3}$$

If we assume that we can approximate the Newtonian field around the saddle to the linear Newtonian force (at least for the purpose of effectuating this matching), remembering that

$$\mathbf{F}_N = -\nabla\Phi_N = Ar\mathbf{N}(\theta,\phi)$$

and we recall A is the Newtonian SP tidal stress and $\mathbf{N}$ is its angular profile. Recall also the definition of the MONDian bubble size, r_0:

$$r_0 = \frac{16\pi^2 a_0}{\kappa^2 A}$$

we therefore have in the Newtonian regime and close enough to the saddle:

$$\mathbf{U} \approx \frac{r}{r_0}\mathbf{N}(\theta,\phi) \tag{4.4}$$

which we see is simply $\mathbf{U} \to \mathbf{U}_0 = \frac{r}{r_0}\mathbf{N}$. This boundary condition allows us to select the homothetic solution (4.2) appropriate to a given saddle and free parameters. To match the boundary conditions, one should set $\lambda = 1/r_0$, so that the solution is

$$\mathbf{U} = \mathbf{F}\left(\frac{\mathbf{x}}{r_0}\right) \tag{4.5}$$

The above argument is still (approximately) valid if one goes beyond the linear approximation, as long as this approximation is good up to a few r_0. If the parameters a_0 and κ lead to a breakdown of this

assumption, however, then scaling is lost. From this we can read off scaling laws for our familiar quantities. We see from the definition before that the MONDian force must have the form:

$$\mathbf{F}_\phi = \frac{a_0}{\kappa}\mathbf{G}\left(\frac{\mathbf{x}}{r_0}\right) \tag{4.6}$$

where $\mathbf{G}$ is another universal function. (This scaling law is obvious by direct inspection of the analytical solutions derived for $\mu_{fiducial}$, however as we see now, it is more general). By taking derivatives we then find that the MONDian tidal stresses must have the form

$$S_{ij} = \kappa A H_{ij}\left(\frac{\mathbf{x}}{r_0}\right) \tag{4.7}$$

where the H_{ij} are also universal. This allows us to templates for general values of κ and a_0 from those for fiducial values, simply by rescaling them according to the above laws.

4.3 Some Applications

As a simple example, we examine in this section the impact of a_0 and κ on the SNR forecast for a LPF flyby. For our noise model, we will use the best estimate at the time of writing (which we denoted Best Case Noise in Figure 3.4). We then inspect the SNR variations with a_0 and κ for different saddle impact parameters b. After a number of studies, following on from [43], an impact parameter $b \leq 10$ km is now considered realistic. Multiple flybys are currently being investigated, for which b may not be as good. We therefore consider SNRs for b up to 1000 km. Recall that for the fiducial values $a_0 = 10^{-10}$ ms^{-2} and $\kappa = 0.03$ (required or suggested by cosmological and astrophysical applications) one forecasts SNRs for the Earth-Sun saddle around 40-60 for $b = 10 - 50$ km, only dropping below 5 beyond $b \sim 700$ km (see Figure 3.6).

Figure 4.3 shows the effect of changing the acceleration scale a_0, doing so results from a change in the MOND bubble size r_0 (as Equation 4.4 shows). Therefore the SNR is roughly constant on lines of constant b/a_0. The slope of the iso-SNR lines is not constant and they are not exactly straight due to the

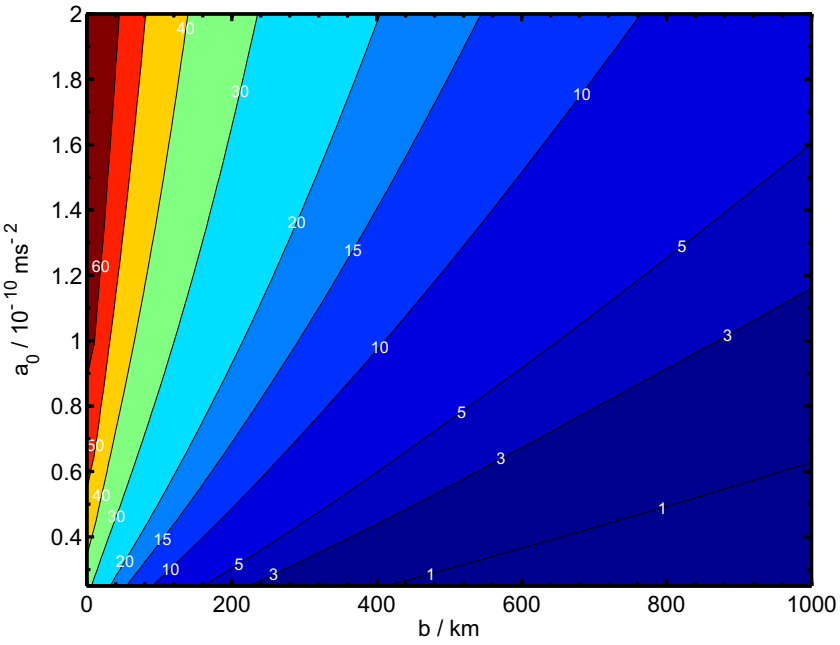

Figure 4.3: The effect on the Signal-to-Noise Ratio (SNR) resulting from varying a_0, assuming different impact parameters b and the "Best Case" estimate for the noise at the time of writing, see Figure 3.2.2 (with κ kept fixed at $\kappa = 0.03$). The fiducial value used in previous publications is $a_0 = 10^{-10}$ ms^{-2}. Generally the larger the a_0 the higher the SNR.

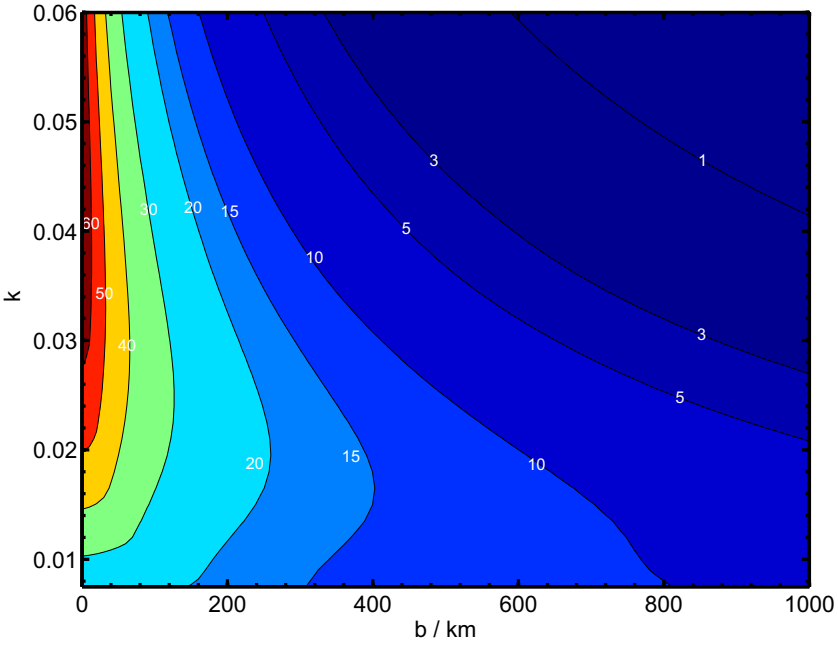

Figure 4.4: Effect on the SNR obtained by varying κ (keeping a_0 fixed at the fiducial value), again with "Best Case" noise model. The fiducial value used in previous publications is $\kappa = 0.03$. At smaller b, changing κ may increase or decrease the SNR, whilst at larger b smaller κ results in large SNR.

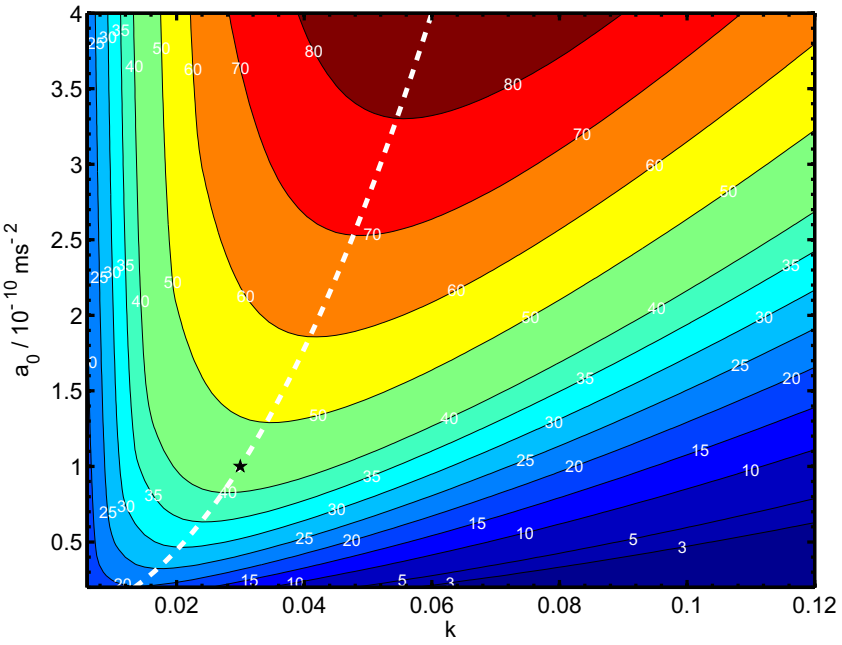

Figure 4.5: Effect on SNR obtained by jointly varying a_0 and κ, for a trajectory with impact parameter $b = 50$km. The fiducial values have been indicated with a star. We also plot (dashed white line) the contour of constant r_0 passing through the fiducial values.

non-linear nature of the SNR algorithm. We see that even at large b it is possible to turn a weak result into a strong positive one by increasing a_0 by a factor of 2. Conversely, if a_0 is halved, a SNR below ~ 5 is now a liability for b as low as ~ 350 km. Without external constraints fixing a_0 to better than an order of magnitude, it is therefore risky to give up on a $b \sim 10 - 50$ km.

The effect of changing κ is plotted in Figure 4.4 and results from two sources: a change in bubble size according to $r_0 \propto 1/\kappa^2$ (cf Equation 4.4) and an overall factor multiplying the amplitude (cf Equation 4.7). The two effects counteract each other, so that unless b is very large, the SNR at first increases with κ, then decreases. For $b \sim 10 - 50$ km it can go either way. For large b (greater than $b \sim 500$ km for the fiducial value of a_0), the bubble size prevails and so the SNR decreases with increasing κ. The interplay of these two effects is best illustrated in Figure 4.5, where we plotted the effect on the SNR of changing simultaneously a_0 and κ for fixed $b = 50$ km. We also plotted the line of constant r_0 passing through the fiducial values. As we see the SNR does change along this line, showing that the bubble size r_0 is not the only consideration.

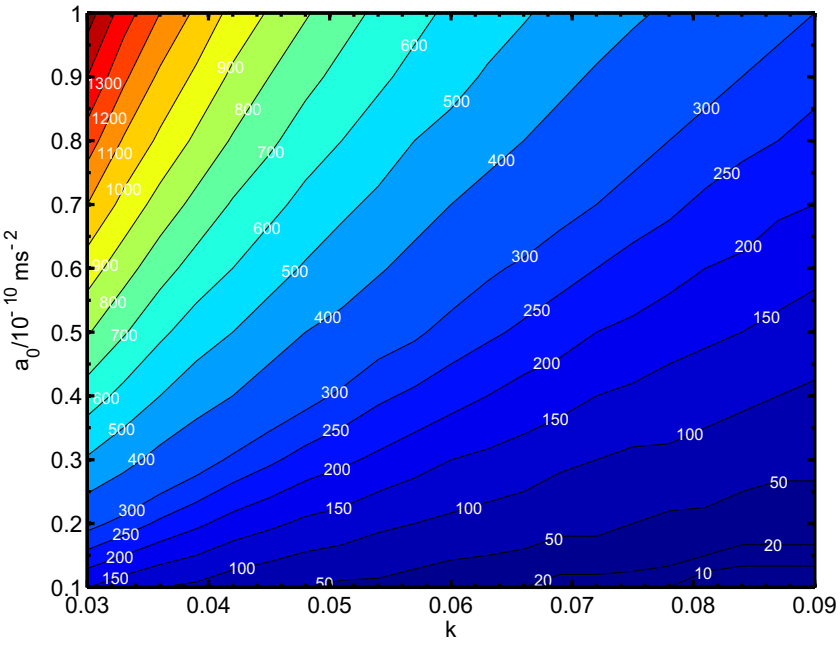

Figure 4.6: Constraints placed on a_0 and κ by a negative result for different impact parameters b (labelling the lines and coding the colours). We pick SNR $= 1$ as the condition on our signal here and then find an upper bound for a_0, κ at a given impact parameter. For a given b, the admissible parameter space would be "outside" the corresponding b line (i.e. towards the right lower corner).

Supposing we get a negative result, what constraints can we place upon a_0 and κ? As in Section 3.4, we may get a preliminary estimate by seeking the region where the SNR for an optimal filter drops below 1. This is plotted Figure 4.6 for various values of b (in this figure, b labels the lines and codes the colours). For a given b, the admissible parameter space is "outside" the corresponding b line (i.e. towards the right-bottom corner). In general, a negative result forces a_0 to be smaller and κ to be larger than the fiducial values, the more so, the smaller the impact parameter b. As we see, if we were to miss the saddle by 1500 km or more, the fiducial values of a_0 and κ would survive a negative result. For an approach any closer, however, a negative result would rule them out and squeeze the parameter space towards the right-bottom corner. For $b \sim 10$ km, the a_0 (the κ) would have to be smaller (larger) than the fiducial values by an order of magnitude.

These constraints may now be combined with other pressures upon the theory, such as those arising from limits on G renormalisation, Big Bang nucleosynthesis, fifth force Solar System tests, galaxy rotation curve data, and cosmological structure formation. However, as advocated in the introduction, by allowing

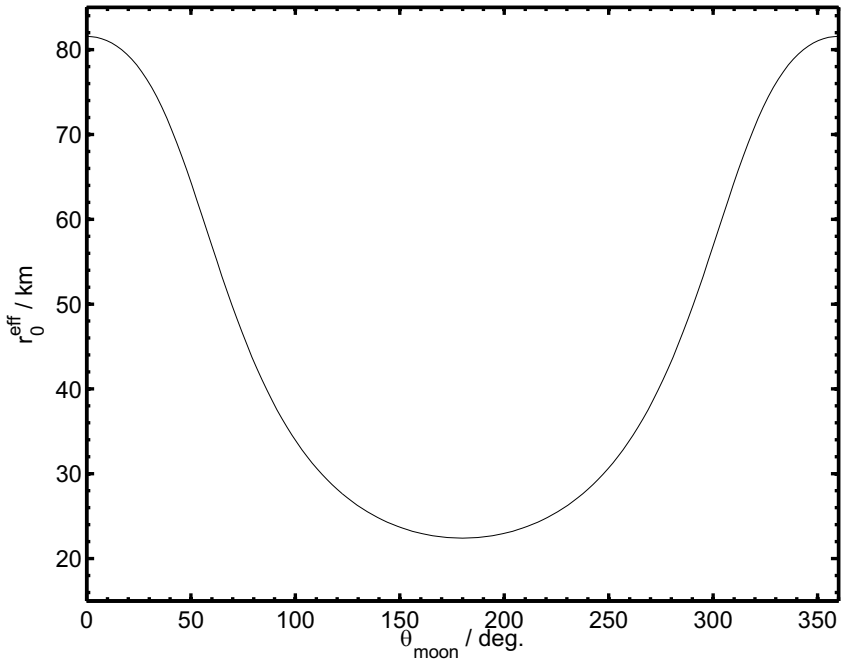

Figure 4.7: The effective MONDian bubble radius r_0 for the Moon-Earth saddle as a function of the lunar phase, where $\theta_{moon} = 0$ deg denotes new Moon and $\theta_{moon} = 180$ deg denotes Full Moon.

complete freedom in a_0 and κ in a saddle test, we have achieved a clear separation of the issues confronting these theories.

4.3.1 The moon saddle as a LPF target

Our techniques can also be applied to a very topical issue: whether the Moon saddle is a good alternative target for LPF. Practical matters may render this saddle more amenable to multiple flybys, an issue that could be essential in dismissing a "false alarm", should a positive detection be found. Application of the algorithm in Section 4.2 to the moon saddle is straightforward (and indeed it motivated the argument presented therein). As noted in [5], r_0 for the Moon saddle is smaller than the 380km found for the Earth-Sun saddle, and this size is more variable, depending strongly on the phase of the Moon (as Figure 4.7 shows, it varies between around 25km and 80km), however as A is bigger, so the tidal stresses have a larger amplitude. Nevertheless, what really matters for SNRs is the FT of the signal as seen in time, with the satellite going through the bubble. The large SNRs obtained for the Sun-Earth saddle result from a miraculous coincidence between the sweet spot in the ASD, and the size of the bubble as transformed

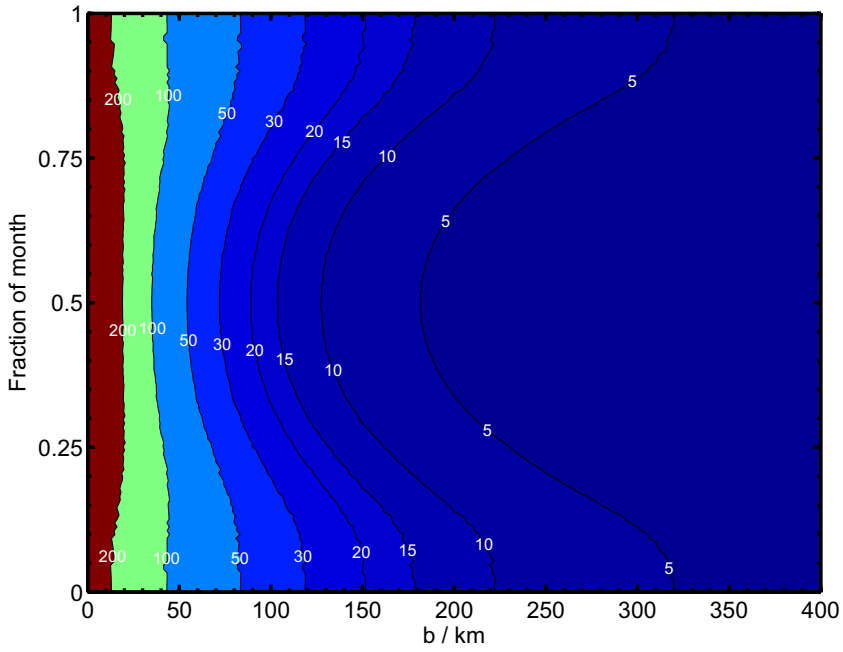

Figure 4.8: SNRs for the Moon-Earth saddle, assuming our best case noise model and approach velocity $v = 0.3$ km s^{-1}, for different impact parameters and day of the month (0 and 1 represent the New Moon, 0.5 the Full Moon). We see that this saddle is less forgiving if you miss it by more than 150 km and more rewarding if you get close to it (SNRs of 200 within reach). If the former, we see that new moons generate higher SNRs.

into a time-signal by the typical velocities found in transfer orbits. This miracle could be spoiled by the smaller size of the Moon saddle.

As it happens, orbits crossing the Moon saddle do so with a smaller velocity, typically smaller than 0.5 km s^{-1}. The two effects, smaller bubble combined with a lower speed, we find in fact counteract one another when converting the bubble signal into a time signal. Therefore it is not surprising that the SNRs predicted for the Moon saddle are as high as those for the Earth saddle (albeit more dependent on the phase of the moon).

In Figure 4.8 we plotted SNRs assuming the "Best Case" noise model (see Figure 3.2.2), for a crossing of the moon saddle at $v = 0.3$ km s^{-1}, with varying impact parameters and for different days of the month. On the y axis we see 0 and 1 represent the New Moon and 0.5 the Full Moon. As we can see, in comparison with the Earth-Sun saddle, we find the moon saddle:

- is less forgiving if we miss by more than 150 km.

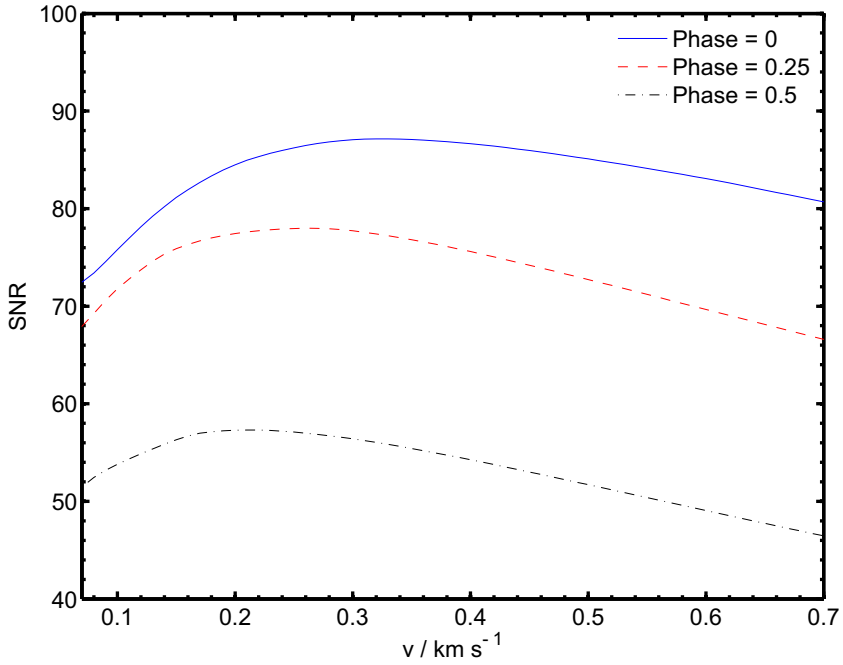

Figure 4.9: SNRs for the Moon-Earth saddle, assuming a standard noise model, impact parameter of $b = 50$km between the New Moon (phase $= 0$) and Full Moon (phase $= 0.5$) for different speeds of approach. We notice that the peak in the signal varies depending on the phase of the moon. Additionally we see that the optimal range of velocities falls around the expected 0.3 km s^{-1} in each case.

- will more rewarding if we get close (with SNRs of 200 within reach).
- depends crucially on the lunar phase, with the new moon producing the best results.

These results show there is great merit in including a moon saddle flyby into the considerations of LPF orbit designers (should a mission extension occur). We consider the impact of approaching the saddle at velocities other than the expected $v = 0.3$ km s^{-1} in Figure 4.9 and find that although the peak in SNR varies at different points in the Moon's cycle, the expected velocity is in the optimal range.

4.4 Varying the Free Function

Suppose that instead of considering rescaling κ and a_0 in our MONDian system, we prefer to alter the μ function. Would similar scaling rules exist? Our aim here is to look at parameterised functions and as a

starting point we will consider μ's of the form:

$$\mu = \frac{z^n}{1+z^n} \tag{4.8}$$

and later we will consider further generalisations (as we will see, the different limits are constrained by very different effects). In such a case we have

$$4m \equiv \frac{d\ln U^2}{d\ln \mu} = \frac{2}{n}\left(n + \frac{1}{1-\mu}\right) \tag{4.9}$$

Now although we cannot (in general) write a closed form for $4m$ in terms of U, we find in the limits

$$z \ll 1 \qquad \mu \approx z^n \Rightarrow 4m \approx \frac{2(n+1)}{n} \tag{4.10}$$

$$z \gg 1 \qquad \mu \approx 1 \Rightarrow 4m \approx \frac{2\,U^n}{n} \tag{4.11}$$

Similarly, the extra acceleration felt by test particles cannot generally be written down as a closed form expression in U, but here we find it can be expressed instead as

$$\delta\mathbf{F} = -\nabla\phi = \frac{4\pi a_0}{\kappa}\mathbf{U}\left(1 + \frac{1}{z^n}\right) \tag{4.12}$$

and from Equations (2.13) and (4.8) it is clear that

$$z \gg 1 \qquad z^n \approx U^n$$

$$z \ll 1 \qquad z^n \approx U^{n/(n+1)}$$

With these results in mind, let us proceed to finding the analytical solutions as before, using the linear Newtonian approximation to solve our system of vector equations, recall (2.17, 2.18):

$$\begin{aligned} \nabla \cdot \mathbf{U} &= 0 \\ 4\,m\,U^2 \nabla \wedge \mathbf{U} + \mathbf{U} \wedge \nabla U^2 &= 0 \end{aligned}$$

4.4.1 QN regime

Given this system of vector equations, we need to specify boundary conditions. For $r/r_0 \gg 1$, we expect the MONDian potential to mimic the Newtonian $\phi \approx \frac{\kappa}{4\pi}\Phi_N$ and so our ansatz has to be of the form

$$\begin{aligned} \mathbf{U} &= \mathbf{U}_0 + \mathbf{U}_2 \\ \mathbf{U}_0 &= \frac{r}{r_0}\mathbf{N}(\psi) \end{aligned}$$

where $\mathbf{U}_2$ will be some subdominant contribution as we move far from the saddle, but a very relevant one closer to the bubble. Additionally although $\mathbf{U}_0$ is curl free, the form of the curl equation (2.18) suggests $\mathbf{U}_2$ could in general have a curl sourced by $\mathbf{U}_0$, satisfying

$$\begin{aligned} \nabla \cdot \mathbf{U}_2 &= 0 \\ \nabla \wedge \mathbf{U}_2 &= -\frac{\mathbf{U}_0 \wedge \nabla |\mathbf{U}_0|^2}{2\,|\mathbf{U}_0|^{n+2}/n} \end{aligned} \tag{4.13}$$

Using the notation

$$\mathbf{U}_2 = U_r \mathbf{e}_r + U_\psi \mathbf{e}_\psi$$

these equations take the form

$$\frac{1}{r^2}\frac{\partial}{\partial r}(r^2 U_r) + \frac{1}{r\sin\psi}\frac{\partial}{\partial \psi}(\sin\psi\, U_\psi) = 0 \tag{4.14}$$

$$\frac{1}{r}\left[\frac{\partial}{\partial r}(r U_\psi) - \frac{\partial U_r}{\partial \psi}\right] = \frac{s_n(\psi)}{r^n} \tag{4.15}$$

$$s_n(\psi) \equiv -3n\frac{2^{3n/2}\sin 2\psi}{(5+3\cos 2\psi)^{1+n/2}} \tag{4.16}$$

and so we have to discuss the effect of varying n on this extra curl force.

The $n = 1$ case

The source function here becomes

$$s_1 \equiv -\frac{6\sqrt{2}\sin 2\psi}{(5+3\cos 2\psi)^{3/2}} \tag{4.17}$$

and Equation (4.15) suggests as ansatz of the form

$$\mathbf{U}_2 = \mathbf{B}_1(\psi) = (F_1(\psi)\mathbf{e}_r + G_1(\psi)\mathbf{e}_\psi) \tag{4.18}$$

This reduces (4.15) to

$$G_1 = F_1' + s_1 \tag{4.19}$$

and hence (4.14) takes the form

$$2F_1 + F_1'\cot\psi + F_1'' = -(s_1' + s_1\cot\psi) \tag{4.20}$$

We can solve this using the standard techniques of inhomogeneous ODEs, to find expansions of F and G

$$\begin{aligned} F_1 &\approx -0.2322 - 0.7201\cos 2\psi + 0.1306\cos 4\psi \\ G_1 &\approx 0.5115\sin 2\psi - 0.0556\sin 4\psi \end{aligned} \tag{4.21}$$

We find the extra acceleration felt by test particles is hence given by

$$\delta\mathbf{F} = -\nabla\phi \approx \frac{4\pi a_0}{\kappa}\mathbf{U}\left(1+\frac{1}{U}\right) \tag{4.22}$$

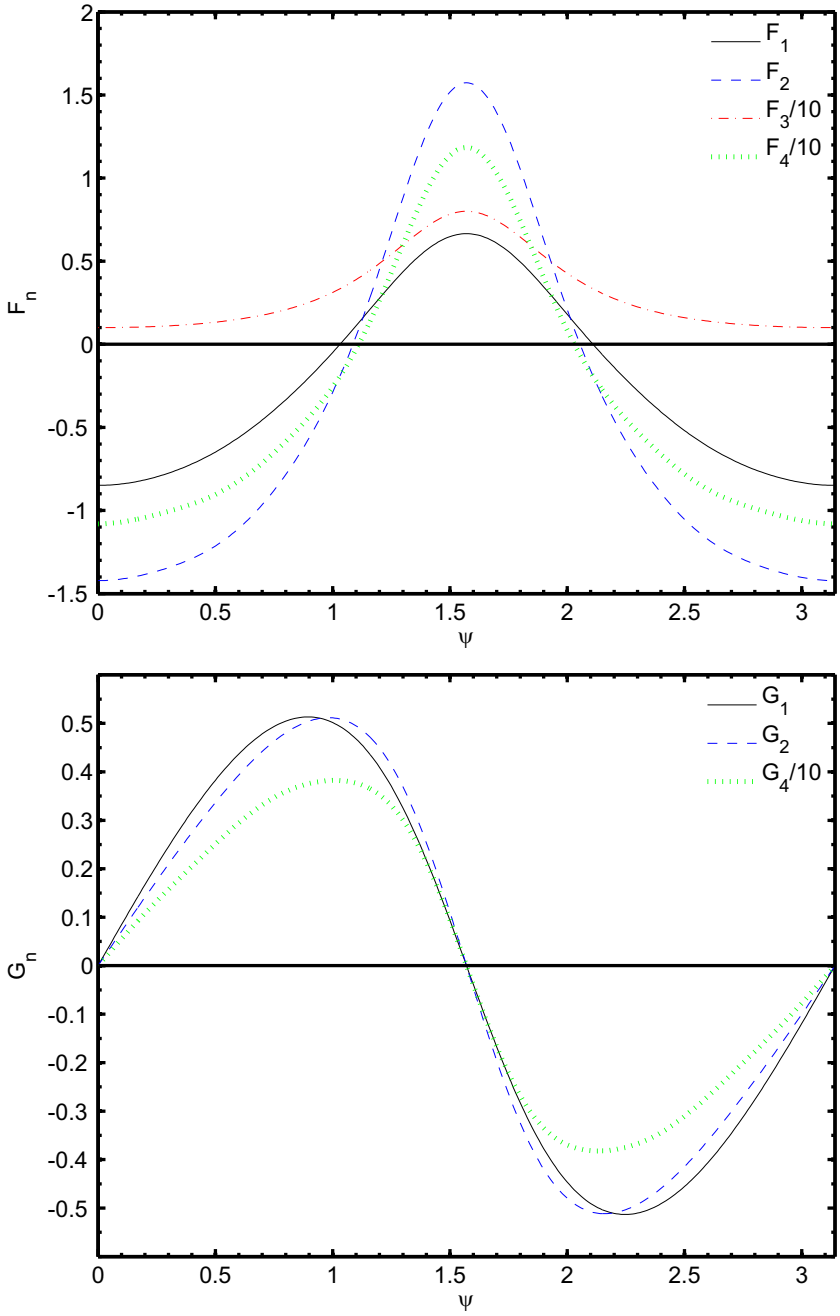

Figure 4.10: The angular profile functions F and G giving the direction of the curl field $B(\psi)$ in the QN region in a few different cases - we omit G_3 here due to it vanishing for all ψ.

which for $U \gg 1$ suggests

$$\delta F \approx \frac{4\pi a_0}{\kappa}\left(\mathbf{U}_0 + \frac{\mathbf{U}_0}{U_0} + \mathbf{U}_2 + ...\right) \tag{4.23}$$

The first term, our $\delta\mathbf{F}_0$, is simply a fully Newtonian term which renormalises the gravitation constant. The second term, our $\delta\mathbf{F}_1$, is here just a rescaled unit vector of the Newtonian potential

$$\delta\mathbf{F}_1 = \frac{16\pi a_0}{\kappa}\frac{\mathbf{N}(\psi)}{\sqrt{10+6\cos 2\psi}} \tag{4.24}$$

The third term, our $\delta\mathbf{F}_2$, is just the curl field contribution

$$\delta\mathbf{F}_2 = \frac{4\pi a_0}{\kappa}\mathbf{B}_1(\psi) \tag{4.25}$$

The $n = 2$ case

In this case, the source reduces to

$$s_2 \equiv -\frac{48\sin 2\psi}{(5+3\cos 2\psi)^2} \tag{4.26}$$

which is just a rescaled solution of those from [41]. The form of (4.15) again suggests both U_r and U_ψ behave as $1/r$, hence we can rewrite our ansatz as

$$\mathbf{U}_2 = \left(\frac{r_0}{r}\right)\mathbf{B}_2(\psi) = \left(\frac{r_0}{r}\right)\left(F_2(\psi)\mathbf{e}_r + G_2(\psi)\mathbf{e}_\psi\right) \tag{4.27}$$

Summarising the results of the calculation here, we find the ansatz collapses equation (2.34), allowing a simple separation of the components of $\mathbf{U}$:

$$\begin{aligned} F_2 &= \frac{8}{5+3\cos 2\psi} + A \\ G_2\sin\psi &= 4\frac{\tan^{-1}(\sqrt{3}-2\tan\frac{\psi}{2}) + \tan^{-1}(\sqrt{3}+2\tan\frac{\psi}{2})}{\sqrt{3}} + A\cos\psi + B \end{aligned} \tag{4.28}$$

finding A, B after imposing the conditions of homogeneity and continuity and that at the boundaries of the bubbles we only have a radial force component (akin to the Newtonian), ie $G(\psi = 0) = G(\psi = \pi) = 0$,

$$A = B = -\frac{4\pi}{3\sqrt{3}}$$

We can then insert this expression into the expansion in equation (4.12) for $\delta\mathbf{F}$ with $U \gg 1$ as before.

The $n = 3$ case

Here the source function becomes

$$s_3 \equiv -\frac{144\sqrt{2}\sin 2\psi}{(5 + 3\cos 2\psi)^{5/2}} \tag{4.29}$$

We find solutions using a separable ansatz of the form

$$\mathbf{U}_2 = \left(\frac{r_0}{r}\right)^2 \mathbf{B}_3(\psi) = \left(\frac{r_0}{r}\right)^2 (F_3(\psi)\mathbf{e}_r + G_3(\psi)\mathbf{e}_\psi) \tag{4.30}$$

with profile functions

$$\begin{aligned} F_3 &= \frac{16\sqrt{2}}{(5 + 3\cos 2\psi)^{3/2}} \\ G_3 &= 0 \end{aligned} \tag{4.31}$$

which satisfy the boundary conditions.

Other cases

For some power $n \geq 1$, we can make a more general ansatz as

$$\mathbf{U}_2 = \left(\frac{r_0}{r}\right)^{n-1} \mathbf{B}_n(\psi) = \left(\frac{r_0}{r}\right)^{n-1} (F_n(\psi)\mathbf{e}_r + G_n(\psi)\mathbf{e}_\psi) \tag{4.32}$$

which we find now does not collapse (4.15), but rather by combining with (4.14), we get a second order

sourced ODE for F_n in

$$F_n(n-2)(n-3) + F_n' \cot\psi + F_n'' = -(s_n' + s_n \cot\psi) \tag{4.33}$$

and from (4.15)

$$(2-n)G_n - F_n' = s_n \tag{4.34}$$

The homogenous solutions of equation (4.33) are simply Legendre polynomials in $\cos\psi$ of order $(n-2)$ and the full inhomogenous solution can be found using standard ODE techniques. We find a generic feature of solutions in this regime is that

$$(\delta\mathbf{F}_1 + \delta\mathbf{F}_2) \propto \frac{1}{r^{n-1}} \tag{4.35}$$

and since further terms in $\delta\mathbf{F}$ tail off ever faster, the relative importance of the curl terms becomes diminished in the large n limit. Also our initial requirement on z that $n \geq 1$ means at worst $U_2 \propto r^0$, which will still be "washed out" for $r/r_0 \gg 1$ in comparison to the Newtonian background.

4.4.2 DM regime

Recall our vacuum equations, here in the coordinate form

$$\frac{1}{r^2}\frac{\partial}{\partial r}\left(r^2 U_r\right) + \frac{1}{r\sin\psi}\frac{\partial}{\partial\psi}(\sin\psi\, U_\psi) = 0$$
$$\left[\frac{4m}{r}\left(\frac{\partial(rU_r)}{\partial r} - \frac{\partial U_\psi}{\partial\psi}\right) + \left(\frac{U_r}{r}\frac{\partial}{\partial\psi} - U_\psi\frac{\partial}{\partial r}\right)\right] U^2 = 0$$

given $4m \to$ constant, our rescaling symmetry is present once again - suggesting a separable ansatz of the form

$$\mathbf{U} = C\left(\frac{r}{r_0}\right)^{\alpha-2}(F(\psi)\mathbf{e}_r + G(\psi)\mathbf{e}_\psi)$$

We will look for solutions which keep U small but make the tidal stresses increasingly divergent as $r/r_0 \ll 1$. We find a pair of coupled ODEs for F and G

$$G' + G\,\cot(\psi) + \alpha F = 0 \tag{4.36}$$

$$F\frac{d(F^2+G^2)}{d\psi} + 2[\alpha' G - 2mF'](F^2+G^2) = 0 \tag{4.37}$$

where we should be clear to distinguish between the radial exponent α and the extended variable α'

$$\alpha' = \alpha(2m-1) + 2(1-m) \tag{4.38}$$

The MONDian force takes the form

$$\delta\mathbf{F} = -\nabla\phi \approx \frac{4\pi a_0}{\kappa}\frac{\mathbf{U}}{U^{\frac{n}{n+1}}} \tag{4.39}$$

which we rewrite in a separable form as

$$\delta\mathbf{F} \approx \frac{4\pi a_0}{\kappa}\,C^{\frac{1}{n+1}}\left(\frac{r}{r_0}\right)^{\frac{\alpha-2}{n+1}}\frac{\mathbf{D}}{D^{\frac{n}{n+1}}} \tag{4.40}$$

where $\mathbf{D}$ is the angular profile in the DM regime. We see $\alpha < n+3$ yields divergent tidal stress solutions. Requiring $n \geq 1$ puts bounds on m as

$$\frac{1}{2} < m \leq 1 \tag{4.41}$$

by substituting in m and which after some manipulation, we find divergent solutions for

$$\alpha < \frac{6m-2}{2m-1} \tag{4.42}$$

and from inverting equation (4.38)

$$\alpha = \frac{\alpha' + 2(m-1)}{2m-1} \tag{4.43}$$

this makes our bound $\alpha' < 4m$ and so $\alpha' \leq 4$. From similar considerations, we see that from requiring $U \ll 1$, $\alpha > 2$ in all cases. These bounds are required when picking out the particular α needed, from the sequence of possible solutions which satisfy the equations and are regular.

The $m = 1$ case

If we consider solutions with $m = 1$ (equivalent to $n = 1$), we are guided to pick $\alpha' = \alpha \approx 3.528$ (allowing us to use the results from Section 2.2) with profile functions

$$\begin{aligned} F_1 &\approx 0.2442 + 0.7246\cos 2\psi + 0.0472\cos 4\psi \\ G_1 &\approx -0.8334\sin 2\psi - 0.0368\sin 4\psi \end{aligned} \tag{4.44}$$

The $\frac{1}{2} < m < 1$ case

Here, we have $\alpha' \neq \alpha$ and so we need to find new solutions to Equations (4.36 - 4.37). We find solutions which neglect the derivative term in (4.37) as

$$\begin{aligned} F &= a\cos\psi \\ G &= \mp a\sin\psi \end{aligned} \tag{4.45}$$

(where a is a constant) here with values of $\alpha_\pm$ given by

$$\alpha_+ = 2 \tag{4.46}$$

$$\alpha_- = \frac{2}{1-2m} \tag{4.47}$$

but in fact the α_- solution only exists when $m = 1$, otherwise Equations (4.36 - 4.37) will not be simultaneously satisfied. We also find regular solutions exist for a discrete sequence of $\alpha(n)$'s for each power n: $\{..., \alpha_{-1}, \alpha_\pm, \alpha_1, ...\}$, however now we have lifted the degeneracy that $\alpha_{-i} = -\alpha_i$ (which only exists in the $n = 1$ case).

For $n = 2$, we have solutions for $\alpha_{-1} \approx -5.206$, $\alpha_1 \approx 3.983$ and we pick solutions where $2 < \alpha < 5$, nicely selecting out α_1, with angular profile functions as

$$\begin{aligned} F_2 &\approx 0.2485 + 0.7373\cos 2\psi + 0.0598\cos 4\psi \\ G_2 &\approx -0.9570\sin 2\psi - 0.0578\sin 4\psi \end{aligned} \tag{4.48}$$

Similarly for $n = 3$, we have $2 < \alpha < 6$ and so $\alpha_1 \approx 4.4057$, with angular profile functions

$$\begin{aligned} F_3 &\approx 0.2574 + 0.7667\cos 2\psi + 0.0624\cos 4\psi \\ G_3 &\approx -1.1099\sin 2\psi - 0.0756\sin 4\psi \end{aligned} \tag{4.49}$$

and we compare a few angular profiles in Figure 4.11.

The $m = \frac{1}{2}$ case

In this large n limit, μ effectively becomes a step function. We have $\alpha' = 1$ and find Equation (4.37) reduces to

$$F\frac{d(F^2+G^2)}{d\psi} + 2[G - F'](F^2+G^2) = 0 \tag{4.50}$$

which can be further manipulated to just

$$\frac{d}{d\psi}\left(\frac{F}{G}\right) = 1 + \left(\frac{F}{G}\right)^2 \tag{4.51}$$

with the simple solution of

$$F = G\tan(\psi + C_1) \tag{4.52}$$

and we pick $C_1 = \pm\pi/2$ to satisfy the boundary conditions. Inserting this into Equation (2.51) gives

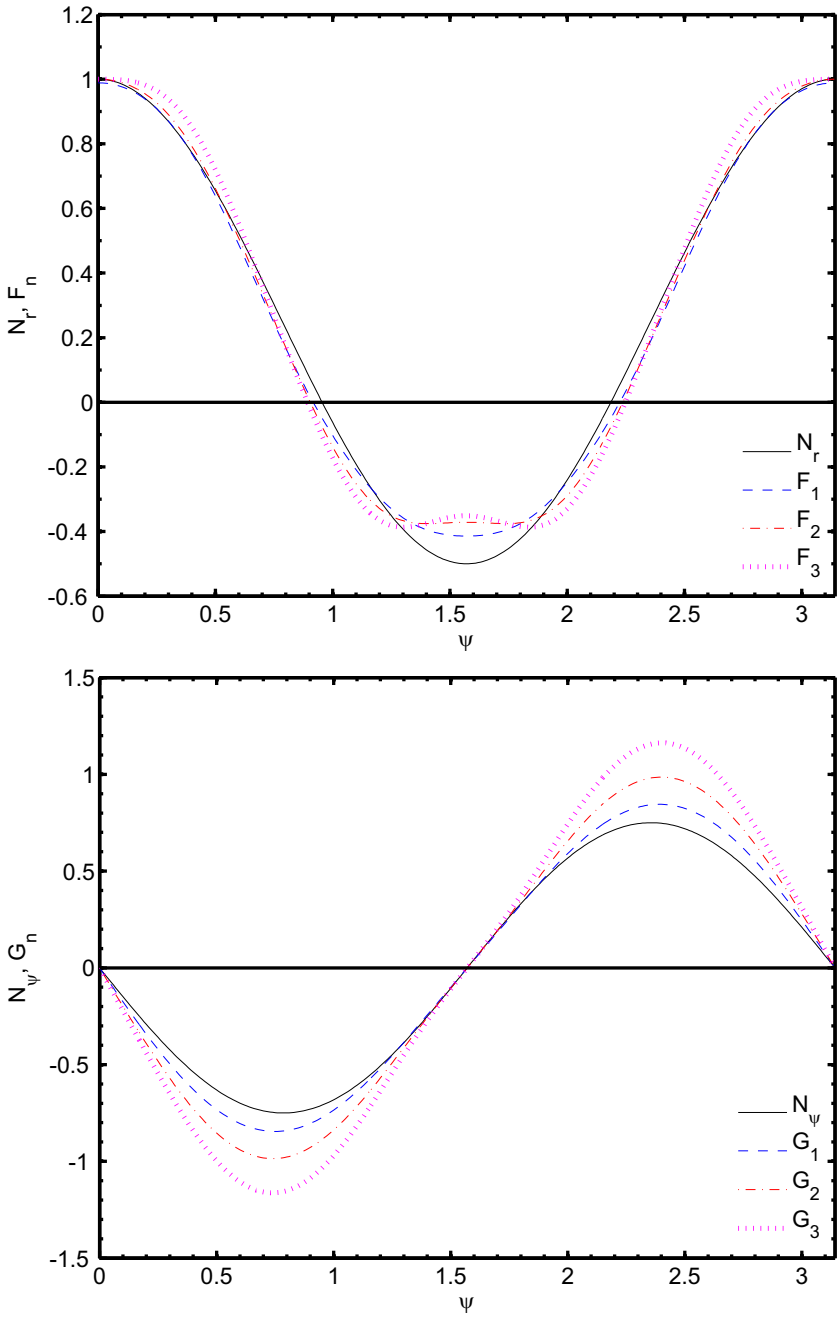

Figure 4.11: A few numerically determined angular profile functions F_n and G_n in the DM region (dotted) compared with the Newtonian profile functions N_r and N_ψ (solid), in each figure respectively. Note the relative invariance of the radial profile and the slight changes in the azimuthal profile.

solutions of the form

$$\begin{aligned} F &= \mp C_2 \cos\psi \, (\sin\psi)^{\alpha-2} \\ G &= C_2 (\sin\psi)^{\alpha-1} \end{aligned}$$

This guides us to pick $C_2 = \mp 1$ and $\alpha = 2$ here, giving

$$\begin{aligned} F &= \cos\psi \\ G &= \mp \sin\psi \end{aligned} \tag{4.53}$$

which mimic the $\alpha = 2$ solutions seen previously. In this extreme case, the additional MONDian force is

$$\delta\mathbf{F} \rightarrow \frac{4\pi a_0}{\kappa} \frac{\mathbf{D}}{D} \tag{4.54}$$

which gives tidal stresses of the form

$$S_{ij} \propto r^{-1} \tag{4.55}$$

which obviously diverges as we approach the saddle (although the divergence is now relatively weaker than the "rule of thumb" approach to MONDian tidal stresses suggests).

4.4.3 Type II theories

An important point to consider is what are the analogous effects of changing free functions in other classes of MONDian theories. For type II theories, changes to each of the regimes are easy to include in the computation of the sourced Poisson equation, as we saw in Section 3.5. Given here

$$\nabla^2\phi = \frac{\kappa}{4\pi} \nabla \cdot (\nu \nabla \Phi_N) = r \, C_1 \, \mathbf{N} \cdot \nabla \nu(r, \psi)$$

where $\nu = \nu(w)$, $w = |\mathbf{U}_0|$ and C_1 is some constant and we used an ansatz of the form

$$\phi = C_2\, r^a\, F_n(\psi)$$

where C_2 is another constant. For some generalised DM limit taking the form $(F_\phi)^{n+1} \propto F_N$,

$$\nu \to \left(\frac{1}{w}\right)^{\frac{n}{n+1}}$$

This fixes the radial exponent a as

$$a = \frac{n+2}{n+1}$$

and also fixes the sourced ODE for the profile function

$$a(a+1)F_n + \cot\psi\, F_n' + F_n'' = g(\psi, n) \tag{4.56}$$

with generalised source term

$$g(\psi, n) = (7 + 9\cos 2\psi)\left(\frac{2^{n-2}}{(5+3\cos 2\psi)^{3n+2}}\right)^{\frac{1}{2(n+1)}} \tag{4.57}$$

Given the results of sourced ODEs like this from Section 4.4.1, it seems unlikely therefore, that in this regime the solutions will remain similar, in stark contrast to the relative invariance of the DM limit in the type I theories. In the QN regime, a similar system of ODEs exist, with varying source functions and parameters depending on the form of the falloff from $\nu \to 1$ and hence a similar conclusion can be reached. A more detailed study of these generalised solutions however we leave for future work.

4.4.4 An intermediate regime

While we have a clear idea of the dynamics of $\mathbf{U}$ in the large and small acceleration regimes, we lack detail in the "near field" or intermediate regime (around $z \simeq 1$), except when we can estimate the size of the DM bubble. Our work thus far has focused on finding the form and solutions to equation (2.18) in

each limit, however really we only need to start at the form of the $4m$ and see how it scales in each limit. We begin by considering the leading order term of $4m$ to be of the form $\sim U^q$ (where q is some power to be found). We begin with the expression

$$\xi = \frac{4m}{C_q U^q} \tag{4.58}$$

where C_q is simply some dimensionless constant and first derive our results in the two well understood regimes. For the $\mu(n)$ models,

$$\xi = \frac{2(n+1+z^n)}{nC_q z^q}\left(1+\frac{1}{z^n}\right)^q \tag{4.59}$$

and we seek solutions for $\xi \to 1$ in each limit. In the $z \ll 1$ regime,

$$\xi \to \frac{2(n+1)}{nC_q}\frac{1}{z^{(n+1)q}} \tag{4.60}$$

which can only approach unity when $q = 0$ and

$$C_q = \frac{2(n+1)}{n} \tag{4.61}$$

as before. Similarly in the $z \gg 1$ limit,

$$\xi \to \frac{2}{nC_q} z^{n-q} \tag{4.62}$$

hence for unity $q = n$ and as before

$$C_q = \frac{2}{n} \tag{4.63}$$

The real power of this technique can be exploited to attempt to solve these models around some general point $z \simeq z_0$, which has the expansion:

$$\xi C_q|_{z_0} \approx 1 + \frac{nz_0^n(1+z_0^n) - q(1+n+z_0^n)^2}{z_0(1+z_0^n)(1+n+z_0^n)}(z-z_0) + \mathcal{O}((z-z_0)^2) \tag{4.64}$$

with dimensionless scaling of the form

$$C_q|_{z_0} = \frac{2}{n}\left(\frac{z_0^{1+n}}{1+z_0^n}\right)^{-q}(1+z_0^n+n) \tag{4.65}$$

which we can solve at first order for q,

$$q|_{z_0} = \frac{z_0^2(1+z_0^n)n}{(1+z_0^n+n)^2} \tag{4.66}$$

and seeing again that in the large and small z_0 limits, we recover the necessary behaviour for U^q. Around $z \simeq 1$, we find the behaviour

$$q = \frac{2n}{(2+n)^2} \tag{4.67}$$

$$C_q = \frac{(2+n)}{n}2^{q+1} \tag{4.68}$$

and here q is bounded for $n \geq 1$ as

$$0 < q \leq \frac{2}{9}$$

meaning that for large n, $C_q \to 2$, akin to an asymptotic DM regime in the large n limit. We plot the full ξ profile to demonstrate the relative stability of this limit around $z \simeq 1$ for different n's in Figure 4.12. We see that, in general, $4m$ is not going to a constant here and so are guided to pick QN-like perturbative solutions, as before taking $\mathbf{U} = \mathbf{U}_0 + \mathbf{U}_2$ with

$$\mathbf{U}_2 = \left(\frac{r}{r_0}\right)^{1-q}\mathbf{B}_q(\psi) \tag{4.69}$$

4.5 An Application - Transients

One important use of these techniques is to look at how different power law transients from $\phi \to \frac{\kappa}{4\pi}\Phi_N$ affect our results and perhaps examine how to rescale existing templates for different μ functions. Whilst the $\mu(n)$ model presents a nice parameterisation here, we should also consider multi-parameter families

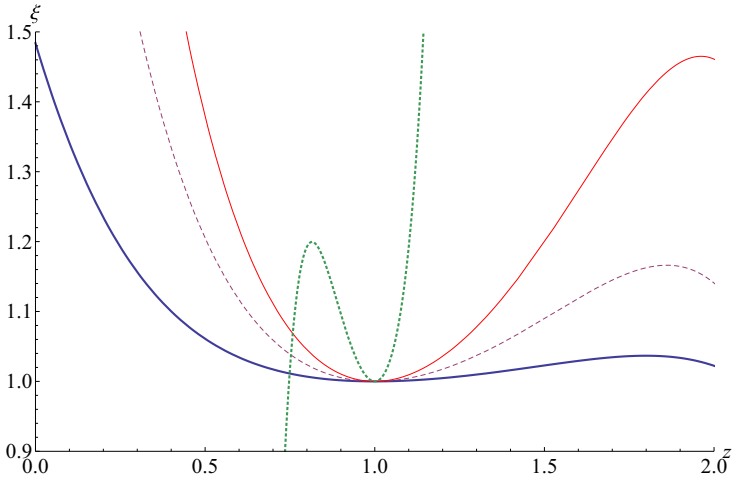

Figure 4.12: The ratio ξ plotted for $z \sim 1$ (for different values of n). The blue (bold) line being $n = 1$, the purple (dashed) line $n = 2$, the red (solid) line $n = 3$ and the green (dotted) line $n = 20$. As we see, for small n, in this regime these models are relatively stable.

of functions, given that the various regimes are constrained by complementary but different physical phenomena. Our usual DM limit with $\mu \propto z$, is motivated by the theory being a good dark matter replacement on low acceleration scales (as we motivated in Section 1.2). Let's consider dropping this requirement *a priori*, working with some generalised limit of $\mu \propto z^n$, and then introduce later (as necessary). In the QN limit, the fall-off from $\mu \to 1$ is governed by agreement with bounds on fifth forces Solar System [8]. We see, therefore, it is prudent to consider at least a two parameter family of free functions. We can consider free functions of the form

$$\mu = \frac{z^a}{(1+z^b)^{a/b}} \tag{4.70}$$

and then as before, we compute

$$\begin{aligned} 4m &= \frac{2}{a}\left(a + \frac{1}{1-\mu^{b/a}}\right) \\ \delta\mathbf{F} &= \frac{4\pi a_0}{\kappa}\,\mathbf{U}\left(1+\frac{1}{z^b}\right)^{a/b} \end{aligned} \tag{4.71}$$

where $z^b \approx U^b$ in the QN regime and $z^b \approx U^{b/(a+1)}$ in the DM regime. For these functions, the intermediate scaling parameter has the form around $z \simeq 1$ of:

$$q = \frac{2b}{(2+a)^2} \tag{4.72}$$

which is clearly greater than unity for $a = 1$ and $b \geq 5$, suggesting that the QN-like behaviour must have already been triggered before $z \simeq 1$, since these intermediate solutions already display the asymptotic-like behaviour (albeit with a "stronger" curl term - in the $z \gg 1$ regime here, $U_2 \propto r^{1-b}$).

We can consider some arbitrary model for $\mu(z)$, where each regime takes the form

$$\mu \simeq \sum_{n=p}^{\infty} a_n z^n \qquad z \ll 1 \tag{4.73}$$

$$\mu \simeq 1 - \sum_{n=q}^{\infty} \frac{b_n}{z^n} \qquad z \gg 1 \tag{4.74}$$

we see each a_n and b_n as telling us the leading order ($n = p, q$) and higher terms of each expansion, with $p, q \geq 1$ in all cases. In the DM regime, we find

$$4m \simeq 2\left(1 + \frac{\mu}{p\, z^p}\frac{1}{a_p}\right) \to \frac{2(p+1)}{p} \tag{4.75}$$

where p is the exponent of the leading order term in $\mu(z)$. We compute the term μ/z^p from Equation (4.73), however at leading order this is obviously a constant - explaining why there is little variability in this limit. Similarly, in the QN limit, we find (using $U \simeq z$ here)

$$4m \simeq \frac{2}{U}\left(\frac{U^{q+1}}{q}\frac{1}{b_q}\right)\left(1 - \sum_{n=q+1}^{\infty}\frac{n b_n}{U^{n+1}}\right) \to \frac{2\,U^q}{q\,b_q} \tag{4.76}$$

where q is the exponent of the leading order term in the expansion of $\mu(z)$. As this result shows, here we are very much at the mercy of the free function we pick - naturally giving rise to the menagerie of solutions we found in Section 4.4.1.

Given these results, perhaps we can consider a similar scaling argument for tidal stresses, akin to

that presented in Section 4.2. A naive approach would be to just consider a window function (as we attempted in Section 3.3.3), which preserves templates for $r < r_0$ (which we can now motivate by the observed relative invariance of the profile functions in this limit), but rescales them altogether differently outside of this. There are however a couple of points that any rescaling algorithm needs to take into account:

1. **The Matching** The constant C in the DM solution is poorly constrained analytically and up to now has only been measured by looking at the ratio of numerical results to $C = 1$ analytical values (over the range $r/r_0 = 0.05 \to 0.5$). Care needs to be taken that the correct normalisation for any rescaled tidal stresses is found.

2. **Loss of Signal** Since our analytical results are valid for $r/r_0 \ll 1$, the nature of the window function could cause us to loose some signal when we rescale. Although these losses would be small compared to the signal deep inside the bubble, at the periphery and in the QN regime, noticeable losses could occur if a naive rescaling is done.

To investigate such issues, we need to consider how the tidal stresses change when we vary the azimuthal and radial components of the MONDian force ($\mathbf{F}_\phi(r, \psi)$). Although in general, our observable tidal stresses take the form

$$S_{ij} = -\frac{\partial^2 \phi}{\partial x_i \partial x_j} + \frac{\kappa}{4\pi} \frac{\partial^2 \Phi^N}{\partial x_i \partial x_j}$$

for simplicity, we will compute $S_{yy}(\mathbf{x})$. It is easy to see however that with a suitable coordinate change, any tidal stress component could be picked. From the form of Equation (4.40), we see we can write the MONDian force (in the linear regime) in the DM region as

$$\begin{aligned} F_r &= C_1\, r^\gamma\, f(\psi) \\ F_\psi &= C_1\, r^\gamma\, g(\psi) \end{aligned} \tag{4.77}$$

where we define

$$\begin{aligned} \gamma &= \frac{\alpha(n)-2}{n+1} \\ C_1 &= \frac{4\pi a_0}{\kappa}\frac{C^{\frac{1}{n+1}}}{r_0^{\gamma}} = \kappa A \frac{C^{\frac{1}{n+1}}}{r_0^{\gamma-1}} \end{aligned}$$

The tidal stresses therefore are

$$S_{yy} = \frac{C_1}{2} r^{\gamma-1}(f(1+\gamma+(1-\gamma)\cos 2\psi) + (g(\gamma-1)+f')\sin 2\psi + 2g'\cos^2\psi)) + \frac{C_2}{2} \quad (4.78)$$

where $C_2 = \frac{\kappa}{4\pi}A$ is the rescaled Newtonian tidal stress at the saddle. We see clearly the previous results for rescaling κ, a_0 remain, such that $S_{yy} = \kappa A H_{yy}(r/r_0)$. Additionally now the effect of changing the exponent in $\mu \simeq z^n$ is clear, the effects are mediated through the variable $\gamma(\alpha(n))$. As Figure 4.11 shows, there is an approximate invariance of the profile functions in this regime, such that

$$\begin{aligned} F_n(\psi) &\simeq F_1 \simeq N_r \\ G_n(\psi) &\simeq \xi(n) N_\psi \end{aligned} \quad (4.79)$$

where $\xi(n)$ is some dimensionless linear scaling (for small n, we see $\xi \simeq 1$). As this shows, a naive window function rescaling of the tidal stresses runs the risk of ignoring relevant scalings dependent on $\gamma(\alpha(n))$ and C. Similarly for the QN regime, in the linear regime, the forces take the form suggested by Equation (4.23):

$$\begin{aligned} F_r &= C_2\, N_r(\psi)\, r + C_3\, f(\psi)\, r^{1-n} \\ F_\psi &= C_2\, N_\psi(\psi)\, r + C_3\, g(\psi)\, r^{1-n} \end{aligned} \quad (4.80)$$

with

$$C_3 = \frac{4\pi a_0}{\kappa} r_0^{n-1} = \kappa A r_0^n$$

and hence the tidal stresses are

$$S_{yy} = \frac{C_3}{2} r^{-n}(f(2+n(\cos\psi-1))+2\cos\psi(\sin\psi(f'-ng)+g'\cos\psi) \tag{4.81}$$

Here clearly we can try to play the same game with f, g - however we are hampered by the fact that the curl term has more variance between models.

Another issue that must be addressed is the effect of the MONDian scaling C in these models. It would be telling if the scaling could indeed be a function of the parameters (perhaps n) in some way. Using the same techniques employed before, we reran our adaptive mesh code (presented in Section 2.3 with simple adaptations detailed in Appendix B) with smaller grids, to compute the ratio of analytical results (*a priori* with $C = 1$) and the numerical results for $r/r_0 = 0.1 \to 0.5$. As Figure 4.13 shows, the results are a little surprising. To try and make some sense of these findings, we will need to look more closely at the matching between the regimes here and find the existence of three types of relevant constant in our system of equations:

- **DM regime** For $z \ll 1$, $4m \to C^{DM}$, which becomes relevant when computing the exponent $\alpha(n)$ in the DM regime solutions.
- **Departures from renormalised** G_N, expanding μ in the $z \gg 1$ limit gives

$$\mu^{-1} \simeq 1 + \frac{C_1^\mu}{z^p} + \frac{C_2^\mu}{z^{2p}} + \dots \tag{4.82}$$

  where for consistency we match each C_i^μ by expanding out μ^{-1} - we see that the coefficients parameterise the departures (at each order) from the usual Newtonian limit.

- **QN regime** For $z \gg 1$, $4m \to U^p/C^{QN}$ where p is the leading order power relevant in the expansion of m, such that we rewrite Equation (2.29) in the form of

$$\nabla \wedge \mathbf{U}_2 = \underbrace{-\frac{\mathbf{U}_0 \wedge \nabla|\mathbf{U}_0|^2}{|\mathbf{U}_0|^{p+2}}}_{\nabla\wedge\mathbf{U}_2^r} C^{QN} \tag{4.83}$$

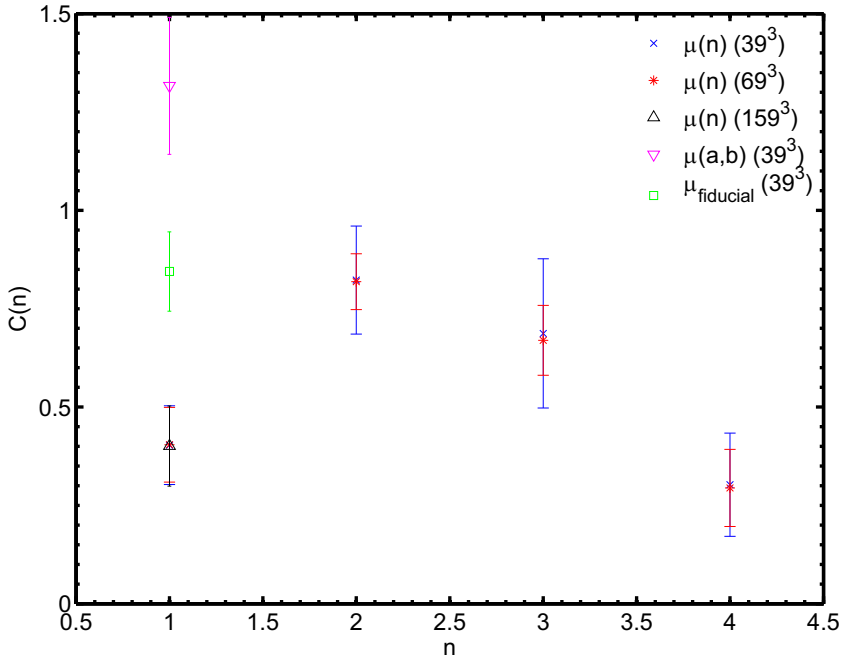

Figure 4.13: Deep MONDian scaling C for different μ parameterisations, using different lattice sizes. We measured the ratio of the linear solutions compared to the full numerical solutions for $r/r_0 = 0.1 \to 0.5$ (since the smaller lattice sizes mean poorer resolution for small r, we raised the starting cutoff). As we see, whilst the errors reduce, the behaviour in n remains as we increase the lattice size (suggesting these effects are not artifacts). An important note is that in order to produce results quickly, models were compared for runtimes of just eight hours, meaning the majority of the error in the $n = 1$ case results from the different lattice sizes all having roughly equal convergence at the end of their run. Such a result varies for different n, however we use it as a "first go" at computing $C(n)$ and suggest that it is unfeasible to rerun our codes for each variation in μ to find C. For comparison, we also present the original scaling for our fiducial μ, as well as a $\mu(a, b)$ model (with $a = 1$, $b = 2$).

where $\mathbf{U}_2^r$ is the (renormalised) curl term (which is just a function of $\mathbf{U}_0$ and exponent p, but free of any scalings) and C^{QN} is the model dependent scaling. As Equation (4.76) shows however, this is related to the expansion of μ as

$$C^{QN} = \frac{p}{2} C_1^{\mu} \tag{4.84}$$

but we will use this notation to be clear where each contribution arises from.

We summarise the values of these for various parameterisations in Table 4.1 and bring attention to the fact that in the $\mu(a, b)$ model, the DM regime parameter a plays a role in both regimes, whilst the $\mu(n)$ model is relatively constrained in the parameter space. Since we require the MONDian force be smooth and continuous, the matching between the different regimes must occur here. From equation (4.12) we

Table 4.1: Scaling Constants for Various Models of μ

$C^{\#}$	$\mu_{fiducial}$	$\mu(n)$	$\mu(a,b)$
C^{DM}	4	$\frac{2(n+1)}{n}$	$\frac{2(a+1)}{a}$
C^{QN}	$\frac{1}{4}$	$\frac{n}{2}$	$\frac{a}{2}$
C_1^{μ}	$\frac{1}{4}$	1	$\frac{a}{b}$
C_2^{μ}	$\frac{1}{32}$	0	$\frac{a(a-b)}{2b^2}$
C_3^{μ}	$-\frac{1}{128}$	0	$\frac{a(a-b)(a-2b)}{3b^3}$

see that

$$\delta\mathbf{F} = \frac{4\pi a_0}{\kappa}\frac{\mathbf{U}}{\mu}$$

which put together with these model independent parameters, in the QN regime, reads as the not unfamiliar expression of:

$$\frac{\mathbf{U}}{\mu} \approx \underbrace{\mathbf{U}_0}_{\mathcal{O}(r^1)} + \underbrace{C_1^{\mu}\frac{\mathbf{U}_0}{U_0^p} + C^{QN}\mathbf{U}_2^r}_{\mathcal{O}(r^{1-p})} + \dots \tag{4.85}$$

where the higher order terms are $\mathcal{O}(r^{1-2p})$ or smaller and represent more complicated combinations of U_0 and U_2^r (see Appendix C for more details). We will match this to the DM force

$$\frac{\mathbf{U}}{\mu} \approx C^{1/(\ell+1)}\left(\frac{r}{r_0}\right)^{(\alpha-2)/(\ell+1)}\frac{\mathbf{D}_\ell}{(D_\ell)^{\ell/(\ell+1)}} \tag{4.86}$$

where ℓ is the leading order exponent in the expansion of μ for $z \ll 1$ and in reality $\alpha = \alpha(C^{DM})$.

Table 4.2: Comparison of Numerical and Matched C Scalings

μ	C_{num}	C_{mat}
$\mu_{fiducial}$	0.8445	-
$\mu(n=1)$	0.4042	0.4050
$\mu(n=2)$	0.8186	0.7903
$\mu(a=1;b=2)$	1.3163	1.3723

While matching the QN and DM regimes to find the scaling C might seem dubious, note that we seek

not to predict the actual values of $C(n)$ (since that would doubtless require knowledge of the system beyond linear order) but rather the scaling *between different* C's. In this way, we assume stricter validity in the linear regime but a more approximate one outside of this (as we have previously suggested with scaling rules). We provide more details about the matching in Appendix C, the broad conclusion being the variation in C between models is an issue that can be dealt with. As Table 4.2 shows, we can predict relatively well how C should scale without resorting to full numerical investigations. Naturally we should question the effectiveness of using these (so-called) "shooting" methods to interpolate between these disparate regimes. Such techniques are commonplace in the field of numerical relativity, where matching asymptotic solutions to those close to a horizon, whilst maintaining regularity, is required. Recent work, however, has looked towards modeling curvature changes as akin to that of heat flows [74, 75]. Such Ricci flow techniques allow for a much cleaner determination of a systems dynamics, without the need for fine-tuning of parameters. We leave the application of these spectral methods for future work.

One bit of house keeping would be to reconsider the effect of the DM scaling in the case of the window function (see Section 3.3.3), involving an exponential fall off for the tidal stresses outside the DM bubble. Naturally if this was a properly motivated model, with behaviour designed to have a sharp fall off (e.g. in the Solar System to avoid conflict with constraints), then the scaling would be different, as we have just shown in this section. Here we present the effect of the sharp fall off on the SNRs, as Figure 4.14 shows, there is only a marginal difference between the original and adjusted results (compared with Figure 3.10). As an illustration of the effects from a more radical scaling, we also present there the effects of a $C \to C/3$ rescaling, which produces a much more apparent result.

4.6 Diverging μ Models

We can, using these techniques, consider altogether different models of free function, such as those which are naturally divergent, as we introduced in Section 3.3.

$$z = \frac{\kappa}{4\pi} \frac{\mu}{\frac{\kappa}{4\pi} + \beta\mu} \frac{1}{(1-\mu)^n} \tag{4.87}$$

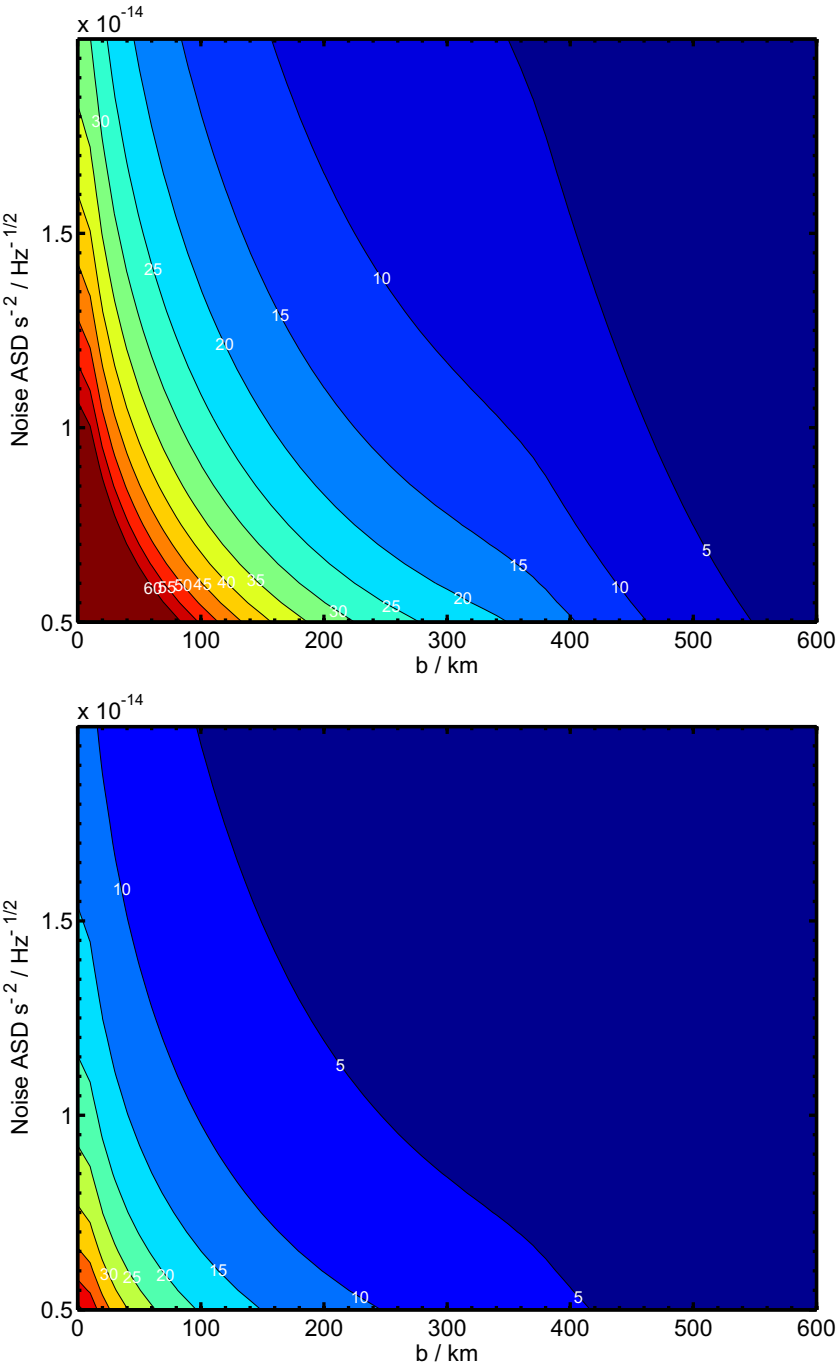

Figure 4.14: Signal to Noise ratio contours for different baseline noise and impact parameters of LPF considering the effect of a exponential fall off for $r > r_0$ and a properly adjusted (**top panel**) and more considerably reduced (**bottom panel**) DM scaling C in the inner bubble.

Our central quantity for analysis has the form

$$4m = 2\left(2 + \frac{\beta(n+1)\mu^2 + (n\frac{\kappa}{4\pi} - \beta)\mu}{(1-\mu)(\frac{\kappa}{4\pi} + \beta\mu)}\right) \tag{4.88}$$

For $n = 0$, these models display the asymptotic behaviour

$$\mu \ll 1 \qquad \delta\mathbf{F} \approx \frac{4\pi a_0}{\kappa} C^{\frac{1}{n+1}} \left(\frac{r}{r_0}\right)^{\frac{\alpha-2}{n+1}} \frac{\mathbf{D}}{D^{\frac{n}{n+1}}}\bigg|_{n=1} \tag{4.89}$$

$$\mu \gg 1 \qquad \delta\mathbf{F} \approx \frac{a_0}{\beta}\frac{\mathbf{F}_N}{F_N} \tag{4.90}$$

with the feature that z saturates as $F_N \to \infty$ (as seen clearly in Figure 3.14). In this case we have

$$4m = 2\left(2 - \frac{\beta\mu}{\frac{\kappa}{4\pi} + \beta\mu}\right) = 2\left(2 - \frac{4\pi\beta}{\kappa}z\right) \tag{4.91}$$

in each limit becoming

$$\mu \ll 1 \qquad 4m \simeq 4$$

$$\mu \gg 1 \qquad 4m \simeq 2$$

suggesting we are moving simply from one DM regime to a different one. The form of the tidal stresses for $\mu \gg 1$ are

$$S_{yy} \quad = \quad \frac{C_4}{r}\cos\psi((f+g')\cos\psi + \sin\psi\,(f'+g)) + \frac{C_2}{2} \tag{4.92}$$

where $C_4 = a_0/\beta$ and as before C_2 is the rescaled Newtonian tidal stress at the saddle. We note that the magnitude of tidal stress scaling is suppressed by a factor of $\frac{\kappa}{4\pi}$ (compared with C_1).

For models where $n \neq 0$, we find again the same DM limit $\mu \to z$, but now a parameterised QN limit,

of the form

$$\begin{aligned} \beta \gg \frac{\kappa}{4\pi} \qquad & \mu \simeq 1 - \left(\frac{\kappa}{4\pi\beta}\frac{1}{z}\right)^{1/n} + \dots \\ \beta \ll \frac{\kappa}{4\pi} \qquad & \mu \simeq 1 - \left(\frac{1}{z}\right)^{1/n} + \dots \end{aligned} \tag{4.93}$$

in the QN limit, equation (4.88) reduces to

$$\begin{aligned} \beta \gg \frac{\kappa}{4\pi} \qquad & 4m \simeq 2n \left(\frac{4\pi\beta}{\kappa}\right)^{1/n} U^{1/n} \\ \beta \ll \frac{\kappa}{4\pi} \qquad & 4m \simeq 2n\, U^{1/n} \end{aligned} \tag{4.94}$$

where we take notice of the limit relevant for suggested value of $\beta \approx 1$ (which provides a good fit to galactic data, as presented in [25]). If we consider a simple case we have encountered before, say $n = 1$, our model parameters now take the form

$$C_1^{\mu} \quad = \quad \frac{\kappa}{4\pi\beta} \ll 1 \tag{4.95}$$

This strongly suggests that the DM scaling C will be suppressed - allowing us to place some constraint on the combination of β, n parameters here. In this case we would expect

$$\begin{aligned} C \quad &\rightarrow \quad \zeta C \\ \zeta \quad &\simeq \quad \left(\frac{\kappa}{4\pi}\right)^{2/n} \end{aligned}$$

which in this example would be small and hence given this suppression in signal, such models could potentially evade the net of an LPF test. For the case of $\beta \ll \frac{\kappa}{4\pi}$, these functions simply fall into the cases we have described before (indeed our $\mu_{fiducial}$ follows a similar functional form).

4.7 Constraining the Parameter Space

A natural question to consider now is where do these results leave us when looking at data, such as measurements from LPF in the event of saddle flyby extension. *How (if at all) can we constrain our theories from data? What exactly is the parameter space of MOND?*

The most likely scenario for an LPF test is a single saddle flyby, which given its likely velocity, suggests data collected with be on the time scale of many minutes (rather than say hours). We posit that *if* any clear signal is seen above the noise and Newtonian background, we can make the following inferences:

- **The 0^{th} Order Approach**, for $b \lesssim r_0$, we assume that the signal is dominated by the DM regime, which given the relative invariance of the profile functions (assuming $F_i(\psi) \simeq F_1$, $G_i(\psi) \simeq G_1$) means that the main scalings in the tidal stresses come from γ and C.

  We can attempt to fit the DM tidal stresses to the signal by varying the value of γ - remembering that $\alpha = \alpha(n)$ and there only exists a strict series of $\gamma(\alpha(n))$ for regular solutions of $\mathbf{U}$. Once we find the correct γ, we can then consider the "amplitude" of this signal, which can tell us (albeit broadly) about the QN regime, from the matching between $C \to C_1^\mu$.

  For $b \gtrsim r_0$, the signal is sampling the QN regime, which means at lowest order

$$\frac{\mathbf{U}}{\mu} - \mathbf{U}_0 \simeq \frac{\mathbf{h}(\psi)}{(r/r_0)^{p-1}} \tag{4.96}$$

  where we have collected together the angular function

$$\mathbf{h}(\psi) = C_1^\mu \left(\frac{\mathbf{N}(\psi)}{N^p} + \frac{p}{2}\mathbf{B}_p(\psi) \right) \tag{4.97}$$

  Given that for small n, $h(\psi) \sim \mathcal{O}(1)$, we can first try fitting the radial fall off from the data (this should provide the order of magnitude contribution) and then once the exponent p is found, the various angular profile functions can be inferred, allowing us to get a bound on C_1^μ.

- **The 1^{st} Order Approach**, we introduce a cutoff in the signal, based on the impact parameter of the spacecraft (between the interior and exterior of the bubble). We fit the DM signal as before (now taking into account the scaling of $G_i(\psi)$) and with the improved matching, make corrections to C_1^μ. We consider each parameter can be written as a perturbative expansion as

$$C_1^\mu \simeq C_1^{\mu(\mathbf{0})} + C_1^{\mu(\mathbf{1})} + \dots \tag{4.98}$$

  etc ... Allowing for improvements in parameter accuracy as we go up in approach.

$$\Downarrow$$

- **The 2^{nd} Order Approach**, if we are blessed with plenty of tracking data and/or multiple flybys, we can make better determinations of our parameters.

In this way, we can convert the distinctive MONDian signal of a positive result into a constraint on the MONDian parameter space akin to converting a negative result into a constraint on μ, just as we considered in Section 3.4.

4.8 More General Free Functions

Suppose we generalise our free functions to the case

$$\nabla \cdot (f \nabla \phi) = \kappa G \rho \tag{4.99}$$

where $f = f(\phi, z, \dots)$, arising for instance if the relativistic "mother theory" is actually some general scalar-tensor theory. Might there still be MONDian effects observable at the SP? Could these theories produce a divergent tidal stress signal of their own? We set up our change to a linear variable and vacuum

equations for this system as

$$\begin{aligned} \mathbf{U} = -f\frac{\kappa}{4\pi}\frac{\nabla\phi}{a_0} &\Rightarrow U = fz \\ \nabla\wedge\left(\frac{\mathbf{U}}{f}\right) = 0 &\Rightarrow 4m_f U^2\nabla\wedge\mathbf{U} + \mathbf{U}\wedge\nabla U^2 = 0 \\ 4m_f &= \frac{\partial\ln U^2}{\partial\ln f} \end{aligned} \tag{4.100}$$

and proceed to solving these equations around the saddle with the knowledge of the linear Newtonian approximation, remembering

$$\begin{aligned} \Phi_N &= -\frac{A}{2}r^2 N_r(\psi) \\ N_r &= \frac{1}{4}(1+3\cos 2\psi) \end{aligned} \tag{4.101}$$

4.8.1 DM Regime

Here $z \ll 1$, so let's expand the free function such that

$$f(\phi, z, \dots) = b_0 + \sum_{n=p}^{\infty} b_n z^n \tag{4.102}$$

and we can take

$$4m_f = \frac{\partial\ln U^2}{\partial\ln f} = 2\left(1 + \frac{f}{z}\frac{\partial z}{\partial f}\right) \tag{4.103}$$

where we will invert the derivative

$$\frac{\partial z}{\partial f} = \frac{1}{\frac{\partial z}{\partial f}} = \frac{1}{f'} \tag{4.104}$$

such that

$$4m_f = 2\left(1 + \left(\frac{b_0}{z} + \sum_{n=p}^{\infty} b_n z^{n-1}\right) \Big/ \sum_{n=p}^{\infty} n b_n z^{n-1}\right) \tag{4.105}$$

The $b_0 = 0$ case

At leading order p, we find

$$4m_f \to \frac{2(p+1)}{p} \tag{4.106}$$

meaning we have a similar DM regime close to the saddle, with solutions of the form

$$\mathbf{U} = C(p)\left(\frac{r}{r_0}\right)^{\alpha(p)-2}\mathbf{D_p}(\psi) \tag{4.107}$$

where the exact form of all the components is detailed in Section 4.4.2.

The $b_0 \neq 0$ case

Here the leading order contribution will be of the form

$$4m_f \to \frac{2b_0}{pb_p z^p} \simeq \frac{2}{pU^p}\frac{b_0^{p+1}}{b_p} \tag{4.108}$$

using $U \simeq b_0 z$. We find solutions of the form:

$$\mathbf{U} = \mathbf{U}_0 + \mathbf{U}_2 \tag{4.109}$$

$$\mathbf{U}_0 = \frac{r}{r_0}\mathbf{N}(\psi) \tag{4.110}$$

$$\nabla \cdot \mathbf{U}_2 = 0 \tag{4.111}$$

$$\nabla \wedge \mathbf{U}_2 = -\frac{\mathbf{U}_0 \wedge \nabla U_0^2}{2(b_0^p/pb_p)U_0^{p+2}} = \frac{s(\psi)}{r^p}\frac{b_p}{b_0^{p+1}} \tag{4.112}$$

In order to solve this system, we need to know the function f to "background order" in (r, ψ), (akin to sourcing $\mathbf{U}_2$ from the background $\mathbf{U}_0$), which we find from the zeroth order relation $f \to b_0$ giving

$$\nabla \cdot (b_0 \nabla \phi) = \frac{\kappa}{4\pi}\nabla^2 \Phi_N \tag{4.113}$$

and if we have the case of simply $f(\phi, z)$, then we can solve for $b_0(\phi)$ close to the saddle first, to find

$\phi(r,\psi)$ and finally substitute into equation (4.117) to find how the curl term is sourced from the ϕ and z dynamics.

4.8.2 QN Regime

Here we take the limit $z \gg 1$ and so make an asymptotic expansion of f of the form

$$f = c_0 + \sum_{n=q}^{\infty} \frac{c_n}{z^n} \tag{4.114}$$

such that to leading order we find

$$4m_f = 2\left(1 - \left(\frac{c_0}{z} + \sum_{n=q} \frac{c_n}{z^{n+1}}\right) \Big/ \sum_{n=q} \frac{nc_n}{z^{n+1}}\right) \tag{4.115}$$

The $c_0 \neq 0$ case

Here we have

$$4m_f \to -\frac{2c_0 z^q}{qc_q} \simeq -\frac{2U^q}{qc_q}\frac{1}{c_0^{q-1}} \tag{4.116}$$

where we have used $U \simeq c_0 z$. Such a result is familiar to us from as a generalised QN limit with the caveat of having additional $\phi(r,\psi)$ dependence here. Finally we find solutions of the form

$$\begin{aligned} \mathbf{U} &= \mathbf{U}_0 + \mathbf{U}_2 \\ \mathbf{U}_0 &= \frac{r}{r_0}\mathbf{N}(\psi) \\ \nabla \cdot \mathbf{U}_2 &= 0 \\ \nabla \wedge \mathbf{U}_2 &= \frac{\mathbf{U}_0 \wedge \nabla U_0^2}{(2/qc_0^{q-1}c_q)U_0^{q+2}} = \frac{s(\psi)}{r^q} c_0^{q-1} c_q \end{aligned} \tag{4.117}$$

The $c_0 = 0$ case

In this case we find

$$4m_f \to \frac{2(q-1)}{q} \tag{4.118}$$

and we can use results from Section 4.8.1 to find (DM like) solutions similarly for this case.

The Bubble Boundary

If we are interested in the boundary between the two regimes, we look for solutions at $|\mathbf{U}|^2 \simeq 1$, which we can see will satisfy

$$|\mathbf{U}|^2 \simeq \left[\frac{\kappa}{4\pi}\frac{|\nabla\phi|}{a_0}c_0(\phi)\right]^2 \simeq 1$$

where as before we source c_0 from

$$\nabla\cdot(c_0\nabla\phi) = \frac{\kappa}{4\pi}\nabla^2\Phi_N \tag{4.119}$$

and using the fact that deviations from spherical symmetry are subdominant at the bubble boundary, we find $c_0|\nabla\phi| \simeq \frac{\kappa}{4\pi}|\nabla\Phi_N|$, giving the same result as before using the linear Newtonian force

$$|\mathbf{N}|^2 r^2 = \left(\cos^2\psi + \frac{1}{4}\sin^2\psi\right) r^2 = \underbrace{\left(\frac{16\pi^2 a_0}{\kappa^2 A}\right)^2}_{r_0^2}$$

suggesting we, in fact, have the same structure with MONDian ellipsoids around the saddle.

4.8.3 An Example

We provide the simple example of a scalar theory coupled with a standard MONDian one

$$f = d_1\mu(z) + d_2\phi + d_3\phi\mu(z) \tag{4.120}$$

$$\mu(z) = \frac{z^a}{(1+z^b)^{a/b}} \tag{4.121}$$

Inner Bubble

Here we expand for $z \ll 1$

$$\begin{aligned} \mu &\simeq z^a + \dots \\ f &\simeq d_2\phi + (d_1 + d_3\phi)z^a + \dots \end{aligned} \tag{4.122}$$

and so our background equations of motion take the form

$$\begin{aligned} \nabla^2\left(\frac{d_2}{2}\phi_0^2\right) &= \frac{\kappa}{4\pi}\nabla^2\Phi_N \\ \phi_0 &= \sqrt{\frac{2}{d_2}\frac{\kappa}{4\pi}\Phi_N} \end{aligned} \tag{4.123}$$

Since our effective $b_0 \neq 0$, we have a modified inner bubble solution, such that

$$\nabla \wedge \mathbf{U}_2 = \frac{s_a(\psi)}{r^a}\frac{d_1 + d_3\phi}{(d_2\phi)^a} \tag{4.124}$$

for simplicity we will pick $a = 1$ and $d_1 = d_2 = d_3 = 1$, making

$$\begin{aligned} s_1(\psi) &= -\frac{6\sqrt{2}\sin 2\psi}{(5 + 3\cos 2\psi)^{3/2}} \\ \nabla \wedge \mathbf{U}_2 &= \frac{s_1}{r}\frac{d_1 + \tilde{d_3}N^{1/2}\,r}{\tilde{d_2}N^{1/2}\,r} \end{aligned} \tag{4.125}$$

where for the Earth-Sun saddle, taking our fiducial value for κ, $\frac{\kappa}{4\pi}A \simeq 10^{-13}$ kg s^{-1} and so $\tilde{d_i} = d_i\sqrt{\frac{2}{d_2}\frac{\kappa}{4\pi}A} \simeq \frac{d_i}{\sqrt{d_2}}5 \times 10^{-7}$ kg m, making

$$\nabla \wedge \mathbf{U}_2 \simeq \sqrt{\frac{4\pi}{\kappa A}}\frac{s_1}{N^{1/2}}\frac{1}{r^2} \tag{4.126}$$

And so we can calculate the form of $\mathbf{U}_2$ and $\delta\mathbf{F}$ in this regime.

$$\delta\mathbf{F} = -\nabla\phi = \frac{4\pi a_0}{\kappa}\frac{1}{b_0(\phi)}\left(\mathbf{U}_0 + \mathbf{U}_2 - \frac{b_1(\phi)}{b_0^2(\phi)}U^2(\mathbf{U}_0 + \mathbf{U}_2) + \dots\right) \tag{4.127}$$

One point to be made is using the typical values of κ described up to now, this term will be of order 10^6 and so not subdominant to the rescaled Newtonian component of $\mathbf{U}$ (as was the case before). Obviously we can account for this in the expansion of $\mathbf{F}_\phi \propto \mathbf{U}/\mu$, but in different theories it may be the case that κ takes on a wholly different value and so our constraints may be somewhat different. The main purpose of this calculation is to show a wholly different inner bubble solution is possible with the presence of a generalised free function.

Outer Bubble

Here we expand for $z \gg 1$

$$\begin{aligned} \mu &\simeq 1 - \frac{a}{b}\frac{1}{z^b} + \dots \\ f &\simeq d_1 + (d_2 + d_3)\phi - \frac{a}{b}(d_1 + d_3\phi)\frac{1}{z^b} + \dots \end{aligned} \tag{4.128}$$

Our background equations of motion take the form

$$\nabla^2\left(d_1\phi + \frac{d_2 + d_3}{2}\phi^2\right) = \frac{\kappa}{4\pi}\nabla^2\Phi_N \tag{4.129}$$

which we can see is a quadratic in ϕ, with solutions of the form

$$\phi = \frac{-d_1 + \sqrt{d_1^2 + 2(d_2 + d_3)\frac{\kappa}{4\pi}\Phi_N}}{d_2 + d_3} \tag{4.130}$$

We find an effective radius r_s for the interplay between these effects, given by

$$r_s = \sqrt{\frac{4\pi}{\kappa A}\frac{d_1^2}{d_2 + d_3}} \simeq 3 \times 10^3 \left(\sqrt{\frac{d_1^2}{d_2 + d_3}}\right) km$$

(with κ taking its fiducial value) and we find for

$$r \ll r_s \Rightarrow \phi_0 \to \frac{1}{d_1}\frac{\kappa}{4\pi}\Phi_N \tag{4.131}$$

$$r \gg r_s \Rightarrow \phi_0 \to \sqrt{\frac{2}{d_2 + d_3}\frac{\kappa}{4\pi}\Phi_N} \tag{4.132}$$

The physical interpretation of r_s should be clarified here. We see on scales below r_s, ϕ_0 just takes on the form of a renormalised Newtonian field and on scales above it, the field takes on a completely different form. Notice in the first case, we just get a renormalisation of G in the usual way, in the second however the field takes on a wholly different form, in this case $\sim \sqrt{\Phi_N}$. This field will *also* generate a divergent tidal stress and there will be some additional force here, but we will assume there is some screening mechanism at play also. What is interesting is that even the effects prevalent far from the saddle can have an effect on the form of the solutions, depending on which "background" regime we are in. Additionally, see that these scalar-tensor effects produce different effects to those from solely MONDian theories and this might provide the possibility of distinguishing between the two.

Also we have $c_0 = d_1 + (d_2 + d_3)\phi \neq 0$ and so a modified outer bubble solution of the form

$$\nabla \wedge \mathbf{U}_2 = \frac{a}{b}\frac{s_b(\psi)}{r^b}\left((d_1 + (d_2 + d_3)\phi)^{b-1}(d_1 + d_3\phi)\right) \tag{4.133}$$

For similar simplicity, let's pick $b = 2$ (again with $d_1 = d_2 = d_3 = 1$) and in the region close to the exterior of the bubble (ie $r \ll r_s$), we find a solution

$$\nabla \wedge \mathbf{U}_2 = \frac{s_2}{r^2}\left(1 + 3\frac{\kappa}{4\pi}ANr^2 + \left(\frac{\kappa}{4\pi}AN\right)^2 r^4\right) \tag{4.134}$$

and with $r_s \simeq 2 \times 10^3$ km, we can see that for $r < r_s$, this can be safely approximated to

$$\nabla \wedge \mathbf{U}_2 \simeq \frac{s_2}{r^2}$$

allowing us to use the usual QN results. As such, the observable force takes the form

$$\delta\mathbf{F} = -\nabla\phi = \frac{4\pi a_0}{\kappa}\frac{1}{c_0(\phi)}\left(\mathbf{U}_0 + \mathbf{U}_2 + \frac{1}{2}\frac{c_1(\phi)}{c_0^2(\phi)}\frac{\mathbf{U}_0}{U_0^2} + \dots\right) \tag{4.135}$$

It is worthwhile saying that in the case of the expansion in this regime taking the form

$$f = b_0 + \sum_{n=p}^{\infty} \left(b_n z^n + \frac{b_{-n}}{z^n} \right) \tag{4.136}$$

then given $z \ll 1$ here, we will have the expression

$$\begin{aligned} 4m_f &\simeq \lim_{q\to\infty} 2\left[1 + \left(\frac{b_0}{z} + \sum_{n=p}^{q} \frac{b_{-n}}{z^{n+1}}\right) \Big/ \left(-\sum_{n=p}^{q} \frac{n b_{-n}}{z^{n+1}}\right)\right] \\ &\simeq \lim_{q\to\infty} 2\left[1 - \frac{b_0 z^q}{q b_{-q}} - \frac{1}{q}\right] \to 2 \end{aligned} \tag{4.137}$$

suggesting that generically if $b_{-n} \neq 0, \forall n$, then we will always have an asymptotic DM regime, as described in Section 4.6. If the series expansion terminates *prematurely*, then we will have the solution $4m_f \to 2(q-1)/q$, where q is the terminating power in the expansion. Similarly for the QN regime, if we are confronted with a free function of the form

$$f = c_0 + \sum_{n=p}^{\infty} \left(c_n z^n + \frac{c_{-n}}{z^n} \right) \tag{4.138}$$

then for similar reasons, $4m_f \to 2$.

4.9 Conclusions

To conclude, we have presented a series of techniques for characterising, evaluating and rescaling the MONDian tidal stresses, which would be measured by LISA Pathfinder, should a saddle flyby be incorporated into the mission. Our argument allows for the variation of the acceleration scale a_0 and κ and for different models of μ function. Our goal was to detach these theories from their "alternative to dark matter duties", considering two-regime functions with $\mu \to 1$ at large z, but $\mu \propto z^n$ (where in general $n \neq 1$), when z is small. We demonstrated how SNRs change by changing the parameters of the theory, giving an indication of how sensitive the experiment is, and therefore how much it will constrain them. As an application of our techniques, we applied this scaling algorithm to the prediction of results for the

Moon saddle. The results were very encouraging and lead us to urge the orbit designers to include it in their considerations. Whilst changing the free function, we found (broadly speaking) an approximate invariance for the angular profile functions in the DM limit irrespective of the model of μ used, although changes do arise from the radial exponent γ and DM scaling C. In the QN limit, we find a menagerie of solutions depending on the form of the fall off from $\mu \to 1$. A very brief investigation into type II MONDian theories suggests that the broad results here do not transfer over into that class of theory and so any rescaling of tidal stresses must be done more carefully, in contrast to the invariance we showed in type I theories. We also considered an intermediate MONDian limit, although it remains somewhat unclear what the solutions here can tell us about the transition to the other regimes.

We suggested potential strategies to constrain the parameter space of MONDian theories from data, identifying a framework of parameters that could be important for an experimental determination around saddle points. In doing so, we demonstrated the interplay between the DM and QN limits by using this framework to calculate how the DM scaling C varies in different models - a previously overlooked issue. The framework also shows the possibility of calculating order by order the coefficient and fall off power in μ if *a priori* we assume values for κ, a_0 - at best we can constrain two parameters. Finally, we demonstrated the power of our techniques in the case of more general free functions, as could perhaps be the case from a more exotic (and therefore complicated!) modified gravity theory or perhaps resulting from some scalar-tensor theory. We leave the computation of scalings in SNRs for future work, as well as other applications of these techniques.

Chapter 5

Conclusions

In this thesis we have considered analytical, numerical and experimental techniques for testing and constraining theories of modified gravity with a preferred acceleration scale. Such ideas were originally conceived in the guise of MOND as a replacement for dark matter but now have been elevated to fully relativistic, consistent alternatives to GR. The weak field limits of these theories can produce phenomenology suitable for such purposes on galactic scales, however cosmological and other probes [45, 46, 76] can be problematic.

In this work, we examined the possibility of testing such theories in the non relativistic limit, notating the generic anomalous tidal stresses such theories would produce. We find the low acceleration regions surrounding gravitational saddle points are a fertile testing ground for these ideas, where these MONDian effects would likely be observed:

- In Section 1.2.5, we showed how to attack these problems by first classifying the different modified poisson equations that result from these theories. Theories we labelled type I and IIB provide the best prospect for such a test, producing large regions of observable MONDian behaviour, due to the triggering nature of their dynamics. In such theories, the fifth force field ϕ present moves from taking the form of a rescaled Newtonian potential ($\phi \rightarrow \frac{\kappa}{4\pi}\Phi_N$, with κ taken suitably small to escape detection on, say, Solar System scales) to producing a truly MONDian form. When the total

acceleration drops some preferred acceleration scale (which we denote a_0), this ϕ field becomes the dominant contribution. Whilst this region around the Earth-Sun SP would only be ~ 2.2m in size, the anomalous tidal stress "bubble" of behaviour would be ~ 383km - providing a viable target for a satellite fly-by test.

- The LPF space probe, designed to test the feasibility of space based, low frequency gravitational wave detection, could provide just the experimental test for a tidal stress experiment. We find the peak of a potential MONDian tidal stress signal would be exactly around the lowest point in the expected noise spectrum - a useful coincidence. Other theories, which we labelled types IIA and III, would fair less favourably, due to their one field approach for producing modified gravity effects - the effects which are the tiny saddle bubbles. In Section 3.1, we used the framework of experimental gravitational waves to estimate the SNRs for a LPF test. Further to this, we considered experimental systematics such as different noise profiles, spacecraft velocity and self gravity and as such the nominal requirements of the mission should be ample, as Figure 3.2 shows.

- In Section 3.4, we considered how these Solar System tests would be able to constrain the parameter space, based on a null result. Whilst a precise statement would be model dependent, we can obtain an order magnitude answer on the functional form of the free functions μ and ν, as Figures 3.13 - 3.15 and 3.19 show. Such constraints suggest it would be hard to wriggle out of a negative result, unless certain types of free functions are considered (e.g. they diverge) - giving a different restriction of the parameter space. The different types of theory appear to have different behaviours in the regime we will be testing and so different constraints will apply to each - perhaps this can be used a discriminator between them.

- An alternative approach considered in Section 4.2, makes use of the systems scaling symmetries. We find homeothetic solutions satisfy our vacuum equations and consequently we can derive a scaling algorithm allowing us to use (previously computed) numerical results for a wide range of parameter values. We applied our techniques in Section 4.3.1, using the example of the Earth-Moon SP and showing that provided we approach "close enough" and at the "right phase" in the moon's cycle,

very high SNRs are within arms reach, as illustrated in Figure 4.8.

- We also considered in Section 4.4 routes to extending our formalism to cover any choice of type I free function - allowing us to investigate strategies for constraining μ in the event of a positive detection. This allows us to produce results for different values of our parameters, κ, a_0 and μ. We also looked at more general free functions, suggesting the divergent tidal stress phenomenology could be present from a much wider set of theories than originally thought (such as scalar-tensor theories).

- We suggest therefore that a mission extension for LPF to probe these ideas would be scientifically feasible and provide good constraints on MG theories (whatever the eventual result).

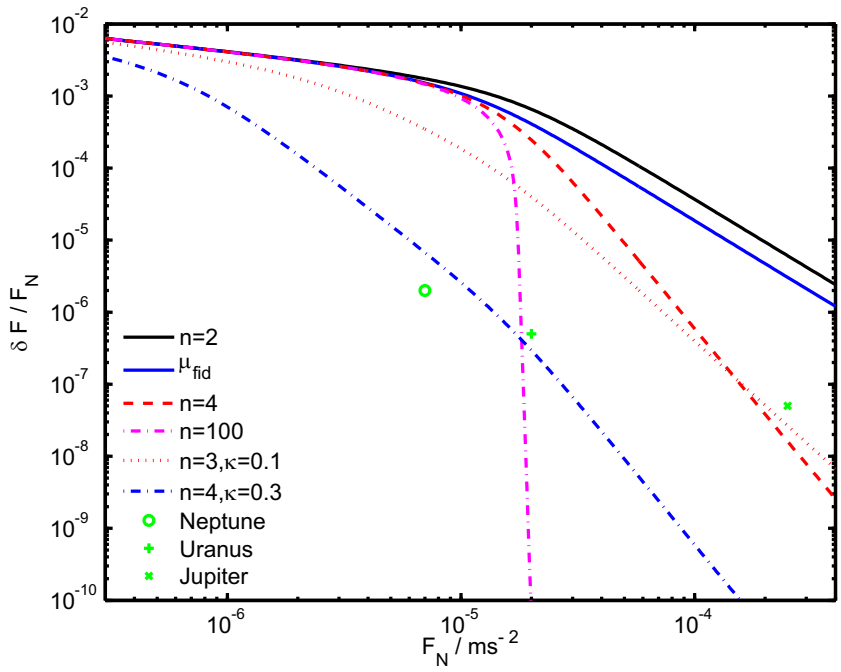

Figure 5.1: Comparing Solar System fifth force constraints [8] with models of free function. Such a plot would a starting point to consider current constraints on MG theories. Recall that for fiducial parameter values, the bubble boundary is at $a_{trig} \simeq \frac{4\pi}{\kappa} a_0 \simeq 10^{-5}$ ms^{-2} and here we have subtracted off the rescaled Newtonian contribution from the δF and $\kappa = 0.03$ unless stated otherwise. The errors on the constraints from Uranus and Neptune remain high, even so note that our fiducial models would not satisfy the constraint from Jupiter - changes to either the fall off n and/or κ would be required.

Looking to the future, we consider a few prospects for further work:

- A consistent study of how to reconcile Solar System based constraints, such as the SP test and fifth

force constraints, with galactic and other astrophysical settings for MOND. As alluded to in Section 3.4.1, a proper fit of all the constraints available over *all* regimes has to date not been considered. By way of a start, we can consider inner and outer Solar System constraints (eg [8]) and see how our free functions compare on these scales, as outlined Figure 5.1.

- Investigating how scalar-tensor theories, such as chameleon models (usually considered in the context of dynamical dark energy models, see [23]) could produce observable effects in a SP test - providing constraints on these ideas from an LPF test.

- A reassessment of the data analysis - developing concrete ideas of how the SNRs scale with changes in the parameters - perhaps similar scaling algorithms also exist for these?

- Proper assessment of the weak-field limits of MG theories - e.g. BiMOND can produce different NR limits [47] using a different form of free function. The FRW cosmology of such theories [76] investigated generalisations of these theories and so the phenomenological implications of such should also be considered in this context.

- Preferred acceleration scale effects are not properly covered by the PPN formalism, e.g. time delay effects across MONDian bubbles as characterised in [77]. Perhaps a way forward would be developing a Post Parametrised Saddle formalism? Characterising MOND from a more geometric point of view, as in [78] could be a starting point.

- Parameter Estimation, akin to those used in cosmology with techniques such as fisher matrix forecasting [79] and using codes such as CosmoMC.

Appendix A

Type II Free Functions

Our plan will be to consider functions similar to those investigated for Type I theories and so easily compare between the two. We start with the idea that *under the assumption of spherical symmetry*

$$\begin{aligned} \nabla \cdot (\mu\, \mathbf{F}_\phi) = \frac{\kappa}{4\pi} \nabla \cdot \mathbf{F}_N \quad &\Rightarrow \quad \mu \mathbf{F}_\phi = \frac{\kappa}{4\pi} \mathbf{F}_N \\ \nabla \cdot \mathbf{F}_\phi = \frac{\kappa}{4\pi} \nabla \cdot (\nu \mathbf{F}_N) \quad &\Rightarrow \quad \mathbf{F}_\phi = \frac{\kappa}{4\pi} \nu \mathbf{F}_N \end{aligned} \tag{A.1}$$

with the natural comparison between

$$\mu(z) \longleftrightarrow \frac{1}{\nu(w)}$$

and so we can use the definition of z to find

$$z = \frac{\kappa}{4\pi} \frac{|\nabla \phi|}{a_0} = \nu \left(\frac{\kappa}{4\pi} \right)^2 \frac{|\nabla \Phi_N|}{a_0} = \nu w \tag{A.2}$$

$$\frac{\mu}{\sqrt{1-\mu^4}} = \frac{1/\nu}{\sqrt{1+1/\nu^4}} = \nu w \tag{A.3}$$

which we can solve to find

$$\nu = \left(1 + \frac{1}{w^2} \right)^{1/4} \tag{A.4}$$

Whilst we stress this derivation is only strictly valid for spherical symmetry, it remains a good starting point for comparison between these theories.

Appendix B

Adaptations to the Numerical Code

Type I

Minimal changes are required to run our code for these parameterised μ functions - the main difference being the term $\frac{\partial \mu}{\partial g^2}$ in the computation of the discrete divergence on the lattice (see section (2.3)), for the $\mu(n)$ models:

$$\frac{\partial \mu}{\partial g^2} = \frac{n}{2}\left(\frac{\kappa}{4\pi a_0}\right)^2 \mu^{1-\frac{2}{n}}(1-\mu)^{1+\frac{2}{n}} \tag{B.1}$$

and the $\mu(a,b)$ models:

$$\frac{\partial \mu}{\partial g^2} = \frac{a}{2}\left(\frac{\kappa}{4\pi a_0}\right)^2 \mu^{1-\frac{2}{a}}(1-\mu^{\frac{b}{a}})^{1+\frac{2}{b}} \tag{B.2}$$

For completeness, we compare with the expression for $\mu_{fiducial}$:

$$\frac{\partial \mu}{\partial g^2} = \frac{1}{2}\left(\frac{\kappa}{4\pi a_0}\right)^2 \mu^{-1}(1-\mu^4)^2(1+\mu^4)^{-1} \tag{B.3}$$

Type IIB

Framing the Poisson equation (1.104) in the form of

$$\nabla \cdot \mathbf{g} = \frac{k}{4\pi}\nabla \cdot (\nu\, \mathbf{g}_N) \tag{B.4}$$

$$\nabla \wedge \mathbf{g} = 0 \tag{B.5}$$

and can compute the discrete divergence

$$D_{\mathbf{x}} = \sum_j \frac{g^j_{\mathbf{x}} - g^j_{\mathbf{x}-\mathbf{j}}}{\Delta^j_-} \tag{B.6}$$

where we use the compact notation

$$\Delta^j_- = r^j_{\mathbf{x}} - r^j_{\mathbf{x}-\mathbf{j}}$$
$$\Delta^j_+ = r^j_{\mathbf{x}+\mathbf{j}} - r^j_{\mathbf{x}}$$

Our source term takes the form

$$D^N_{\mathbf{x}} = \sum_j \frac{\nu_{\mathbf{x}}(g^j_{\mathbf{x}})_N - \nu_{\mathbf{x}-\mathbf{j}}(g^j_{\mathbf{x}-\mathbf{j}})_N}{\Delta^j_-} \tag{B.7}$$

such that at each site we locally solve (B.4) whilst ensuring the discrete curl (B.5) is satisfied globally. As the field changes $g^j \to g^j + \delta g^j$, then at each step, these changes should take the form

$$\begin{aligned} \delta g^j_{\mathbf{x}} &= +\frac{C_{\mathbf{x}}}{\Delta^j_+} \\ \delta g^j_{\mathbf{x}-\mathbf{j}} &= -\frac{C_{\mathbf{x}}}{\Delta^j_-} \end{aligned} \tag{B.8}$$

to keep the discrete curl satisfied. The change in the discrete divergence, $\delta D_{\mathbf{x}}$, at each step will satisfy,

$$D_{\mathbf{x}} + \delta D_{\mathbf{x}} = D^N_{\mathbf{x}} \tag{B.9}$$

such at each site, the change in the field is given by

$$\delta g^j_{\mathbf{x}} = -\frac{D_{\mathbf{x}} - D^N_{\mathbf{x}}}{\delta D_{\mathbf{x}}} \frac{C_{\mathbf{x}}}{\Delta^j_+} \tag{B.10}$$

Then as we cycle through the lattice and the $\mathbf{g}$ field converges, the additional changes to $g^j_{\mathbf{x}}$ lessen. We

achieve faster convergence using a successive over relaxation method (SOR), by scaling the field as

$$\delta g^j_{\mathbf{x}} \rightarrow \lambda \delta g^j_{\mathbf{x}} \tag{B.11}$$

where λ is the over-relaxation parameter and is larger than unity. We begin with $\lambda = 1$ and increase it once the field is settling down, since high values of λ can initially result in the RMS value of $|\delta D_{\mathbf{x}}|$ increasing, whilst we are looking for $|\delta D_{\mathbf{x}}| \rightarrow 0$.

Appendix C

Matching the DM and QN Regimes

Since we require the MONDian force to be smooth and continuous, the matching between the different regimes must occur between $\nabla\phi$ (rather that say $\mathbf{U}$), which takes the form

$$\delta\mathbf{F} = \frac{4\pi a_0}{\kappa}\frac{\mathbf{U}}{\mu}$$

and in the QN limit $\mathbf{U} = \mathbf{U}_0 + C^{QN}\mathbf{U}_2^r$, so we need to make use of

$$\begin{aligned} U &= \sqrt{\mathbf{U}\cdot\mathbf{U}} \\ &= \underbrace{|\mathbf{U}_0|}_{\mathcal{O}(r^1)}\left(1 + 2\,C^{QN}\underbrace{\frac{\mathbf{U}_0\cdot\mathbf{U}_2^r}{U_0^2}}_{\mathcal{O}(r^{-p})} + (C^{QN})^2\underbrace{\frac{\mathbf{U}_2^r\cdot\mathbf{U}_2^r}{U_0^2}}_{\mathcal{O}(r^{-2p})}\right)^{1/2} \end{aligned} \tag{C.1}$$

finally all put together up to 3^{rd} order in the QN regime becomes

$$\begin{aligned}\frac{\mathbf{U}}{\mu} &\approx \underbrace{\mathbf{U}_0}_{\mathcal{O}(r^1)} + \underbrace{C_1^\mu \frac{\mathbf{U}_0}{U_0^p} + C^{QN}\mathbf{U}_2^r}_{\mathcal{O}(r^{1-p})} + \underbrace{\frac{C_1^\mu C^{QN}}{U_0^p}\left(\mathbf{U}_2^r - p\frac{\mathbf{U}_0\cdot\mathbf{U}_2^r}{U_0^2}\mathbf{U}_0\right) + C_2^\mu\frac{\mathbf{U}_0}{U_0^{2p}}}_{\mathcal{O}(r^{1-2p})} \\ &- \underbrace{\frac{C^{QN}}{U_0^p}\left[\left(\frac{p}{2}C_1^\mu\left(U_2^r\right)^2 - p_2\frac{(\mathbf{U}_0\cdot\mathbf{U}_2^r)^2}{U_0^2}\right)\frac{C^{QN}\mathbf{U}_0}{U_0^2} + \mathbf{U}_2^r\left(\frac{p}{2}C_1^\mu C^{QN}\frac{\mathbf{U}_0\cdot\mathbf{U}_2^r}{U_0^2} - \frac{C_2^\mu}{U_0^p}\right)\right]}_{\mathcal{O}(r^{1-3p})} \\ &+ \underbrace{\frac{\mathbf{U}_0}{U_0^{2p}}\left(\frac{C_3^\mu}{U_0^p} - pC_2^\mu C^{QN}\frac{\mathbf{U}_0\cdot\mathbf{U}_2^r}{U_0^2}\right)}_{\mathcal{O}(r^{1-3p})} + \dots\end{aligned} \tag{C.2}$$

where $p_2 = p(p+2)/2$ and here the higher order terms are $\mathcal{O}(r^{1-4p})$ or smaller and represent much more complicated combinations of U_0 and U_2^r. This must be matched to the DM regime force

$$\frac{\mathbf{U}}{\mu} \approx C^{\frac{1}{\ell+1}}\left(\frac{r}{r_0}\right)^{\frac{\alpha-2}{\ell+1}}\frac{\mathbf{D}_\ell}{(D_\ell)^{\frac{\ell}{\ell+1}}}$$

where for $z \ll 1$, $\mu = z^\ell + \dots$ and D_ℓ are just the angular profiles for this case. Using these parameters, we can perform the matching between the two regimes, here choosing the intermediate MONDian regime as

$$\frac{\mathbf{U}_{DM}}{\mu}\left[\frac{r}{r_0} \simeq 0.5 \to 1\right] \xleftrightarrow{\mathbf{C}^{\frac{1}{\ell+1}}} \frac{\mathbf{U}_{QN}}{\mu}\left[\frac{r}{r_0} \simeq 1 \leftarrow 3\right]$$

and we present the results from such a matching and compare with numerical values in Table C.1.

Table C.1: Numerical and Matched C Scalings

μ	C_{num}	C_{mat}	λ_{num}	λ_{mat}	C_{mat}^{improv}
$\mu_{fiducial}$	0.8445	1.0523	-	-	-
$\mu(n=1)$	0.4042	0.5046	2.0893	2.0852	0.4050
$\mu(n=2)$	0.8186	0.9847	1.0316	1.0686	0.7903
$\mu(a=1;b=2)$	1.3163	1.7098	0.6416	0.6154	1.3723

where $\lambda_\# = (C_{fiducial}/C_\mu)_\#$ represents the ratio between the fiducial DM scaling and the value for each model of μ, which we do for both the numerical and matched cases. As we see, the values of C predicted in each case (using the matching techniques) typically overestimate its value. If we consider,

however, the ratio between fiducial scaling value (from matching) with the same models scaling found numerical and use this as our conversion factor. Thus we can convert all the C_{mat} into $\sim C_{num}$ for *any* model of μ we pick - compare the first, second and last columns in Table C.1. Since this regime matching process is considerably less computationally intensive than running our code, this represents an improvement on constraints for C.

Bibliography

[1] J. Magueijo and A. Mozaffari, "The case for testing MOND using LISA Pathfinder," *Phys. Rev. D*, vol. 85, p. 043527, Feb 2012.

[2] A. Mozaffari, "Testing Different Formulations of MOND Using LISA Pathfinder," *arXiv*, 2011.

[3] J. Magueijo and A. Mozaffari, "Saddle stresses for generic theories with a preferred acceleration scale," *Phys. Rev. D*, vol. 86, p. 123518, Dec 2012.

[4] A. Mozaffari, "Parameterised free functions and saddle stresses in modified gravity," 2012.

[5] N. Bevis, J. Magueijo, C. Trenkel, and S. Kemble, "MONDian three-body predictions for LISA Pathfinder," *Class. Quant. Grav.*, vol. 27, p. 215014, 2010.

[6] F. Antonucci and M. A. et al, "The lisa pathfinder mission," *Classical and Quantum Gravity*, vol. 29, no. 12, p. 124014, 2012.

[7] B. Famaey and S. S. McGaugh, "Modified Newtonian Dynamics (MOND): Observational Phenomenology and Relativistic Extensions," *Living Reviews in Relativity*, vol. 15, p. 10, Sept. 2012.

[8] R. Sanders, "Solar system constraints on multi-field theories of modified dynamics," *Mon.Not.Roy.Astron.Soc.*, vol. 370, pp. 1519–1528, 2006.

[9] Planck Collaboration, P. A. R. Ade, N. Aghanim, C. Armitage-Caplan, M. Arnaud, M. Ashdown, F. Atrio-Barandela, J. Aumont, C. Baccigalupi, A. J. Banday, and et al., "Planck 2013 results. I. Overview of products and scientific results," *ArXiv e-prints*, Mar. 2013.

[10] G. D'Amico, M. Kamionkowski, and K. Sigurdson, "Dark Matter Astrophysics," July 2009.

[11] P. Scott, *Searches for Particle Dark Matter: Dark stars, dark galaxies, dark halos and global supersymmetric fits.* PhD thesis, PhD Thesis, University of Stockholm, Faculty of Science, Department of Astronomy (2010). Advisors: Joakim Edsjö, Lars Bergström, Jan Conrad. ISBN 978-91-7447-031-4, May 2010.

[12] M. Milgrom, "A Modification of the Newtonian dynamics as a possible alternative to the hidden mass hypothesis," *Astrophys. J.*, vol. 270, pp. 365–370, 1983.

[13] J. Bekenstein and M. Milgrom, "Does the missing mass problem signal the breakdown of Newtonian gravity?," *Astrophys. J.*, vol. 286, pp. 7–14, 1984.

[14] J. D. Bekenstein, "Relativistic gravitation theory for the MOND paradigm," *Phys. Rev.* ***D70****, 083509 (2004); Erratum-ibid.*, vol. D71, p. 069901, 2005.

[15] T. Jacobson and D. Mattingly, "Gravity with a dynamical preferred frame," *Physical Review D*, vol. 64, p. 024028, July 2001.

[16] T. G. Zlosnik, P. G. Ferreira, and G. D. Starkman, "The vector-tensor nature of Bekenstein's relativistic theory of modified gravity," *Phys. Rev.*, vol. D74, p. 044037, 2006.

[17] T. G. Zlosnik, P. G. Ferreira, and G. D. Starkman, "Modifying gravity with the Aether: an alternative to Dark Matter," *Phys. Rev.*, vol. D75, p. 044017, 2007.

[18] J. Zuntz, T. G. Zlosnik, F. Bourliot, P. G. Ferreira, and G. D. Starkman, "Vector field models of modified gravity and the dark sector," *Physical Review D*, vol. 81, p. 104015, May 2010.

[19] C. Bonvin, R. Durrer, P. G. Ferreira, G. Starkman, and T. G. Zlosnik, "Generalized Einstein-Aether theories and the Solar System," *Physical Review D*, vol. 77, p. 024037, Jan. 2008.

[20] C. Skordis, "Generalizing tensor-vector-scalar cosmology," *Physical Review D*, vol. 77, p. 123502, June 2008.

[21] M. Milgrom, "Bimetric MOND gravity," *Physical Review D*, vol. 80, p. 123536, Dec. 2009.

[22] R. H. Sanders, "A tensor-vector-scalar framework for modified dynamics and cosmic dark matter," *Mon. Not. Roy. Astron. Soc.*, vol. 363, p. 459, 2005.

[23] T. Clifton, P. G. Ferreira, A. Padilla, and C. Skordis, "Modified Gravity and Cosmology," 2011.

[24] B. Famaey and S. S. McGaugh, "Modified Newtonian Dynamics (MOND): Observational Phenomenology and Relativistic Extensions," *Living Reviews in Relativity*, vol. 15, p. 10, Sept. 2012.

[25] H.-S. Zhao and B. Famaey, "Refining MOND interpolating function and TeVeS Lagrangian," *Astrophys. J.*, vol. 638, pp. L9–L12, 2006.

[26] B. Famaey and J. Binney, "Modified Newtonian Dynamics in the Milky Way," *Mon. Not. Roy. Astron. Soc.*, vol. 363, pp. 603–608, 2005.

[27] I. Ferreras, M. Sakellariadou, and M. F. Yusaf, "The necessity of dark matter in MOND within galactic scales," *Phys. Rev. Lett.*, vol. 100, p. 031302, 2008.

[28] N. E. Mavromatos, M. Sakellariadou, and M. F. Yusaf, "Can TeVeS avoid Dark Matter on galactic scales?," *Phys. Rev.*, vol. D79, p. 081301, 2009.

[29] I. Ferreras, N. E. Mavromatos, M. Sakellariadou, and M. F. Yusaf, "Incompatibility of Rotation Curves with Gravitational Lensing for TeVeS," *Phys. Rev.*, vol. D80, p. 103506, 2009.

[30] G. W. Angus, B. Famaey, and H. Zhao, "Can MOND take a bullet? Analytical comparisons of three versions of MOND beyond spherical symmetry," *Mon. Not. Roy. Astron. Soc.*, vol. 371, p. 138, 2006.

[31] D. Clowe *et al.*, "A direct empirical proof of the existence of dark matter," *Astrophys. J.*, vol. 648, pp. L109–L113, 2006.

[32] D.-C. Dai, R. Matsuo, and G. Starkman, "Gravitational Lenses in Generalized Einstein-Aether theory: the Bullet Cluster," *Phys. Rev.*, vol. D78, p. 104004, 2008.

[33] G. W. Angus and S. S. McGaugh, "The collision velocity of the bullet cluster in conventional and modified dynamics," 2007.

[34] J. R. Brownstein and J. W. Moffat, "The Bullet Cluster 1E0657-558 evidence shows Modified Gravity in the absence of Dark Matter," *Mon. Not. Roy. Astron. Soc.*, vol. 382, pp. 29–47, 2007.

[35] A. Mahdavi, H. Hoekstra, A. Babul, D. D. Balam, and P. L. Capak, "A Dark Core in Abell 520," *Astrophys. J.*, vol. 668, pp. 806–814, Oct. 2007.

[36] B. Withers, "Einstein-aether as a quantum effective field theory," *Classical and Quantum Gravity*, vol. 26, p. 225009, Nov. 2009.

[37] J. A. Zuntz, P. G. Ferreira, and T. G. Zlosnik, "Constraining Lorentz Violation with Cosmology," *Physical Review Letters*, vol. 101, p. 261102, Dec. 2008.

[38] L. Blanchet and J. Novak, "Testing MOND in the Solar System," 2011.

[39] M. Sereno and P. Jetzer, "Dark matter vs. modifications of the gravitational inverse-square law. Results from planetary motion in the solar system," *Mon. Not. Roy. Astron. Soc.*, vol. 371, pp. 626–632, 2006.

[40] M. Milgrom, "MOND effects in the inner solar system," 2009.

[41] J. Bekenstein and J. Magueijo, "MOND habitats within the solar system," *Phys. Rev.*, vol. D73, p. 103513, 2006.

[42] P. McNamara, S. Vitale, and K. Danzmann, "LISA Pathfinder," *Class. Quant. Grav.*, vol. 25, p. 114034, 2008.

[43] C. Trenkel, S. Kemble, N. Bevis, and J. Magueijo, "Testing MOND/TEVES with LISA Pathfinder," *submitted*, 2009.

[44] C. Skordis, "The Tensor-Vector-Scalar theory and its cosmology," *Class. Quant. Grav.*, vol. 26, p. 143001, 2009.

[45] C. R. Contaldi, T. Wiseman, and B. Withers, "TeVeS gets caught on caustics," *Phys. Rev. D*, vol. 78, p. 044034, Aug. 2008.

[46] F. Bourliot, P. G. Ferreira, D. F. Mota, and C. Skordis, "Cosmological behavior of Bekenstein's modified theory of gravity," *Phys. Rev. D*, vol. 75, p. 063508, Mar. 2007.

[47] M. Milgrom, "Quasi-linear formulation of MOND," *Mon. Not. Roy. Astron. Soc.*, vol. 403, pp. 886–895, Apr. 2010.

[48] M. Milgrom, "Bimetric MOND gravity," *Phys. Rev.*, vol. D80, p. 123536, 2009.

[49] M. Milgrom, "Matter and twin matter in bimetric MOND," *Mon. Not. Roy. Astron. Soc.*, vol. 405, p. 1129, 2010.

[50] E. Babichev, C. Deffayet, and G. Esposito-Farèse, "Improving relativistic modified Newtonian dynamics with Galileon k-mouflage," *Phys. Rev. D*, vol. 84, p. 061502, Sept. 2011.

[51] S. M. Carroll and E. A. Lim, "Lorentz-violating vector fields slow the universe down," *Phys. Rev. D*, vol. 70, p. 123525, Dec 2004.

[52] K.-i. Umezu, K. Ichiki, and M. Yahiro, "Cosmological constraints on newton's constant," *Phys. Rev. D*, vol. 72, p. 044010, Aug 2005.

[53] J. Laraudogoitia, "On norton's dome," *Synthese*, 2012.

[54] M. Milgrom, "Solutions for the modified Newtonian dynamics field equation," *Astrophys. J.*, vol. 302, pp. 617–625, 1986.

[55] W. Press and al. al. al. al. 1992. Numerical Recipes in C, Cambridge University Press, UK.

[56] N. Bevis and M. Hindmarsh.

[57] F. Antonucci and M. A. et al, "Lisa pathfinder: mission and status," *Classical and Quantum Gravity*, vol. 28, no. 9, p. 094001, 2011.

[58] S. Vitale, "The LTP Experiment on the LISA Pathfinder Mission," *ArXiv General Relativity and Quantum Cosmology e-prints*, Apr. 2005.

[59] K. Danzmann and the LISA study team, "Lisa: laser interferometer space antenna for gravitational wave measurements," *Classical and Quantum Gravity*, vol. 13, no. 11A, p. A247, 1996.

[60] C. Helstrom 1968. Statistical Theory of Signal Detection, Pergamon Press, Oxford; New York.

[61] B. S. Sathyaprakash and B. F. Schutz, "Physics, Astrophysics and Cosmology with Gravitational Waves," *Living Rev. Rel.*, vol. 12, p. 2, 2009.

[62] P. McNamara, S. Vitale, K. Danzmann, and LISA Pathfinder Science Working Team, "LISA Pathfinder," *Classical and Quantum Gravity*, vol. 25, p. 114034, June 2008.

[63] F. e. a. Antonucci, "From laboratory experiments to LISA Pathfinder: achieving LISA geodesic motion," *Classical and Quantum Gravity*, vol. 28, p. 094002, May 2011.

[64] F. e. a. Antonucci, "LISA Pathfinder data analysis," *Classical and Quantum Gravity*, vol. 28, p. 094006, May 2011.

[65] B. Famaey, G. Gentile, J.-P. Bruneton, and H.-S. Zhao, "Insight into the baryon-gravity relation in galaxies," *Phys. Rev.*, vol. D75, p. 063002, 2007.

[66] J. Magueijo and R. D. Sorkin, "Occam's razor meets WMAP," *Mon.Not.Roy.Astron.Soc.*, vol. 377, pp. L39–L43, 2007.

[67] G. Gentile, B. Famaey, and W. de Blok, "THINGS about MOND," *Astron.Astrophys.*, vol. 527, p. A76, 2011.

[68] J.-P. Bruneton and G. Esposito-Farese, "Field-theoretical formulations of MOND-like gravity," *Phys.Rev.*, vol. D76, p. 124012, 2007.

[69] S. McGaugh, "Milky Way Mass Models and MOND," *Astrophys.J.*, vol. 683, pp. 137–148, 2008.

[70] H. Zhao, "An ecological approach to problems of Dark Energy, Dark Matter, MOND and Neutrinos," *J.Phys.Conf.Ser.*, vol. 140, p. 012002, 2008.

[71] P. Galianni, M. Feix, H. Zhao, and K. Horne, "Testing QMOND in the Solar System," *Phys. Rev. D*, vol. 86, p. 044002, Aug. 2012.

[72] E. Bertschinger, "The self-similar evolution of holes in an Einstein-de Sitter universe," *ApJS*, vol. 58, pp. 1–37, May 1985.

[73] E. Bertschinger, "Self-similar secondary infall and accretion in an Einstein-de Sitter universe," *ApJS*, vol. 58, pp. 39–65, May 1985.

[74] M. Headrick, S. Kitchen, and T. Wiseman, "A new approach to static numerical relativity and its application to Kaluza-Klein black holes," *Classical and Quantum Gravity*, vol. 27, p. 035002, Feb. 2010.

[75] A. Adam, S. Kitchen, and T. Wiseman, "A numerical approach to finding general stationary vacuum black holes," *Classical and Quantum Gravity*, vol. 29, p. 165002, Aug. 2012.

[76] T. Clifton and T. G. Zlosnik, "FRW cosmology in Milgrom's bimetric theory of gravity," *Phys. Rev. D*, vol. 81, p. 103525, May 2010.

[77] J. Magueijo and A. Mozaffari, "Time delays across saddles as a test of modified gravity," *Classical and Quantum Gravity*, vol. 30, p. 092002, May 2013.

[78] C. Skordis and T. Zlosnik, "Geometry of modified Newtonian dynamics," *Phys. Rev. D*, vol. 85, p. 044044, Feb. 2012.

[79] D. B. Thomas and C. R. Contaldi, "Testing model independent modified gravity with future large scale surveys," *Journal of Cosmology and Astroparticle Physics*, vol. 12, p. 13, Dec. 2011.